



# LUND UNIVERSITY

## Stochastic Reactor Models for Engine Simulations

Tunér, Martin

2008

[Link to publication](#)

*Citation for published version (APA):*

Tunér, M. (2008). *Stochastic Reactor Models for Engine Simulations*. [Doctoral Thesis (monograph), Combustion Physics]. Division of Combustion Physics, Department of Physics, Lund University.

*Total number of authors:*

1

### General rights

Unless other specific re-use rights are stated the following general rights apply:

Copyright and moral rights for the publications made accessible in the public portal are retained by the authors and/or other copyright owners and it is a condition of accessing publications that users recognise and abide by the legal requirements associated with these rights.

- Users may download and print one copy of any publication from the public portal for the purpose of private study or research.
- You may not further distribute the material or use it for any profit-making activity or commercial gain
- You may freely distribute the URL identifying the publication in the public portal

Read more about Creative commons licenses: <https://creativecommons.org/licenses/>

### Take down policy

If you believe that this document breaches copyright please contact us providing details, and we will remove access to the work immediately and investigate your claim.

LUND UNIVERSITY

PO Box 117  
221 00 Lund  
+46 46-222 00 00

# **Stochastic Reactor Models for Engine Simulations**

Martin Tunér

Doctoral Thesis

Division of Combustion Physics  
Faculty of Engineering, LTH  
Lund University  
Sweden, 2008

Division of Combustion Physics  
Faculty of Engineering, LTH  
Lund University  
P.O. Box 118  
SE-22100 Lund  
Sweden

ISSN 1102-8718  
ISBN 978-91-628-7416-2  
ISRN LUTFD2/TFCP-126-SE

© 2008 by Martin Tunér. All rights reserved.  
Printed in Sweden by Tryckeriet i E-huset, Lund 2008

To my mother  
who never saw me  
reach adulthood  
and  
to my father  
who had to...





## Abstract

The aim of the thesis work is the further development of practical engine simulation tools based on Stochastic Reactor Models, SRMs. Novel and efficient implementations were made of a variety of SRMs adapted to different engine types. The models in question are the HCCI-SRM, the TwoZone SI-SRM and the DI-SRM. The specific models developed were incorporated into two different interfaces: DARS-ESSA, which is a stand-alone tool, and DARS-ESM through which all the models can be operated in a simple and effective manner with use of several commercial 1-D engine simulation tools. The tools and couplings to commercial 1-D codes were successfully developed and employed to simulate such complex combustion processes as of HCCI engines with NVO combustion.

SRMs are able to model cyclic variations, but these may be overpredicted if discretization is too coarse. It was found that for studies of cyclic variations in HCCI engines, by using the HCCI-SRM, discretization needs to have a level of resolution of 500 particles and of 0.5 CAD time steps, to provide the correct range of the cyclic variations. To get correct predictions of average values, of for example the pressure, temperature and species mass fractions, as few as 10 cycles are usually required, even when employing as coarse discretization of 100 particles and time steps of 0.5 CAD.

Investigations to study the effects of turbulence and heat transfer in HCCI combustion were performed. In the case of high levels of turbulence and evenly distributed heat transfer, the in-cylinder conditions become homogeneous more quickly. The results indicate that in HCCI engines, inhomogeneities tend to promote earlier ignition and lower pressure rates as well as more stable operating conditions with lesser cyclic variations. Turbulence and the heat transfer distribution had little impact on the duration of combustion or on the amount of HC and NO at EVO.

The calculated concentrations of hydroxyl radicals and formaldehyde were compared with LIF-measurements made in an optically accessed iso-octane / n-heptane fuelled HCCI engine. The averaged and distributed concentrations of  $\text{CH}_2\text{O}$  and OH could be predicted with quite high accuracy by the SRM. This clearly proves the validity of the stochastic reactor model.

The formation of exothermic centers was modeled with the SRM to investigate their impact on HCCI combustion. By varying the exhaust valve temperature, and thus assigning more realistic wall temperatures, the formation of exothermic centers and the ignition timing was shifted in time. It was shown that promoting exothermic centers provide more inhomogeneous conditions before ignition, and lead to earlier ignition. This in turn leads to more homogeneous conditions after combustion, counteracting emissions of hydrocarbons and CO which are a problem in HCCI engines.

# Stochastic Reactor Models for Engine Simulations

---

Studies involving the use of a novel approach with adaptive chemistry, POSM, were performed. Incorporated into the Two-Zone SI-SRM code, calculations showed almost no accuracy to be lost, while there was a decrease in calculation time by a factor of 3. For a further gain in calculation speed of a factor of 12, clear losses in accuracy were experienced, although the global conditions were well captured.

Simulations of diesel engine combustion, DICI, using the newly developed DI-SRM coupled with a 1-D full engine simulation tool were found to agree well with the results of experiments that were conducted. Parametric studies were performed to indicate the sensitivity of the modeling parameters. The DI-SRM behaved as predicted, and even with use of coarse discretization the results were comparable to those of the experiments.

# Acknowledgements

---

## Acknowledgements

So here I am, 4 years and many thousands of SRM calculations after starting my PhD studies. This marks in a way the end of my second round of education, which started in 1998 after a successful decade in the Chemical Industry. Yet this is what I wanted and I can say that I have really found myself in more ways than one. I feel grateful to so many good people who have contributed with so much knowledge, fun and life experiences, too many to be named in here, but none forgotten.

First I would like to express my gratitude to my supervisor Professor Fabian Mauss, who offered me a position as a PhD student. He has profound knowledge in the field of combustion modeling and surprises me continually by being able to keep so much of it in his head. Complex and so hardworking that he is almost the epitome of the overloaded scientist, but indeed a joyful and goodhearted person who continues to care about his students long after they have finished their studies. Dr. Per Amnéus, who co-supervised me the first two years, showed me many useful secrets of chemical modeling. We shared not only an office, but much laughter as well. Professor Ingemar Magnusson, who co-supervised me the final two years, showed me many secrets of flamelets but also good sense in project cooperation and in the ethics of science.

Professor Marcus Aldén, has responsibility for the running of a first class science department, the Division of Combustion Physics, and Anneli and Cecilia see to it that everything work, which surely would make each and any department manager envious. My dear colleagues in the kinetics group, now most of whom spread and contributing to a better world: Raffaella, Gladys, Kalle, Aida, Ned, Andreas, Marie, Ngozi, Sayeed, Fikret and Hadi. Special thanks to Harry, who with a happy smile always would help anybody in the group. Per-Erik, Joakim, Per, Fredrik, Henrik, Johan, Hans, Robert, Mattias and all the others at the division. Thank you all!

Professor Bengt Johansson, for the fruitful discussions and collaborations. The knowledge of engines he possesses is truly humbling. All the other people at the Combustion Engines Department are thanked as well. Professor Xue-Song Bai, is thanked as well, for providing me insights into turbulence phenomenon.

My happy and talented colleagues at LOGE AB, Karin and Anders. Best!

My symbiotic and catalytic partner in life, Adina, and our mini catalysts, Fredrik, Daniel, Sofia and Tudor, the ones most important to me.

# Stochastic Reactor Models for Engine Simulations

---

I kindly acknowledge the financial support for this work provided by the following:

## **Projects:**

### **The Competence Center for Combustion Processes, KCFP.**

[www.kcfp.se](http://www.kcfp.se)

The KCFP of Lund University is concerned with research on combustion processes, in the range from conventional HCCI (Homogeneous Charge Compression Ignition) to classical Otto and Diesel engines.

The ATAC engine Project 2003-2006, financed by: (Volvo Powertrain, Scania CV, Volvo Cars, Volvo Penta, SAAB Automobile (GM Powertrain), Hino Motors Ltd (2003-2005), Nissan (2003-2005), Cummins (2003-2005), Caterpillar Inc, Toyota Motor Corp and STEM).

The KCFP-Modeling Project (2006-2009), financed by: (Volvo Powertrain, Scania CV, Volvo Cars, Volvo Penta, SAAB Automobile (GM Powertrain), Caterpillar Inc, Toyota Motor Corp. and STEM).

### **The Green Car Project.**

The National Green Car project collected the Swedish automotive industry and the Swedish state in support on research for clean vehicles, providing a total funding of 1.8 billion SEK.

I took part in the HCCI horizontal project, GIHR, aimed at developing models and regulation techniques for HCCI engines.

The GIHR project took place from 2000 to 2005, financed by: (Volvo Trucks, Scania CV, Volvo Cars, SAAB Automobile, The Swedish Energy Agency STEM, The Swedish Governmental Agency for Innovation Systems Vinnova, and The Swedish Road Administration Vägverket)

### **The MinKnock Project.**

<http://cordis.europa.eu>

The MinKnock Project was a European Community Project aimed at improving engine performance and efficiency by reducing the probability of knock. It provided total funding of 1.6 million EURO, and took place from 2003 to 2006.

## Acknowledgements

---

### ***Direct financers:***

#### **Volkswagen AG**

[www.volkswagen.com](http://www.volkswagen.com)

The Volkswagen group consists of several brands producing a total of 5.7 million vehicles annually.

#### **CD-adapco**

[www.cd-adapco.com](http://www.cd-adapco.com)

CD-adapco is a global provider of engineering simulation (CAE) solutions for fluid flow, heat transfer and stress.

#### **Diganars**

[www.diganars.com](http://www.diganars.com)

Providers of the DARS software suite.

#### **LOGE AB**

[www.loge.se](http://www.loge.se)

Loge develops software for simulation of the chemical systems.

## List of Publications

The contents of the thesis are in part based on work reported only in the projects GIHR, KCFP and MinKnock or in work reported directly to specific clients. This work was either carried out by the author independently or was reported in the following papers, with the author's contribution listed:

*Tunér, M., Blurock, E. S., Mauss, F., "Phase Optimized Skeleton Mechanisms for Stochastic Reactor Models for Engine Simulation", SAE 2005-01-3813.*

The author developed, programmed and prepared most of the models, ran all of the calculations and wrote most of the paper, also presenting the results at the 2005 SAE Powertrain & Fluid Systems Conference. The results are taken up in section 6.2 (Investigation 1).

*Amnéus, P., Tunér, M., Mauss, F., Collin, R., Nygren, J., Richter, M., Aldén, M., Kraft, M., Bhawe, A., Hildingsson, L., Johansson, B., "Formaldehyde and Hydroxyl Radicals in an HCCI Engine - Calculations and LIF-Measurements", SAE 2007-01-0049.*

The author developed, programmed and prepared the models, ran some of the calculations and wrote parts of the paper, also presenting the results at the 2007 SAE Fuels and Emissions Conference. The results are presented in section 5.2 of the thesis.

*Tunér, M., Pasternak, M., Bensler, H., Mauss, F., "A PDF-Based Model for Full Cycle Simulation of Direct Injected Engines", accepted for publication by the 2008 SAE International Powertrains, Fuels and Lubricants Congress.*

The author did essentially all the work except for the calculations. The results are presented in chapter 7 of the thesis.

During the PhD work the author supervised the following M.Sc. and B.Sc. works:

*Hung, N., Trajkovski, K., "Implementation of kinetic algorithms on a hardware emulator". M.Sc. Thesis, Lund University, 2005.*

This is a study of how the algorithms needed to solve the kinetics in the SRM code can be changed to permit the efficient implementation of them in an FPGA. Simulation using a virtual prototype suggested that performance in solving the chemistry could be improved by a factor 900, as compared with the standard solver in use today. The study is not included in this PhD thesis.

## List of Publications

---

*Andersson, R., "Systematic Testing and Validation of Simulation Programs for Combustion Processes". M.Sc. Thesis, Lund University, 2007.*

This is an exhaustive study of how to validate and test the Combustion Simulation software, as the SRM developed at LOGE. The study aims at finding strategies for developing accurate and robust models in Fortran and Java programming. The issues taken up relate to the demands placed on commercial codes as compared with research codes, which generally lack the robustness and generality needed commercially. Although the subject is an important and interesting one, it is primarily related to programming techniques rather than to research on combustion simulation, it is for this reason not being included in the thesis.

*Karlsson, M., "The Influence of microscale inhomogeneties on the combustion process in an HCCI engine". B.Sc. Thesis, Lund University, 2007.*

This work is directly related to the HCCI-SRM and the results are presented in section 5.1 of the thesis. The author contribution is the planning and organization of the work, the development, programming and preparing of the models, but also the analyzing and the concluding of the results.

*Borg, A., "The optimization of a laminar premixed flame solver". M.Sc. Thesis, Lund University, 2008.*

This is a study of whether use of higher accuracy diffusion coefficients can decrease the number of Jacobian calculations needed in the numerical solver, in order to reduce calculation times. The method was successfully implemented, small reductions in calculation times being achieved. Since this work has little to do with the SRM work carried on in the thesis, it is not included there.



## Nomenclature

### 1. Symbols

$a$	Area [m <sup>2</sup> ]
$B$	Cylinder bore [m]
$c_p$	Specific heat at constant pressure [J kg <sup>-1</sup> K <sup>-1</sup> ]
$C_d$	Valve flow discharge coefficient -
$E$	Energy transported into a zone [J]
$F/A$	Fuel-air ratio -
$H$	Mass specific enthalpy [J kg <sup>-1</sup> ]
$h_c$	Heat transfer coefficient [W m <sup>-2</sup> K <sup>-1</sup> ]
$H$	Molar specific enthalpy [J kmole <sup>-1</sup> ]
$k$	Constant in the Woschni equation -
$M$	Molar weight [kg kmole <sup>-1</sup> ]
$m$	Mass [kg]
$N$	Crankshaft rotational speed [rev s <sup>-1</sup> ]
$nm$	Number of soot moments -
$p$	Pressure [Pa]
$Pr$	Prandtl number -
$QLHV$	Lower heating value [J kg <sup>-1</sup> ]
$Q_{loss}$	Heat loss [J]
$Q_i$	Source/ sink term for the variable $i$
$\Psi$	[kmole s <sup>-1</sup> ]
$rc$	Compression ratio -
$Sp$	Mean piston speed [m s <sup>-1</sup> ]
$T$	Temperature [K]
$t$	Time [s]
$\mathbf{u}$	Velocity field vector [m s <sup>-1</sup> ]
$U_{eff}$	Effective velocity outside boundary layer [m s <sup>-1</sup> ]
$V$	Cylinder volume [m <sup>3</sup> ]
$W$	Work [J]
$\mathbf{x}$	Vector of spatial coordinate [m]
$x_b$	Burned mass fraction -
$Y$	Mass fraction -

### 2. Greek Symbols

$\alpha$	Heat transfer coefficient [W K <sup>-1</sup> m <sup>-2</sup> ]
$c\alpha$	Convection heat transfer coefficient [W K <sup>-1</sup> m <sup>-2</sup> ]
$P\alpha$	Plank radiation coefficient [m <sup>-1</sup> ]
$\gamma$	Specific heat ratio -
$\varepsilon$	Emissivity coefficient -

# Nomenclature

---

$\eta$	Efficiency of engine -
$\nu \eta$	Volumetric efficiency -
$\theta$	Crank angle [degree]
$\lambda$	Air-fuel equivalence ratio -
$\rho$	Density [kg m-3]
$\sigma$	Stefan – Boltzmann constant [W m-2 K-4]
$\nu$	Net stoichiometric coefficient -
$\psi$	Realization (sample space) variable -
$\varphi$	Vector of random variable -
$\omega$	Global reaction rate [kmole m-3 s-1]
$\tau$	Characteristic time for mixing [s]

## 3. Subscripts

amb	Ambient conditions
b	Burned gas
f	Flame
fg	Fresh gas conditions
I	Species
loss	Heat loss
r	Chemical reactions
total	Total
u	Unburned
v	Valve
ve	Valve exiting flow
vi	Valve inflow
w	Wall
z	Zone (used if an expression is valid for both burned and unburned zone)
1	High pressure side
2	Low pressure side

## 4. Abbreviations

CAD	Crank Angle Degree
C/D	Coalescence dispersal
CFD	Computational Fluid Dynamics
EGR	Exhaust Gas Recycling
EVC	Exhaust Valve Closure
EVO	Exhaust Valve Opening
EST	Engine Simulation Tool
HCCI	Homogeneous Charge Compression Ignition
IEM	Interaction by exchange with the mean
IVC	Inlet Valve Closure

# Stochastic Reactor Models for Engine Simulations

---

IVO	Inlet Valve Opening
LHV	Lower Heating Value
NTC	Negative Temperature Coefficient
ODE	Ordinary Differential Equation
PaSPFR	Partially Stirred Plug Flow Reactor
PDF	Probability Density Function
MDF	Mass Density Function
PFR	Plug Flow Reactor
PSR	Perfectly Stirred Reactor
RPM	Revolutions Per Minute
SI	Spark Ignition
SRM	Stochastic Reactor Model
TDC	Top Dead Center

# Contents

Abstract .....	i
Acknowledgements .....	iii
List of Publications .....	vi
Nomenclature .....	viii
<b>1 Introduction.....</b>	<b>1</b>
1.1 Background .....	1
1.2 Motivation .....	8
1.3 Objectives.....	8
1.4 Outline of the work .....	10
<b>2 Different Engine Types and Their Principles .....</b>	<b>13</b>
2.1 The SI engine.....	13
2.2 The CI engine .....	14
2.3 The HCCI engine.....	15
2.4 DI engines.....	16
2.5 HCCIDISIDICI engine.....	16
<b>3 Chemical Modeling.....</b>	<b>17</b>
3.1 Reduced Chemical Models.....	19
3.1.1 <i>Lumping</i> .....	21
3.1.2 <i>Skeletal Mechanism</i> .....	22
3.1.3 <i>The QSSA</i> .....	23
<b>4 Physical Modeling.....</b>	<b>25</b>
4.1 The Homogeneous Reactor Model (HRM).....	26
4.2 The Stochastic Reactor Model (SRM) .....	28
4.2.1 <i>Operator splitting and numerical solution</i> .....	31
4.2.2 <i>Piston movement</i> .....	34
4.2.3 <i>Mixing</i> .....	34
4.2.4 <i>Chemical reaction</i> .....	39

# Stochastic Reactor Models for Engine Simulations

---

4.2.5 Heat transfer.....	39
<b>5 The HCCI-SRM.....</b>	<b>41</b>
5.1 Effects of modeling parameters and discretization on the HCCI-SRM.....	41
5.1.1 The range of cycle-to-cycle variations in HCCI-SRM.....	44
5.1.2 Effects of modeling parameters that affect mixing and heat transfer.....	49
5.1.3 Effects of discretization; time step size and number of particles.....	59
5.2 Formaldehyde and hydroxyl in HCCI combustion.....	73
5.2.1 Introduction.....	73
5.2.2 Engine configuration and experimental procedures.....	74
5.2.3 Chemical model used.....	79
5.2.4 Results and discussion.....	79
5.2.5 Conclusions.....	89
5.3 Modeling and investigation of Exothermic Centers in HCCI-combustion.....	91
5.3.1 Introduction.....	91
5.3.2 Experiment.....	92
5.3.3 Calculation and results.....	93
5.3.4 Conclusions.....	102
5.4 Coupling to GT-Power.....	103
<b>6 The Two Zone SI-SRM.....</b>	<b>107</b>
6.1 Flame propagation model.....	107
6.2 Phase Optimized Skeletal Models.....	109
6.2.1 Introduction.....	109
6.2.2 The POSM strategy.....	110
6.2.3 Investigation 1.....	115
6.2.4 Investigation 2.....	123
6.2.5 Analysis of the calculation with POSM.....	127
6.2.6 Investigation 3.....	130
6.2.7 Conclusions.....	133
<b>7 The DI-SRM.....</b>	<b>135</b>
7.1 Introduction.....	135
7.2 Direct injection model.....	136
7.3 Coupling to Wave.....	142

7.4 Validation of DI-SRM coupled to a 1-D-EST .....	146
7.5 Conclusions.....	154
<b>8 Modeling of HCCI-NVO engines .....</b>	<b>157</b>
8.1 Modeling approaches.....	158
8.2 Direct injection model.....	159
8.3 Reactor Network.....	159
8.4 Validation .....	161
8.5 Peculiarities of NVO engines. Modeling and chemistry issues. ....	162
<b>9 Conclusions .....</b>	<b>165</b>
<b>References .....</b>	<b>169</b>



## 1 Introduction

Stochastic reactor models for engine simulations, what does that mean? If one consults Wikipedia, one finds the following: *Stochastic*, comes from the Greek word stocos which means “a guess”. A *reactor* is a device which uses atomic energy to produce heat. A *model* is an abstraction or a simplification of a real object. An *engine* is something that produces an output effect from a given input, and a *simulation* is an imitation of a real thing, state of affairs or process.

So a stochastic reactor model for engine simulation is merely a simple guess of atomic heat produced with an imitated output?

And one guess is as good as any?

Probably not, an educated guess is surely a better one...as will be shown...

### 1.1 Background

In a perfect world, one would have an endless amount of energy without any costs, pollution or other setbacks. This is not reality, however. Still, the majority of our energy needs are fulfilled by hydrocarbon combustion, involving mainly use of fossil fuels. Combustion is one of the most important keys to the enormous progress and development of humankind. But there are not only positive consequences.

Although on a day to day basis, most people are probably more concerned with the direct impact of costs related to the heating of their homes, to transportation and to cooking, than with more far-ranging energy problems that are far more serious. With the use of combustion come the problem of emissions that result in pollution, poisoning and global warming, as well as erosion and the creation of wastelands through the extracting and harvesting of fuels, and even wars.

Important steps must be taken to counteract this, no doubt, and should include measures to increase the efficiency of combustion and to find alternative energy sources. Research in the fields of combustion and of engines is clearly very important here, particularly since there is a lack of practical and for most people economically sound alternatives.

Today, the focus is very much on the issue of global warming (Figure 1.1). According to most scientists, the greenhouse gases (GHG), generate this phenomenon, CO<sub>2</sub> having been pointed out as being a key species involved.



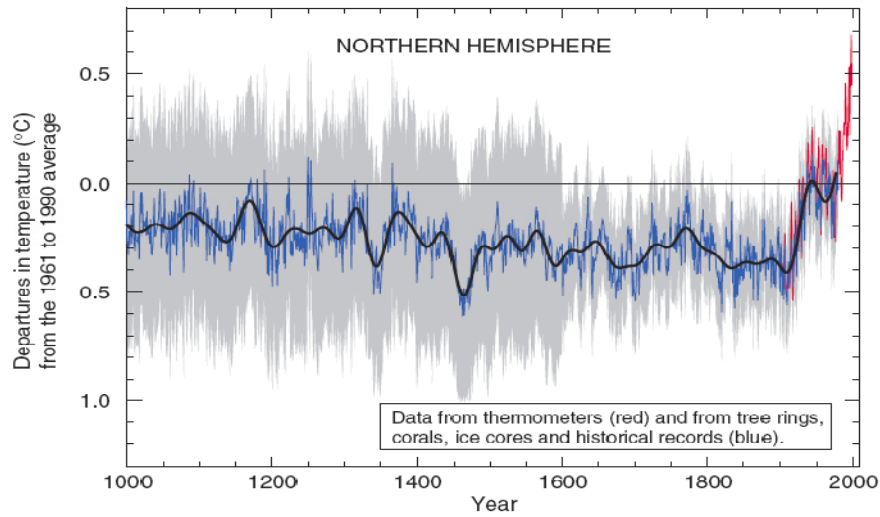


**Figure 1.1** Temperature variations the last millennium [1]

GHG attributed from human activity come from a variety of sources, such as land use, agriculture and above all energy production. Combustion is the major contributor to “human” GHG, combustion engines producing some 14 % of them [2]. The dominant GHG species contributing to global warming is actually water vapor,  $H_2O$ , but since its concentration is controlled directly by the temperature of the atmosphere rather than by human activity, it will not be taken up here further. The other major GHGs in order of importance are carbon dioxide ( $CO_2$ ), methane ( $CH_4$ ) and nitrous oxide ( $N_2O$ ).

The consequences of higher global levels of  $CO_2$  and the global warming it contributes to are discussed in the Stern Report [3]. There is no doubt that actions need to be taken to counteract such a scenario.

$CO_2$ , carbon dioxide, is produced by combustion when a fuel that contains carbon is involved. For combustion in engines a simplified and general combustion formula can be used, where the hydrocarbon fuel can be gasoline, diesel, kerosene, methane, and ethanol and so on. The fuel is burned with air constituting of mainly  $O_2$  and  $N_2$ . This results in work, but also in exhaust gases as  $CO_2$ ,  $H_2O$  and  $N_2$  being produced. The amount of  $CO_2$  produced is related to the amount of carbon atoms the fuel contains. The more efficiently the fuel burns, the higher the amount of  $CO_2$  is produced, until complete combustion is reached. However, in relation to the work produced, efficient combustion reduces the amounts of  $CO_2$  produced.

## Chapter 1 Introduction

---

$$C_a H_b O_c + \left(a + \frac{b}{4} - \frac{c}{2}\right) (O_2 + 3.76 N_2) \rightarrow work + a CO_2 + \frac{b}{2} H_2O + \left(a + \frac{b}{4} - \frac{c}{2}\right) 3.76 N_2 \quad (1.1)$$

This fundamental formula applies to log fires, as well as to any other combustion of hydrocarbon fuels with air. Since combustion is so closely related to human activities one can easily follow human development by looking at the levels of  $CO_2$  found in the atmosphere (Figure 1.2).

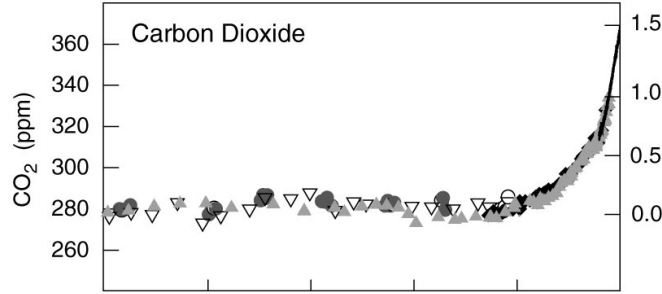


**Figure 1.2** Levels of  $CO_2$  in the atmosphere the last 1000 years [4].

So, what can be done to reduce  $CO_2$ ?

Since the production of  $CO_2$  is a direct and basically proportional consequence of the combustion of fossil fuels, one option would be to limit combustion of this type and to rely on other sources of energy. But since fossil fuels are so cheap and will probably still be available for another 50 years in the case of oil and for hundreds of years in the case of coal, the alternatives are either too expensive or too unpractical that, energy production through combustion of fossil fuels will probably continue to play a major role for many decades to come. In fact, in the emerging economies in the world, new coal power plants are opened every week. Since the combustion of fossil fuels is likely to continue for many years, strong efforts need to be made to achieve much more efficient energy production and energy usage and also possibly combined with active aftertreatment to reduce the emissions that are produced.

Energy conversion efficiency is generally very low (Figure 1.3). It is possibly here where the greatest potential for improvement is found. Nevertheless, the efficiency of combustion itself and the energy production systems, also have the potential for being improved considerably. The efficiency of combustion engines, which is of more direct interest in the present work, is in practical use in the range of 10 - 55%, where the main losses can be attributed to heat losses (Figure 1.4).

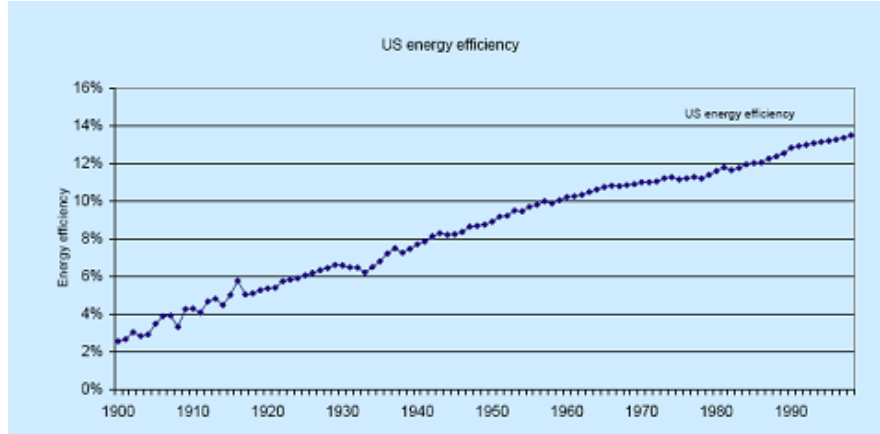


**Figure 1.3** Energy conversion efficiencies in USA, 1900-1998 [3].

Another way of decreasing the  $\text{CO}_2$  produced by combustion is to use biofuels or hydrogen as fuels. In the case of biofuels,  $\text{CO}_2$  is still produced, but the idea is that it is supposed to be “neutral” in the sense that the  $\text{CO}_2$  is all consumed to create the biomass used as fuel. However the reduction of  $\text{CO}_2$  when using biofuels or hydrogen has still to be realized due to the amount of energy needed for the production of these fuels.

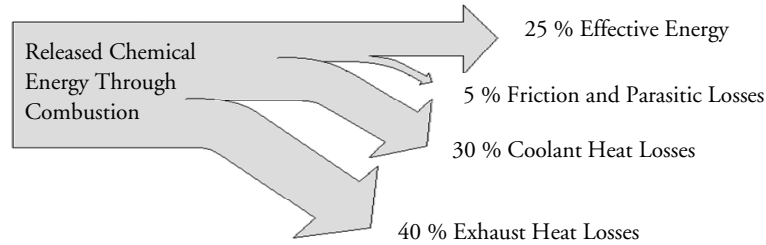


**Figure 1.4** Typical energy diagram for a Gasoline Internal Combustion Engine.

GHGs are not the only problem related to combustion. The reduction of emissions like  $\text{NO}_x$ , soot, hydrocarbons and sulfur oxides and many others has for long been on the agenda of engineers and researchers of combustion devices.

**$\text{NO}_x$**  is poisonous and contributes to the smog problem.  $\text{NO}_x$  is a group of species ( $\text{NO}$ ,  $\text{NO}_2$ ,  $\text{NO}_3$  and  $\text{N}_2\text{O}$ ) emitted in practical combustion.  $\text{NO}_x$  has quite successfully been treated by aftertreatment.

# Chapter 1 Introduction

**Soot** is a particulate matter (PM) that consists mainly of coal (C) covered with hydrocarbons. The particles are cancerogenic. The treatment consists mainly of combustion strategies minimizing the production of soot or by aftertreatment with for example particulate filters.

**Hydrocarbons** is a term referring to a collective (>100) of species which are not completely oxidized to  $\text{CO}_2$  and  $\text{H}_2\text{O}$  during combustion. These species can be poisonous and do also contribute to acidification. The production and presence of hydrocarbons is a sign of inefficient combustion, and is mostly dealt with, with more efficient engines and through after-treatment by use of catalytic converters.

**Sulfur oxides** contribute markedly to acidification by forming sulfuric acid when reacting with atmospheric water and oxygen. It has for long been regulated by minimizing the amount of sulfur in the fuel for land going vehicles. In shipping and energy production rules are not as strict.

For land going vehicles with combustion engines, regulations have been enforced for more than 40 years. In some countries and regions earlier and more stringent, while in others later or to a lesser extent. Today there is a plethora of rules applying to different regions and countries and to different engine types as well as to different vehicle types, not to mention related to emissions of different species as well. Figures 1.5-1.6 show the evolution of regulations for  $\text{NO}_x$  and PM emissions for petrol and diesel fuelled passenger cars respectively, within the European Union.

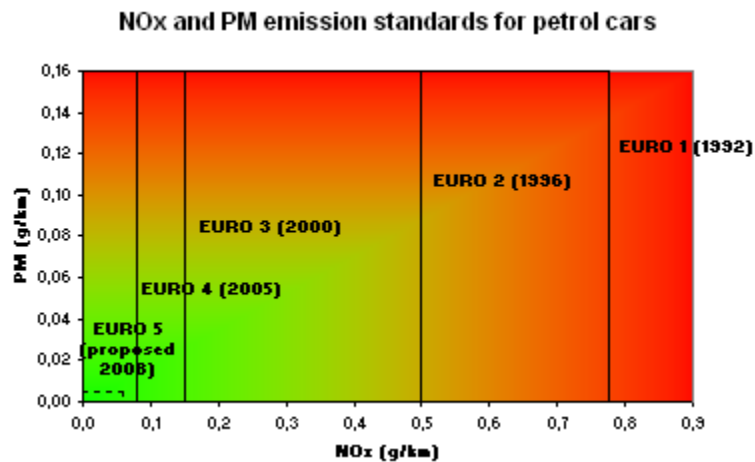


*Figure 1.5 NO<sub>x</sub> and PM emission standards for petrol cars, within EU [5].*

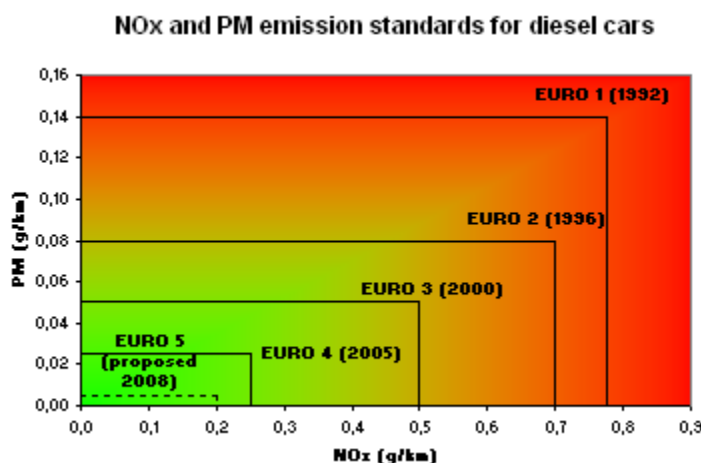


*Figure 1.6 NOx and PM emission standards for diesel cars, within EU [5].*

For trucks, often referred to as heavy duty vehicles (HD), as well as buses, tractors and other vehicles, other rules apply. Fortunately enough, most of these rules develop towards similar levels so that the manufacturers still can produce vehicles that comply with most of them at the same time. The differences in rules reflect partly the conscientiousness and ambitions and the level of development of the societies. It is good to see that evolving economies, such as India have higher ambitions in this respect than some of the more traditional economies do.

Most emissions can be minimized by optimizing the combustion systems, and indeed there has been much work and research done in this area. If one compares the performance of a present-day engine with that of one manufactured 20 years ago, the improvement is massive. Yet there is still very much that can be done. Development tends to follow paths of either known or guessed ways of improvement, in a steady fashion with the available allocated resources. I have always been amazed by the powers of man to manage to solve difficult and complex problems. The downside of our beings, in this respect, is that when thinking that things are working well enough, they are often left as they are, or when others say there is problem one rather fight against those than work together to solve the problem. It seems, in fact, that the saying “Crises is the mother of all inventions” is very true. If there is political will to put harsher rules I am perfectly convinced that we would manage to solve the technical issues needed to reach them.

Since real emissions come from real engines, research has always used real experiments for testing and development purposes. For sure there has always been an element of thinking and calculating along the development process. However, modern simulations capture centuries of knowledge into models and with the advances in knowledge and development of highly effective computers this can be used very efficiently indeed. Instead of doing real tests

## Chapter 1 Introduction

which can be complicated, time consuming, expensive and sometimes dangerous, it is possible to carry out the experiments with computers. Simulations are a powerful complement to experiments using real engines. In fact with the increasing understanding of the underlying physics and chemistry and with the use of increasingly powerful computers to support the investigations, simulations are becoming more and more a part of the regular development of engines. In addition, many questions that cannot be investigated experimentally can be answered with reasonable accuracy by simulations.

Research on combustion engines is both very important and very active today. The automotive sector has a major contribution to the emissions produced, and since the number of vehicles is increasing, thanks to the better conditions of life for people generally and the growth of the newer economies in the world, emissions can be expected to increase unless engine development is able to counteract this. It also appears that engine development in the automotive sector has a leading role, possible because the exhaust pipes (and the exhausts effects) being so close to people compared to the high chimneys of energy production or the chimneys of the ships on the oceans (a Swedish writer once suggested half jokingly that the exhaust pipes of vehicles should be placed at the front, so as to speed up development). It is important that research in this sector continues to be a priority and also that the scientific advances achieved be transferred rapidly to the energy production sector, where global gains can be realized much more effectively (Figure 1.7). Transfer of technology and knowledge transfer in the combustion community is vital, but need also to be encouraged by efficient political decisions.

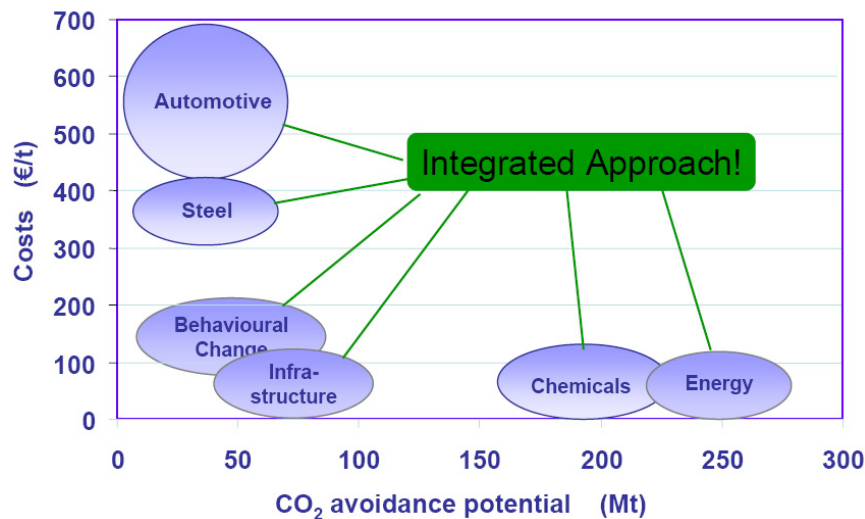


**Figure 1.7** Cost versus CO<sub>2</sub> avoidance potential [4]. According to the figure reduction of CO<sub>2</sub> is almost 10 times more expensive in the automotive sector compared with the energy sector.

## 1.2 Motivation

Engines and vehicles which I have always had a deep devotion and interest in, are a personal matter for me. I am at times reminded by my father that the first word I could speak was not “pappa” or “mamma” but “bil” (car) and that long before that I imitated the sound of engines. During childhood I learned how to disassemble (and eventually to assemble) engines. The latter evolved to the point of where I would build my own racing engines and racing cars and manufacture myself most of the parts that were needed. The practical issues were increasingly matched and prepared by reading all available theory. Knowing the theory and driven towards optimization of the physical problems, lead to the development of whole suite of simulation programs to analyze and optimize as various things as; crankshafts systems, camshaft and valvetrain, coil- rocker and damper systems, chassis and suspension systems (used for example by the Lund University Formula Student team). Whenever needed for the manufacturing and the design of something complex it would usually start by the creation of optimizing software. The most advanced of these programs is a 1-D full engine simulation tool [6], which was the result of my master thesis work at Lund University. During these studies I came in contact with the Division of Combustion Physics and with Professor Fabian Mauss there. When the possibility was given, it felt natural at specializing in the combustion modeling of engines. For me the love of engines as well as the love for life is the strongest motivators.

The work presented here is about the modeling of combustion in engines. It relates to the latest Stochastic Reactor Models, SRMs, their development and their ability and performance in modeling combustion in a wide range of engine types. The work presented in the thesis is also about how to make such tools practical to use and the development of coupling to commercial tools.

The SRM’s are a balance between detailed calculations for engine performance and emissions, and the time needed for the calculations. So perhaps they are one of the most important tools of today for the development of clean and efficient engines.

## 1.3 Objectives

Ideally, computer models should be able to answer all possible questions and show all the properties for an engines performance already during its development, and helping in designing the perfect engine. This is not the case though. There are limitations to the physical understanding of engine processes (especially of the combustion process) as well as to the ability of computers in terms of their calculating power and memory resources. This has limited investigators and developers to the use of simplified models. The limitations involved also mean that there is a tradeoff between the complexity of a computer model and its execution time. For engine developers, there is the choice of either running many cases with use of simpler models, or running fewer cases with more complex models. The choices

# Chapter 1 Introduction

---

also relates to the possibility to validate the calculation with experiments because no models yet are good enough to be fully predictive. The available models of today range from very simple deterministic ones to complex multidimensional full engine models.

For the developer and researcher of engine simulation tools the objectives are to develop models that have the ability to provide the engine developers with vital information which is predictive, accurate and easy to understand and correlate. To be of practical use, the models also need to be easy to use and fast in their execution so that exhaustive studies can be made to predict all possible operating conditions of an engine.

The SRMs have emerged as an attractive approach to engine simulations, attractive in the sense that they have promise of providing useful predictions of the combustion processes in an engine, with high levels of detail and accuracy, at the same time as they are fast and easy to use. The objectives of the present work were as follows:

- The further development of practical engine simulation models based on SRMs for HCCI, SI and DICI engines.
- The development of couplings for the SRMs to commercial 1-D engine simulation tools.
- Investigation of the performance of a novel direct injection model for the SRMs.
- The development of the SRMs to be applied to modeling NVO engines with or without coupling to commercial 1-D engine simulation tools.
- Studying the validity of the SRMs to simulate different engine types as HCCI, SI, and DICI.
- Studying the effects of the assumptions and modeling parameters contained in the SRMs.
- Determining the execution times and investigating an alternative approach to speed up the calculations.



## 1.4 Outline of the work

The different models, tools and interfaces developed and reported in the thesis are all integrated in commercial tools the author has developed. DARS-ESSA is a self sustained interface through which different reactor models can be operated (Figure 1.7). DARS-ESM contains DARS-ESSA but has the additional capability of being coupled to a number of other commercial codes.

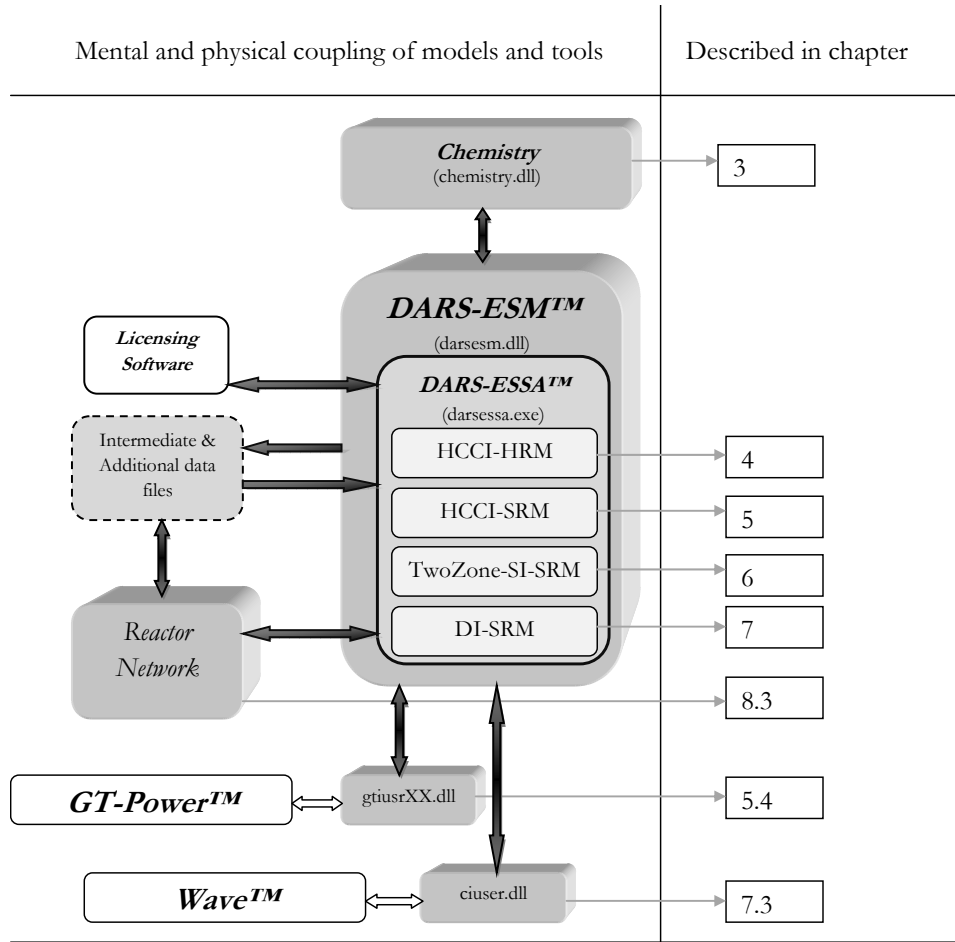


**Figure 1.7** Outline of the thesis. The gray boxes represent developments by the author.

# Chapter 1 Introduction

---

The subject of modeling engine combustion involves many different scientific fields as chemistry, physics, mathematics, informatics and engineering. All these fields needed to be covered by the research group where this work was performed. The different fields are all covered in this thesis although some more in depth.

The thesis can be divided into three parts.

- **Introduction:** Chapter 1.
- **Theory:** Chapters 2, 3 and 4.
- **Investigations and results:** Chapter 5 to 9.

Since the work relates to the simulation of engines, an account of the basic principles of the modern internal combustion engines is provided in **Chapter 2**.

**Chapter 3** is an overview of chemical modeling and how chemical kinetics is employed in Stochastic Reactor Models. It also demonstrates common techniques that are used to simplify chemical models to make them practical for use in engine simulations. This is of particular interest in a novel approach involving adaptive chemistry used and demonstrated later in the thesis.

**Chapter 4** describes the theory behind the Stochastic Reactor Models and their practical implementation.

Comprehensive studies of the practical implementation of the HCCI-SRM, demonstrating its ability to predict individual species and temperature distributions, and also the effect of the modeling parameters based on the SRMs simplifications, can be found in **Chapter 5**.

**Chapter 6** demonstrates how adaptive chemistry can be used to speed up the calculations in a specifically implemented two zone SRM applicable to SI engines.

A novel direct injection model is studied in **Chapter 7** and issues related to the modeling of NVO engines are discussed in **Chapter 8**.

**Chapter 9** presents the conclusions from this work.

Figure 1.7, contains a picture of the connection of all the described models, and in which chapters and sections the detailed descriptions can be found.



### 2 Different Engine Types and Their Principles

This work relates to the simulation of engines. Or more precisely, the simulation of the combustion process in the most common piston engines with internal combustion. This means that this work does not include engines like gasturbines and Wankel type engines (no piston) nor Stirling and steam engines (external combustion) or other types of combustion engines. Many of the approaches described would be perfectly valid for those engines as well, though, with some minor changes and additions.

Why are there different engine types?

People might not think of it, but one very important reason why there are both SI and CI engines is the fact that when oil is cracked several different fractions are produced. The largest fraction is in general diesel, and then comes gasoline and the smallest fraction is kerosene. If one could produce diesel at the expense of gasoline, possibly, there would only be CI engines in use. But since gasoline is produced, it is a pretty strong motivator to also have SI engines and use it.

*Early US refineries processed crude oil to recover the kerosene. Other products (like gasoline) were considered wastes and were often dumped directly into the nearest river [7].*

One important thing to remember, and being the sole reason for the kind of work in this theses is:

A combustion engine is a device that converts chemical energy into motion.

#### 2.1 The SI engine

The engine that most people think of in connection with the word “engine” is most likely the SI engine. SI stands for “Spark Ignition” and is more a group of engines rather than one single engine type. For instance the common gasoline or petrol engine that one have in cars, motorcycles, mopeds, chainsaws and gardening equipment are SI engines. It is a group of engines that in relative terms are simple, lightweight, cheap to produce and very simple to use and regulate. Indeed a very flexible engine. The main disadvantage of SI engines is a relatively lower efficiency which limits their use to consumer products where price and flexibility has high priority.

The nomination SI or Spark Ignition relates to the combustion in the engine and says very little about the engines other properties. It has been presented in many different shapes and

# Stochastic Reactor Models for Engine Simulations

---

principles during history and a wide variety still exist. For instance, the 2-stroke SI engine, which is the simplest SI engine and the most produced combustion engine of any kind. Simple, with high power to weight ratio and extremely low price it is commonly used for mopeds, chainsaws and other small engine applications. Its rather low efficiency and high HC-emissions has limited its use to that category of small engines.

The 4-stroke SI engine, also known as the Otto engine, has for many years been the favorite for regular passenger cars, small aircraft, boats, motorcycles, lawnmowers and more. Being the master of compromise, it has reasonable efficiency, power to weight ratio and level of complexity combined with an attractive production cost and options for very low emissions.

As mentioned, the term SI relates to the combustion principle of the engine. Inside the combustion chamber, when the conditions for combustion are met, meaning that fuel, oxidizer and residual gases ratios, as well as pressure and temperature are favorable, combustion is started by the spark from the spark plug. The combustion commences through a flame front moving through the combustion chamber until all the fuel or the oxidizer is consumed or the flame front is quenched, typically by the cooler combustion chamber walls.

## 2.2 The CI engine

For more professional use in terms of continues running and heavy loads, fuel costs or in other words engine efficiency, becomes a more critical issue. For these applications the CI engine or the “Compression Ignition” engine, and typically what is often referred to the diesel engine is used. Just as for the SI engine the name CI engine relates to the combustion process of the engine and similarly there are several different types of CI engines. Most common is the 4-stroke CI engine used in trucks, busses, cars, boats, ships, trains, power stations and so on.

Often described as diesel engines from the fuel they are often used with, and ultimately from the name of the inventor of the CI engines, Rudolf Diesel, they can in fact be used with a number of liquid and gaseous fuels. High in efficiency, flexible, durable but also quite expensive has meant that these engines has been the choice for semiprofessional or professional use. In the extreme end of professional use and demand for efficiency comes the range of big 2-stroke CI engines which are used in large ships and power stations. The peculiarities of their applications with steady state running, energy recovering systems but also from their sheer size and complicated production, makes almost every single engine of this kind a type in themselves. As for all CI engines they share the drawbacks and concerns for emissions like soot and NO<sub>x</sub>.

The CI engine combustion does not use any external source, like spark plugs, for initiating the combustion. The typical CI process is to compress the oxidizer within the combustion

chamber to reach a suitable pressure and temperature and then inject the fuel which will start to burn as soon as it has mixed with the oxidizer to reach an ignitable mixture. The combustion continues as long as there is fuel injected. For the CI engine, mixing processes and fuel spray formation (for liquid fuels) are very much the heart of the matter.

### 2.3 The HCCI engine

Although the process of HCCI has been around for as long as internal combustion engines, as both a wanted and unwanted effect, and also partly understood for long, it was more clearly explained by Onishi 1979 and has been considered as a future option the latest 10 or so years. The name HCCI, “Homogeneous Charge Compression Ignition” relates to the ambition of creating an engine using this principle. Just as for SI and CI engines the name relates to the combustion process and just the same the HCCI engine can be of several types and configurations, such as 2-stroke and 4-stroke.

The basic idea behind the HCCI engine is that the ignitable mixture of fuel and oxidizer is prepared and mixed in advance as in the SI engine but that the combustion starts as a consequence of temperature and pressure rise created by compression, reminding about the CI engine. Strictly speaking, it is quite far from the CI engine, and the ignition process is determined by what is known as chemical kinetics. Since the charge is homogenous the combustion takes place everywhere simultaneously within the combustion chamber. It does not contain any flame front, but the fuel rather goes through a low temperature oxidation. This is the key to the advantage of the HCCI. Low temperature combustion leads to lower emissions of NO<sub>x</sub> (nitrous oxides) and lower amounts of heat losses, which lead to high efficiency. The reasons that pure HCCI engines are not commonplace are mainly twofold: they are not as flexible as the SI and CI engines in terms of regulation when one wants to change the speed or the load; and they are not that easy to run with the high loads reached by similar sized SI or CI engines. The reason for these drawbacks is related to the combustion process. Since all the fuel is present in the combustion chamber and supposed to burn simultaneously, there is a limitation to how much fuel there can be, or the combustion becomes too fast and violent. Too fast and violent in this case means noisy, which is unacceptable in commercial applications, or destructive which is even worse and certainly unacceptable in commercial applications. Issues of HC emissions have also been a concern.

Fundamentally the concept of HCCI has many advantages and it is also used already in several applications combining it with either SI or CI approaches. Those approached will be discussed later on.

## 2.4 DI engines

First it should be made clear that a DI engine is not an alternative to a SI, CI or HCCI engine. It is merely an addition. In fact DI or “Direct Injection” relates to the means of providing fuel to the combustion chamber. So there can be SI engines with DI (DISI) or without DI, although traditionally SI engines would seldom be direct injected. Direct injection in SI engines should not be confused with injected SI engines which actually refers to indirect injection and is very common for SI engines.

Modern CI engines are almost always DI engines, although some prechamber designs still exist. Although not referred to as DI the prechamber designs pretty much work as DI engines. For HCCI engines the basic principle of “homogenous charge” implies that fuel/oxidizer mixture is prepared and mixed outside the combustion chamber. This means that pure HCCI engines are usually not of the DI type.

## 2.5 HCCIDISIDICI engine

The rules are changing and the development is towards engines that are capable of multiple combustion strategies or modes of operation. One of the early approaches around the HCCI engine is the pHCCI, “partial HCCI”, engine that has both indirect injection (normal HCCI) and early direct injection (pHCCI). The word early here has great significance, since the timing of the injection decides whether the combustion will be of HCCI or CI type.

Very early DI means that the fuel and oxidizer has a relatively long time to mix and create a homogeneous mixture needed for pure HCCI combustion. Medium early DI means that the fuel and oxidizer has a short time to mix and create a homogeneous mixture needed for pure HCCI combustion, but has the advantage of realizing a local island of mixture that is not in contact with the combustion chamber walls. This minimizes quenching and HC emissions. The later the injection becomes, the more CI like the combustion becomes, with its advantages and disadvantages. In effect, with precise DI strategies one can have both HCCI and CI in the same engine.

The current research is focused on investigating the combination of different approaches to be able to create efficient, clean and practical engines. Some of the approaches are PPC (Partially Premixed Combustion) [8] and SACI (Spark Assisted Compression Ignition) [9] both in the borderland of HCCI, SI and CI (and using DI of course).

### 3 Chemical Modeling

Chemical kinetics is the study of reaction rates of different species in chemical processes. It is one of the fundamentals behind and necessary for this work and the provider to determine and describe the factors important not only in combustion, but also in food decomposition, the hardening of dental materials, the reproduction of micro-organisms, the speed at which stratospheric ozone is destroyed, and how the enzymes influence chemical processes in biological systems.

Combined with thermodynamics the reaction rates from chemical kinetics can be used to determine the extent to which reactions occur. According to the collision theory of chemical reaction, concentration plays an important role since molecules must collide in order to react and form new species. The collision theory is straight forward: as the concentration of the reactants increases, the frequency of reactions increases as well. The main factors that influence the reaction rate include: the physical state of the reactants, the concentrations of the reactants, the temperature at which the reaction occurs, and whether or not any catalysts are present in the reaction.

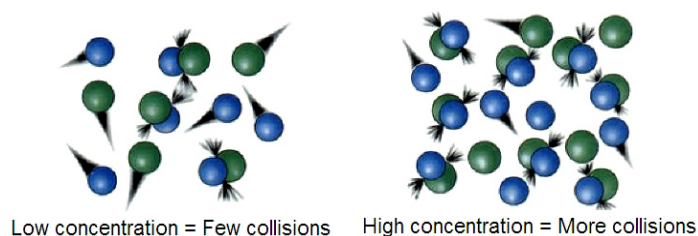


**Figure 3.1** Collision theory.

The chemical model can be thought of as a map, describing the different reaction rates between the different species. For a typical reaction between atomic or molecular species  $A + B \rightarrow C$  the rate  $r$  is given in its simplest form by:

$$r = k(T)[A]^m[B]^n \quad (3.1)$$

where  $m$  and  $n$  are the stoichiometric coefficients, representing the degree of consumption or formation for each species involved in the reaction. For each reaction the reaction rate coefficient  $k$  is given by the Arrhenius equation:

$$k = A \cdot e^{-E/(RT)} \quad (3.2)$$



## Stochastic Reactor Models for Engine Simulations

The preexponential factor  $A$  is related to the physical properties of the reaction: molecular sizes, angular effects, average molecular speeds, etc.  $E$  is the activation energy, the energy needed to break up the molecular bonds.  $R$  is the gas constant and  $T$  the temperature. Often the temperature dependence of the preexponential factor in Equation 3.2 is expressed individually with the modified Arrhenius equation. In the present work and for a system of reactions  $r$  this can be written as:

$$k_r = A_r T^{n_r} \cdot e^{-E_r/(RT)} \quad (3.3)$$

The temperature dependency of the specific reaction is defined by  $n_r$  a dimensionless power. For a system of species  $i$  and reactions  $r$ , Equation 3.1 can be written:

$$r_r = \prod_i^{N_i} c_i^{v_{i,r}} k_r \quad (3.4)$$

The stoichiometric coefficient  $v_{i,r}$  is defined for each of the species  $i$  with concentration  $c_i$  participating in reaction  $r$ . Leading to the expression of production or consumption  $\omega_i$  of all species in the closed system:

$$\omega_i = \sum_r^{N_r} v_{i,r} r_r \quad (3.5)$$

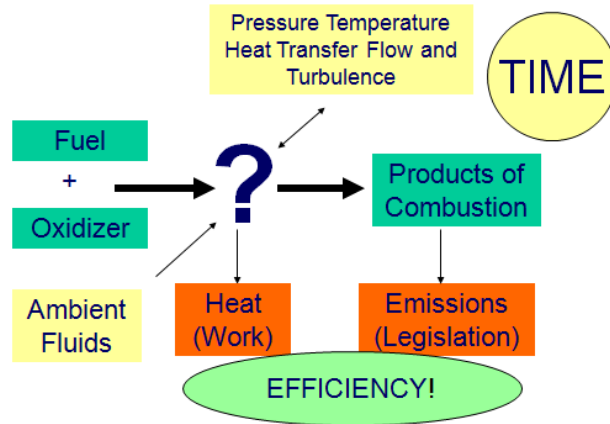


**Figure 3.2** Representation of the problem to solve in simulating engine combustion.

In the simulation of combustion in engines, by use of chemical kinetics, the results are strongly affected by the quality of the chemical model. The problem to solve is how the

initial conditions of fuel, oxidizer, pressure and temperature and so on, translates over time to work and also to the products of combustion (Figure 3.2). The description of the intermediate reactions and their release of heat are clearly important but also difficult to define.

Each chemical model is based on the fuel and oxidizer it is developed for. Typically the more complex the fuel, the more complex the chemical model will be. For example, a small fuel species like hydrogen has a chemical model of less than 10 species, while more complex fuel species like isooctane can have several hundreds of species included in the chemical model. Not only the fuel itself decides the size, but features as NO<sub>x</sub> and soot emission calculations need a chemical model that includes those specific species and reactions.

### 3.1 Reduced Chemical Models

In the interest of reducing the size and thus the computing time, reduced chemical models are developed for complex fuels. The problem is to reduce the size of the chemical model without losing its ability to correctly calculate the chemical process under the conditions specified. DARS-ESM is constructed in such a manner that the chemical model can be exchanged. Of course, this applies to when the engine simulation models different fuels, but also depending on the purpose of the simulation for any given fuel. Typically, an increase in the size of the chemical model results in an exponential increase of computing time.

Although stochastic reactor models are lightweight compared with CFD models regarding the physical properties, this advantage is often used to employ heavier and more detailed chemical models. Generally speaking, there is always a tradeoff in how much information or quality you can obtain from a simulation in relation to how long it takes to perform the calculations. Nevertheless there is a constant development towards faster and often at the same time more detailed simulations. This reflects not only there being a constant development of faster computers, but also considerable effort is also invested in methods to simplify the calculations without losing accuracy or other properties. Modern solver solution is a research area of its own [10], and several of the novel approaches can be used for stochastic models.

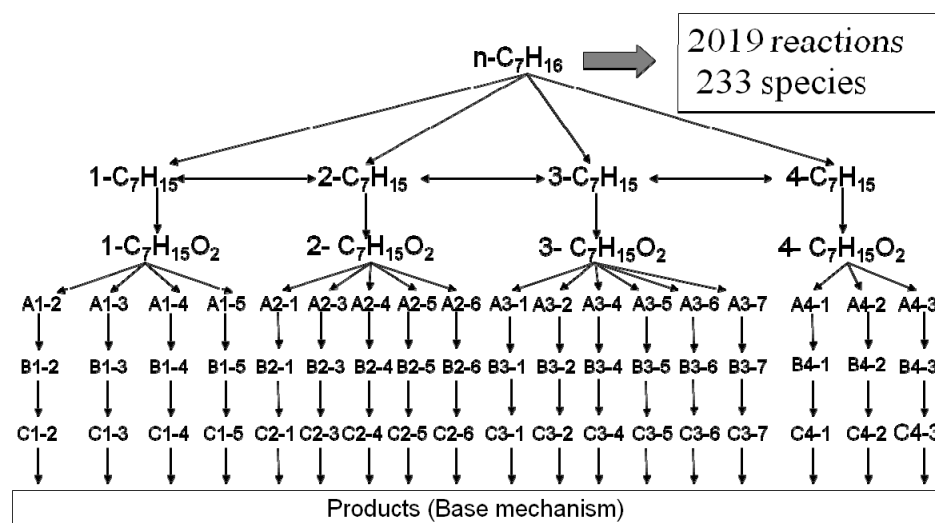


**Figure 3.3** Detailed chemical model of *n*-heptane [11].

From the standpoint of computers, DARS-ESM is not in itself too complex or time consuming to solve. What is really demanding for the computer is the solving of the chemistry. Generally speaking an increase of the size of chemical model will lead to an exponential increase of the computational time. This is the case, since solving the chemistry at a specific moment normally requires the use of numerical methods and in general, the size of the numerical matrix to solve is the number of species, together with any other unknown you like to solve, like temperature, to the power of 2. In addition, when increasing the number of species, typically, less important species or species with extremely low concentrations are included. In practice, with a larger number of species the differences in the concentrations of the species are extended, with the effect from a numerical point of view, that the differences of the size of the numbers is extended.

Let me give a practical example:

A simple chemical model contains  $O_2$  and  $N_2$  (air) and a hydrocarbon fuel, let's say Ethanol in these bio fuel days  $C_2H_5OH$ , and other species like  $CO$ ,  $CO_2$ ,  $H_2O$ ,  $OH$ ,  $NO$ ,  $N$ ,  $O$ ,  $H$ , less than 20 species altogether. Actually this is typically the species accounted for in commercial engine simulation tools in their standard combustion models. For many types of engine simulations, this is no problem.

But, to cover the entire regime of what happens in, for example, a diesel fuelled combustion one would need to include hundreds of species. In the simplified model above, intermediate species like  $CH_2O$ ,  $CH_3$  and hundreds of others are not included, and thus hidden in the

fuel and combustion products, for example  $\text{CO}_2$ . In the simplified model the mass fraction of  $\text{C}_2\text{H}_6\text{O}$  can be 0.01870, while in the detailed model it would be 0.01869 mass fractions of  $\text{C}_2\text{H}_6\text{O}$  together with the  $0.1 \cdot 10^{-13}$  mass fractions of each of 99 other species. To be of any relevance it is still needed to solve those extremely small numbers with accuracy. The differences in mass fractions are not the only differences to consider while solving the chemistry. The evolution of the mass fractions over time is solved within discrete and finite time-steps, and since the lifetimes of different species are of extremely different magnitude, yet another difference is introduced.

In a numerical solver it is needed to solve both the smallest numbers and largest numbers simultaneous and all with some accuracy on the significant digits. When introducing large differences in the size of the numbers, the system to solve is known to be stiff. And with increased stiffness, the longer the calculation will take to perform. In fact to solve chemistry in combustion is known to be very stiff problems.

It is obvious that it is possible to save computing time and also memory space by using smaller chemical models. General reduction of chemical models is one approach, but to be able to have high levels of detail and accuracy combined with fast calculations is more difficult. More information on the subject can be found in [11,22].

### 3.1.1 Lumping

If certain species have similar properties, they may be lumped together into one single species representing them all (Figure 3.4). This is a very general and efficient way of reducing the size of the chemical model. One should be careful, of course, not to lump together any species of particular interest to analyze.

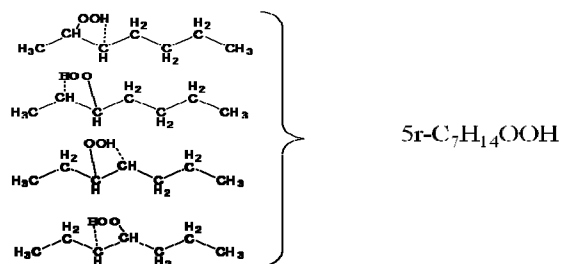


*Figure 3.4 The lumping procedure.*

The result of the lumping procedure can be seen in Figure 3.5. The original mechanism of 233 species and 2019 reactions in Figure 3.3 has been reduced to a mechanism of 143 species and 1374 species. Roughly a division of 2 in size but the gain in calculation time is rather in the order of a factor of 4. The lumped mechanism should in principle be applicable for all the conditions as for the original mechanism and of very minor deviation.

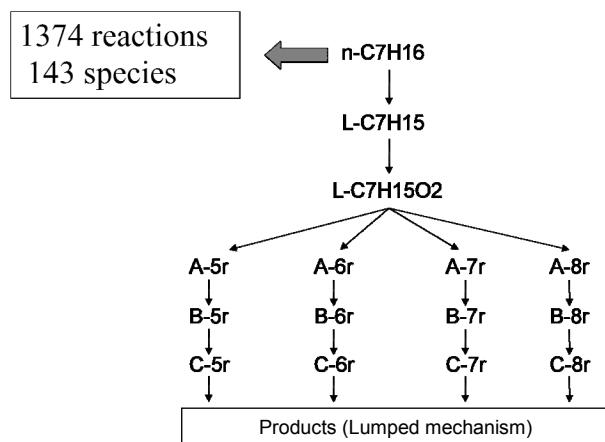


**Figure 3.5** Lumped chemical model of *n*-heptane after the lumping procedure has been applied to the base chemical model shown in Figure 3.3.

## 3.1.2 Skeletal Mechanism

If the problem to solve is within a limited range of conditions, of for instance pressure and temperature, some of the species may be of little or no consequence. If this is the case, then these species can be removed altogether. One should remember though that the skeletal mechanism loses the generality of the detailed model it was based on, and is only applicable under the conditions it was created for.

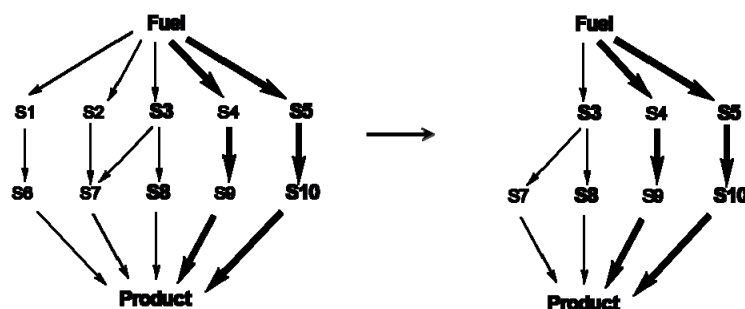


**Figure 3.6** Principle of the skeletal mechanism.

Figure 3.7 demonstrates a skeletal chemical model that has undergone both skeletizing and lumping from the base mechanism in Figure 3.3. The size is a reduction from 233 species and 2019 reactions down to 64 species and 482 species, in effect a reduction in size of almost 4 times, but a computational speedup in the range of a factor of 20. Still the produced

skeletal model should for the applicable conditions be able to predict emissions and engine performance to a high level of accuracy.

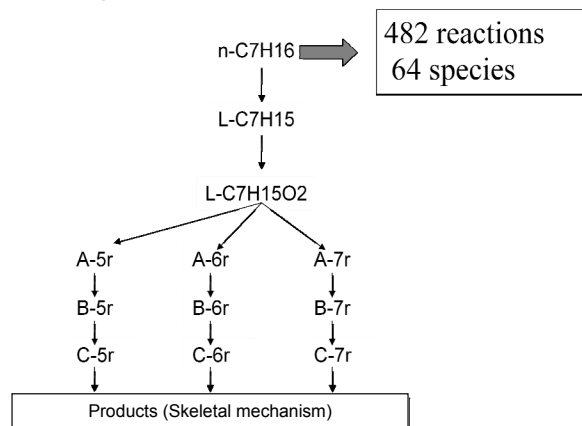


**Figure 3.7** Skeletal chemical model of *n*-heptane after the skeletal procedure has been applied to the lumped chemical model in Figure 3.5.

## 3.1.3 The QSSA

Under certain conditions, certain species may be so short lived, or rather consumed and formed so fast that their concentration remains almost unchanged so that they can be thought of being in steady state. In this case it is generally beneficial to relax the numerical system by removing these species, that with their short lifetime would impose significant stiffness, and solve them outside algebraic. The approach is known as the Quasi Steady State Assumption.

$$\begin{bmatrix} a_{11} & a_{12} & \cdots & \cdots & \cdots & a_{1n} \\ a_{21} & a_{22} & & & & a_{2n} \\ \vdots & & \ddots & & & \vdots \\ \vdots & & & \ddots & & \vdots \\ \vdots & & & & \ddots & \vdots \\ a_{n1} & a_{n2} & \cdots & \cdots & \cdots & a_{nn} \end{bmatrix} \begin{bmatrix} x_1 \\ x_2 \\ \vdots \\ \vdots \\ \vdots \\ x_n \end{bmatrix} \Rightarrow \left\{ \begin{array}{l} \text{QSSA-} \\ \text{reduction} \end{array} \right\} \Rightarrow \begin{bmatrix} a_{11} & a_{12} & \cdots & a_{1k} \\ a_{21} & \ddots & & \vdots \\ \vdots & & \ddots & \vdots \\ a_{k1} & \cdots & \cdots & a_{kk} \end{bmatrix} \begin{bmatrix} x_1 \\ \vdots \\ \vdots \\ x_k \end{bmatrix} + \sum_{i=1}^n \sum_{j=k+1}^n a_{ij} x_j$$

**Figure 3.8** Representation of the QSSA.



### 4 Physical Modeling

In simulating engines the models used can be divided into two categories, physical and chemical modeling. This chapter describes physical modeling and details of chemical modeling have been considered in the previous chapter.

When referring to physical modeling it is meant a model that has physical properties like volume, size, time, temperature, pressure and so forth. The physical model contains a solver for the temporal evolution of the chemistry based on the information from the attached chemical model. The physical models used here are known as reactors and are in the present work restricted to only be used for calculations of the closed cycles of an engine. For four-stroke engines, closed cycles appears usually every fourth stroke as the main combustion period, but more recent with specific valve timing strategies, a second so called Negative Valve Overlap (NVO) period closed cycle may be applied as well.

3-dimensional, detailed engine simulations using Computational Fluid Dynamics (CFD) are amazing in the detailed results they provide, results that are useful to give insight in the phenomenon of engine combustion [12-16]. CFD calculations are however very demanding on computational powers and also quite complex to set up, run and post process. For simulations in which computational time or memory needs are restricted, Homogeneous Reactor Models (HRM) and Stochastic Reactor Models (SRM) are attractive alternatives and complements to CFD. Typically, HRM and SRM can be used for simulations where large chemical models are employed or when transient effects need to be studied or when fluid mechanics or turbulence is of little consequence. Both HRM and SRM are 0-D and there is no spatial information to be gained from calculations of the combustion within the cylinder. The SRM is known as a quasi-0-D tool where the spatial description is replaced with by a statistical description of the distributions.

In full engine simulation tools, like 1-D codes, that are perfectly capable of determining the flow conditions in an engine, combustion modeling is most often performed either with deterministic or empirical models [17,18]. Replacing those simplistic combustion models, these 1-D tools can be coupled to the SRM and thus create a computational efficient and predictive full engine simulation tool. The coupled 1-D SRM is useful for parametric studies of engine emissions and performance for the full operating range and transients of different engines. If the flow conditions in the engines are known, the SRM can also be used on its own.



## 4.1 The Homogeneous Reactor Model (HRM)

The fastest way to calculate engine combustion with a solver for detailed chemistry would be to employ a homogenous reactor model. The model is based on the PFR (Plug flow Reactor) with the assumption that conditions within the cylinder are homogenous at all times. The model uses the Woschni-correlation [19] for calculation of heat transfer and has successfully been applied to calculate the combustion process of HCCI engines [20, 21].

The numerical model is basically a set of zero-dimensional time dependent differential equations, solving the energy conservation and species balances [22]. The matrix system of balance equations is solved using Newton's method and the time is resolved with higher order backward differential functions. The pressure is calculated as a function of the piston movement and of the pressure increase due to chemical reactions. The pressure is then calculated from the equation of state:

$$p = \rho \frac{RT}{M} \quad (4.1)$$

Since combustion in the engines modeled here, occur during the closed period, inflow and out-flow calculations are omitted and a closed system assumed. The conservation equation for the chemical species is then given by:

$$\frac{dY_j}{dt} = \frac{M_j}{\rho} \sum_{k=1}^{N_r} \nu_{j,k} r_k \quad (4.2)$$

and the energy conservation equation is given by:

$$m \sum_{j=1}^{N_s} \left( u_j \frac{M_j}{\rho} \sum_{k=1}^{N_r} \nu_{j,k} r_k \right) + h_g A_{wall} (T - T_{wall}) + p \frac{dV}{dt} + m C_v \frac{dT}{dt} = 0 \quad (4.3)$$

For both these balance equations,  $\nu_{j,k}$  is the stoichiometric coefficient for species  $j$  in reaction  $k$  and  $r_k$  is the reaction rate of reaction  $k$ .  $Y_j$ ,  $u_j$  and  $M_j$  are the mass fraction, specific internal energy and the mole mass respectively, of species  $j$ .  $A_{wall}$  is the in-cylinder wall area and  $h_g$  is the heat transfer coefficient which is obtained with the Woschni correlation [19] and from the engine geometry with an additional factor to account for the clearance volume.  $V$ ,  $p$ ,  $T$ ,  $T_{wall}$  and  $t$  are cylinder pressure, instantaneous volume, in-cylinder temperature, cylinder wall-temperature and time.

$$h_g = 3.26 B^{-0.2} p^{0.8} T^{0.55} \omega^{0.8} \quad (4.4)$$

The instantaneous volume is calculated following the expression [23]:

$$V = V_c + \frac{\pi B^2}{4} \left( L_{cr} + R_{ct} - L_{cr} \cos(\theta) + \sqrt{L_{cr}^2 - R_{ct}^2 \sin^2(\theta)} \right) \quad (4.5)$$

where  $V_c$  is the clearance volume,  $B$  the engine bore,  $L_{cr}$  the connecting rod length, and  $R_{ct}$  crank throw radius.

The calculation approach is similar to that of an ideal constant volume process, with the exceptions that the volume is changed from one time-step to another, and that heat is transferred to and from the system through the cylinder wall.

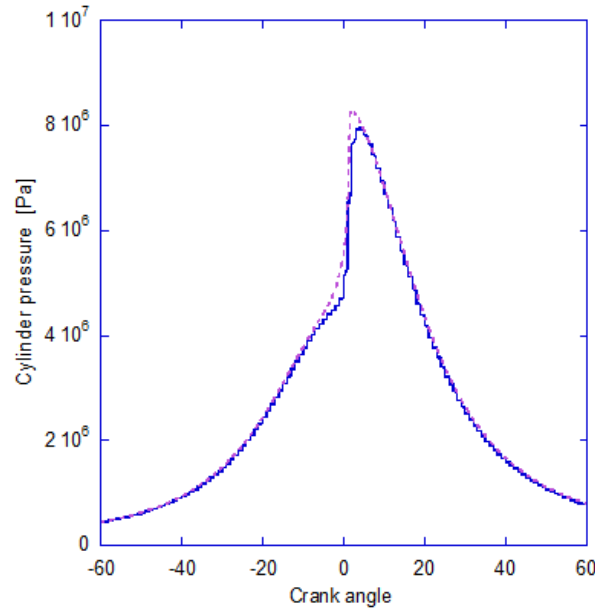


**Figure 4.1** Comparison of experimental results (solid) and HRM calculations (dotted).

The HRM is a fast and efficient tool that provides considerable useful information and trends in emissions and engine performance, but with limitations. Figure 4.1 exemplifies the difference between a calculation with the HRM and an experiment. Since the HRM only contains one single volume, everything happens at once. This is evident in the pressure peak which for the HRM is sharp. The result is that the maximum pressure, maximum pressure rate and maximum temperature are overpredicted. From this follows that hydrocarbon and CO emissions are underpredicted but that NO<sub>x</sub> emissions are overpredicted. Further, the combustion duration can-

not be determined although both the total amount of heat release and the ignition timing are predicted quite reasonable. To be able to get better predictions of emissions and engine performance, the SRM for engine simulations was developed.

### 4.2 The Stochastic Reactor Model (SRM)

The SRM or stochastic reactor model is the model inside DARS-ESM, developed for this investigation. The SRM is based on the partially stirred reactor model (PaSPFR) developed by Kraft [24] which has been presented in several publications for use in combustion modeling of HCCI engines[25-28]. The model developed for the present study contains the same PDF based Monte Carlo type simulation assumption with a MDF and an operator splitting loop.

The strength of the SRM is that it provides means to include effects of inhomogeneties and turbulence. The idea behind the SRM is that the assumption of homogeneity within the combustion chamber is replaced by the one of statistical homogeneity, with physical quantities described by PDF distributions. This is realized by dividing the mass within the cylinder into an arbitrary number of virtual packages called particles. Each of these particles has a chemical composition, a temperature and a mass and is able to mix with other particles and exchange heat with the cylinder walls. Since the SRM is 0-dimensional no information is provided on the position of the particles.

#### The PDF and the MDF

In a real engine or in a CFD model the chemical composition, temperature and mass, have distributions in space, but in the space dimensionless SRM the distributions of the particles variables can be described with probability density functions (PDFs), with one PDF for each variable. The PDF can be compared with the distributions from CFD calculations or from measurements in real engines.

Figure 4.2 shows a theoretical bell-shaped PDF for temperature, where the largest number of particles having temperatures of 1010 – 1040 K, and no particles having temperatures below 950 K or above 1100 K. In reality most PDFs have shapes that are skewed and with several peaks. During a calculation with the SRM the shape of the PDFs as well as their range of the variables changes with each time step.

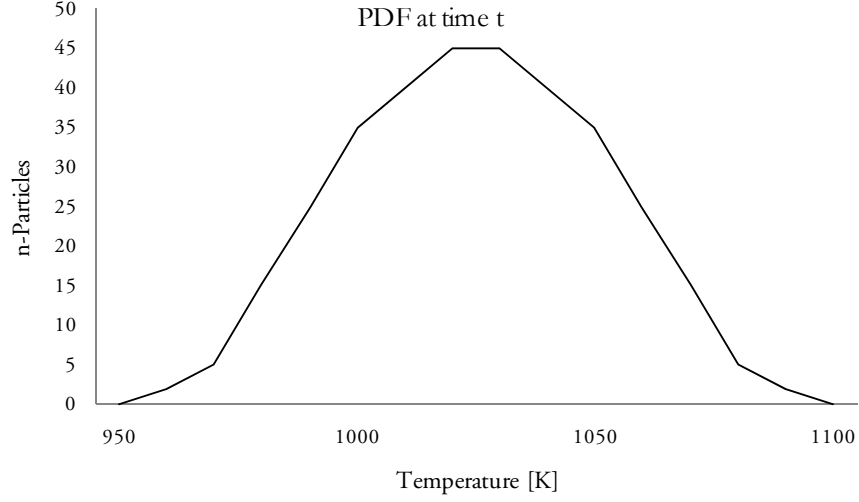


**Figure 4.2** Example of a bell-shaped PDF for temperature.

Since the models implemented in the present work all contain equiweighted particles, the mass density functions (MDF) are always equal to the PDFs.

The MDF can be written as  $F_\Phi(\psi_1, \dots, \psi_{S+1}, t)$ , where

$$\Phi(t) = (\Phi_1, \dots, \Phi_S, \Phi_{S+1}; t) = (Y_1, \dots, Y_S, T; t) \quad (4.6)$$

denotes the vector that contains the random variables, mass fractions,  $Y_i(t)$ ,  $i = 1, \dots, S$ , and temperature,  $T(t)$  represented in the MDF.  $\psi_1, \dots, \psi_{S+1}$  are the realizations (sample space variables) of the corresponding random variables  $\Phi_1, \dots, \Phi_S, \Phi_{S+1}$ .  $S$  is the number of species and  $t$  is the time. The MDF particles are assumed to follow the same physical laws as a gas cluster and the time evolution of the MDF, assuming statistical homogeneity as proposed in the PaSPFR model is given by:

$$\frac{\partial}{\partial t} F_\Phi(\psi, t) + \frac{\partial}{\partial \psi_i} (Q_i(\psi) F_\Phi(\psi, t)) = \text{mixing term} \quad (4.7)$$

The differential Equation 4.7 is derived from the conservation equations for mass and energy as for the Navier-Stokes equations for reactive flows [29]. The initial conditions are set to

## Stochastic Reactor Models for Engine Simulations

---

$F_\phi(\psi, 0) = F_\phi^0(\psi)$ , and  $Q_i$  denotes the source term for variable  $\psi$  which give the changes of the MDFs due to chemical reactions, heat transfer and volume work:

$$Q_i(\psi) = \frac{M_i}{\rho} \omega_i(\psi), i = 1, \dots, S \quad (4.8)$$

$$Q_{S+1}(\psi) = \frac{1}{c_p} \sum_{i=1}^S h_i \frac{M_i}{\rho} \omega_i(\psi) - V \frac{1}{c_p} \frac{dp}{dt} - \frac{h_g A}{c_p} (T - T_w) \quad (4.9)$$

where  $h$  is the Woschni heat transfer coefficient. To include the stochastic heat transfer step [27] the original Equation 4.7 is modified to:

$$\frac{\partial}{\partial t} F_\phi(\psi, t) + \frac{\partial}{\partial \psi_i} (G_i(\psi) F_\phi(\psi, t)) + \frac{\partial}{\partial \psi_{S+1}} (U(\Psi_{S+1}) F_\phi(\psi, t)) = \text{mixing term} \quad (4.10)$$

where:

$$U = -\frac{h_g A}{mc_p} (T - T_w) \quad (4.11)$$

$$G_i = \frac{M_i}{\rho} \omega_{ij} \quad i = 1, \dots, S \quad j = 1, \dots, r \quad (4.12)$$

$$G_{S+1} = \frac{1}{c_p} \sum_{i=1}^S h_i \frac{M_i}{\rho} \omega_{ij} - V \frac{1}{c_p} \frac{dp}{dt} \quad (4.13)$$

To introduce the fluctuation, the third term in the L.H.S., Equation 4.10 is replaced by a finite difference scheme:

$$\frac{1}{h} \left[ \frac{U(\Psi_{S+1}) F(\Psi, t) - U(\Psi_{S+1} - h) F(\Psi_1, \dots, \Psi_S, \Psi_{S+1} - h, t)}{h} \right], \text{ if } U(\Psi_{S+1}) < 0 \quad (4.14)$$

and

$$\frac{1}{h} \left[ \frac{U(\Psi_{S+1}) F(\Psi, t) - U(\Psi_{S+1} + h) F(\Psi_1, \dots, \Psi_S, \Psi_{S+1} + h, t)}{h} \right], \text{ if } U(\Psi_{S+1}) > 0 \quad (4.15)$$

The fluctuation in temperature  $h$  is in this work a modeling parameter, and is described in more detail in section 4.2.5. The mixing term of scalars by turbulent diffusion depends on the used mixing model and is given explicitly in section 4.2.4. The Ideal gas law is assumed to always be valid:

$$pV = nRT \quad (4.16)$$

## 4.2.1 Operator splitting and numerical solution

To simplify the solving of the partial differential equation (Equation 4.10), at each time step an operator splitting loop approach is employed [30]. The differential operator is decomposed and parts of the differential operator describing different physical processes are solved sequentially. The resulting PDE can be seen in Equation 4.17.

$$\begin{aligned}
 & \underbrace{\frac{\partial}{\partial t} F_{\Phi}(\psi, t)}_{\text{Change of MDF}} \\
 &= \\
 & \underbrace{\frac{\partial}{\partial \psi_{S+1}} \left( V \frac{1}{C_p} \frac{dp}{dt}_{\Delta V} F_{\Phi}(\psi, t) \right)}_{\text{Piston movement}} \\
 &+ \\
 & \underbrace{\frac{c_{\Phi} \beta}{\tau} \left[ \int_{\Delta \Phi} F_{\Phi}(\psi - \Delta \psi, t) F_{\Phi}(\psi + \Delta \psi) d(\Delta \psi) - F_{\Phi}(\psi, t) \right]}_{\text{Mixing}} \\
 &+ \underbrace{\frac{\partial}{\partial \psi_{S+1}} \left( V \frac{1}{C_p} \frac{dp}{dt}_{\text{mix}} F_{\Phi}(\psi, t) \right)}_{\text{Mixing}} \\
 &- \\
 & \underbrace{\left( \frac{\partial}{\partial \psi_{S+1}} \left( \frac{1}{C_p} \sum_{i=1}^s h_i \frac{M_i}{\rho} \omega(\Phi) F_{\Phi}(\psi, t) \right) - \sum_{i=1}^s \frac{\partial}{\partial \psi_i} \left( \frac{M_i}{\rho} \omega(\Phi) F_{\Phi}(\psi, t) \right) \right)}_{\text{Chemical reaction}} \\
 &+ \underbrace{\frac{\partial}{\partial \psi_{S+1}} \left( V \frac{1}{C_p} \frac{dp}{dt}_{\text{chem}} F_{\Phi}(\psi, t) \right)}_{\text{Chemical reaction}} \\
 &- \\
 & \underbrace{\frac{\partial}{\partial \psi_{S+1}} \left( \frac{h_g A}{C_p} (\psi_{S+1} - T_w) F_{\Phi}(\psi, t) \right) + \frac{\partial}{\partial \psi_{S+1}} \left( V \frac{1}{C_p} \frac{dp}{dt}_{\text{heat transfer}} F_{\Phi}(\psi, t) \right)}_{\text{Heat transfer}}
 \end{aligned} \quad (4.17)$$

## Stochastic Reactor Models for Engine Simulations

---

The MDFs are updated at each step under the assumption of constant pressure. This approach introduces a small error compared to solving Equation 4.10 directly, so to assure that the thermodynamic conditions are valid for the next operator a pressure correction calculation is performed after each operator. The operator splitting approach has been proved to be first order accurate [31].

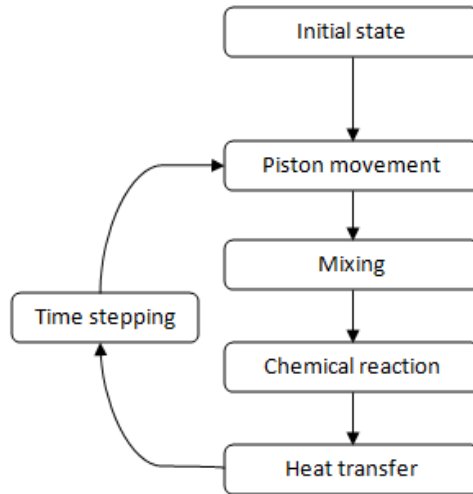


*Figure 4.3 The steps in the operator splitting algorithm.*

The basic functionality is represented in Figure 4.3. The initial state or starting conditions are applied at the closing of the intake valve. The starting conditions include global pressure, temperature, air/fuel ratio, EGR amount, cylinder wall temperature, etc. At the initialization the mass within the cylinder is divided to an arbitrary pre-set number of particles. Residual gas and EGR can be handled in two ways. EGR or Exhaust Gas Recirculation is in a real engine an active measure where residual gas is being fed back into the induction system. In the model it is assumed that the EGR is perfectly mixed with the incoming air, and thus the EGR mass is spread equally over the existing particles. Residual gas is the gas remaining in the cylinder from the last cycle and that was not expelled during the open valve periods. The assumption in the model is that residual gas is not mixed with the incoming gas at all and thus a number of EGR particles are introduced.

At each time step, the volume work of the piston movement, the mixing of the particles scalars, the chemical reaction (with sub cycling), and heat transfer are solved one after each other. After each of the steps a pressure correction is performed. The pressure correction is described below.

## Model for the pressure correction

Since the different steps in the operator loop in fact are supposed to be solved simultaneously and during constant pressure, a small error is introduced while solving the different steps individually. For this reason after each single event in the operator split loop the pressure of the particles are recalculated, so that they all have exactly the same pressure. Especially for zonal models, as the TwoZone SI SRM in chapter 5, where the conditions may be quite different such a procedure is necessary.

In relation to Eq. (4.10) this means that the term corresponding to the pressure change:

$$-V \frac{1}{c_p} \left( \frac{dp}{dt} \right) \quad (4.18)$$

has to be accordingly divided in subterms for each split event (piston movement, mixing, chemistry, and heat transfer):

$$-V \frac{1}{c_p} \left( \frac{dp}{dt} \right) = -V \frac{1}{c_p} \left( \frac{dp}{dt} \right)_{pistonm.} - V \frac{1}{c_p} \left( \frac{dp}{dt} \right)_{mix.} - V \frac{1}{c_p} \left( \frac{dp}{dt} \right)_{chem.} - V \frac{1}{c_p} \left( \frac{dp}{dt} \right)_{heatt.} \quad (4.19)$$

These subterms are solved with the pressure correction.

For introducing the procedure consider a system of particles  $i$ , ( $i = 1, n$ ), each particle having its own species composition and temperature, giving individual specific heat ratios  $\gamma_i$ , and own pressure  $p_i$ . The pressure  $p_i$  is calculated based on the equation of state, written with the particles properties. The model equalizes the pressure of all the particles in the system, by considering they perform an isentropic compression or expansion to a value.

$$p_i V_i^{\gamma_i} = \bar{p} (V_i + \Delta V_i)^{\gamma_i} \quad (4.20)$$

The adiabatic exponents of the particles are assumed to be constant, but even so the system cannot be solved analytically. In order to solve the system (for  $\bar{p}$ ) one additional constraint is needed. This is obtained from the condition that the sum of the volume of all the particles is equal to the total cylinder volume:

$$\sum_{i=1}^n \left[ V_i \left( \frac{p_i}{\bar{p}} \right)^{1/\gamma_i} \right] = V_{tot} \quad (4.21)$$



Equation 4.21 is solved using Newton iteration. After the pressure correction, the temperature and the density of all of the particles are updated accordingly. Further details can be found in [32].

## 4.2.2 Piston movement

A piston engine can be seen as a pump that draws in air and fuel, compress and combust the gas mixture, use the expansion to convert the heat into work, and then pump out the exhaust gases. The SRM codes in the present work are employed to model the closed cycles. The gas filling and emptying through pumping is left to be modeled by 1-D codes which are specific tools for this kind of problems. Coupling of the SRMs to such tools are described in sections 5.4 and 7.3.

In the closed cycle the piston movement works against a closed cylinder, decreasing the volume and thus increasing the pressure. This is a fundamental step to be modeled in a piston engine for predicting the compression, combustion and expansion. In this work the equation for the cylinder volume due to piston position was extended to include the effects of piston pin offset. Piston pin offset, which is the offsetting of the cylinder axis in relation to the crank center, is quite often used to reduce the mechanical stresses on the cylinder walls, friction and noise. The equation for the instantaneous cylinder volume from crank angle degree CAD  $\theta$  can thus be expressed as:

$$V = V_c + \frac{\pi B^2}{4} \left( \sqrt{(L_{cr}^2 + R_{ct}^2) - Of_{pin}^2} - \sqrt{L_{cr}^2 - (R_{ct}^2 \sin(\theta) - Of_{pin})^2} - L_{cr}^2 \cos(\theta) \right) \quad (4.22)$$

where  $V_c$  is the clearance volume,  $B$  the cylinder bore,  $L_{cr}$  the length of the connecting rod,  $R_{ct}$  the radius of the crank throw and  $Of_{pin}$  the piston pin offset.

## 4.2.3 Mixing

Turbulence is modeled with mixing models. The main function of turbulence is to spread and disperse inhomogenities. Turbulence is one of the essential processes for the combustion process in engines, and one necessary for engines in which the incoming charge is not prepared and mixed in advance. Turbulence is also important to reach sufficiently fast flame speed in SI engines as well as for the mixing of fuel and cylinder gas in direct injection engines. This is especially true of DICI engines, in which the combustion is to a great extent decided by the turbulent mixing [23, 33].

## Chapter 4 Physical Modeling

---

Mixing and turbulence phenomena are themselves stochastic processes that are not easily modelled [34], although the flow fields can be determined with DNS [35].

Several models that can be used for the mixing of the particles within an SRM have been developed earlier. The IEM [36,37] and the Binomial Langevine [38] as well as the multi weighted C/D (Coalescence/dispersal) model [39,40] and the modified C/D model as presented by Janicka [39,41] were used in the present work. All of the SRM results presented in the thesis were calculated either with the IEM or the multi weighted C/D mixing model. For this reason, only these two models are presented here.

The mentioned mixing models have in common that the turbulence is modeled with simplified models where typically the turbulence mixing time needs to be provided by the user. Ideally the turbulence mixing time can be provided from experiments or from CFD calculations, for instance as the prescribed Favre mean of the global  $k/\varepsilon$  ratio [42]:

$$\tau = c \frac{\bar{k}}{\varepsilon} \quad (4.23)$$

Usually, this information is not obtainable. This means that user usually is left with the necessity to tune the SRM code with the turbulence mixing time.

The turbulence mixing time  $\tau$  is defined [23] as the ratio between the integral length scale  $l_I$  and the mean velocity in the gas  $\bar{U}$ :

$$\tau = \frac{l_I}{\bar{U}} \quad (4.24)$$

where the integral length scale,  $l_I$ , is the measure of the largest scale structure of the flow field, defined according to the formula:

$$l_I = \int_0^\infty R_x dx \quad (4.25)$$

with  $R_x$  the autocorrelation coefficient of the fluctuating velocity. For engines with little charge motion, the mean flow is the same order of magnitude as the fluctuation of velocity  $u$ , the turbulence mixing time is sometimes expressed as:

$$\tau = \frac{l_I}{u'} \quad (4.26)$$

where  $u'$  the turbulence intensity is defined as:

$$u' = \lim_{t \rightarrow \infty} \left( \frac{1}{t} \int_{t_0}^{t_0+t} u^2 dt \right)^{1/2} \quad (4.27)$$

The level of turbulence changes in general with the engine geometry, but also with engine speed. Turbulence is also a function of the time in the cycle and thus very time dependent.

### The IEM mixing model

The interaction by exchange with the mean model [36, 37], even though still deterministic, is a simple and computationally efficient model. The model works on the principle that the scalar value of each particle approaches the mean scalar value of all the particles with a decay that is controlled by a characteristic time, which is a fraction of the mixing time  $\tau$ :

$$\tau_\Phi = \frac{\tau}{C_\Phi} \quad (4.28)$$

$C_\Phi$  is a constant of the model which was set to 1.0 throughout this work. The expression for the mixing term is:

$$\begin{aligned} \text{mixing term} = & \sum_{i=1}^S \frac{\partial}{\partial \psi_i} \left( \frac{1}{2} \frac{C_\Phi}{\tau} (\psi_i - \langle \Phi_i \rangle) F_\Phi(\psi, t) \right) + \frac{\partial}{\partial \psi_{S+i}} \left( \frac{1}{2} \frac{C_\Phi}{\tau} (h_i - \right. \\ & \left. \langle h_{i,\Phi} \rangle) F_\Phi(\psi, t) \right) \end{aligned} \quad (4.29)$$

where  $C_\Phi/\tau$  is the mixing scalar intensity and  $h_{i,\Phi}$  is the cylinder specific species enthalpy. Since the temperature is not an extensive variable, the enthalpy is used instead. For a MDF particle this gives for the species massfractions and enthalpy respectively:

$$\frac{dY_i^j(t)}{dt} = -\frac{1}{2} C_\Phi (Y_i^j(t) - \langle Y_i^j \rangle(t)) \quad (4.30)$$

$$\frac{dh_i^j(t)}{dt} = -\frac{1}{2} C_\Phi (h_i^j(t) - \langle h_i^j \rangle(t)) \quad (4.31)$$

The result is an exponential change of the particle properties towards the mean. Since the mean value is constant during the operation, this can be written as:

$$Y_i^j(t + \Delta t) = Y_i^j(t) e^{-\frac{1}{2} C_\Phi \Delta t} + \left[ 1 - e^{-\frac{1}{2} C_\Phi \Delta t} \right] \langle Y_i^j \rangle \quad (4.32)$$

$$h_i^j(t + \Delta t) = h_i^j(t) e^{-\frac{1}{2} C_\Phi \Delta t} + \left[ 1 - e^{-\frac{1}{2} C_\Phi \Delta t} \right] \langle h_i^j \rangle \quad (4.33)$$

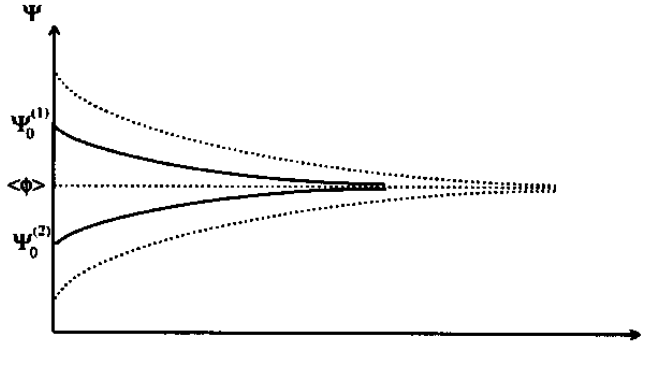


**Figure 4.4** Schematic representation of the time evolution of two particles moving towards the mean according to the IEM model.

All of the MDF particles are moved towards the global mean proportionally at each timestep, so that the evolution of the PDF is rather smooth (Figure 4.4). One disadvantage is that the MDF shape does not relax to a Gaussian.

## C/D mixing model

The coalescence/ dispersal (C/D) model, also known as the Curl model, was originally suggested by Curl [39] and later further developed by Janicka [41]. The implementation in this work is based on the development by Janicka, but with the additional consideration of the particle weights. The expression for the mixing term in this model is:

$$\text{mixing term} = \frac{c_{\Phi\beta}}{\tau} \left[ \int_{\Delta\Phi} F_{\Phi}(\psi - \Delta\psi, t) F_{\Phi}(\psi + \Delta\psi) d(\Delta\psi) - F_{\Phi}(\psi, t) \right] \quad (4.34)$$

The idea is that out of the  $N$  particles,  $n$  random selected particle pairs mix and “take” their mutual mean. The resulting PDF with this model is not continuous, but rather consists of an ensemble of delta functions. The mixing process modeled with this approach does not affect the mean value of the properties. The C/D model is relatively simple to implement and has been reported to perform better for multiple reacting scalars [27, 40] compared to the deterministic IEM. Also this model gives results closer to the Gaussian distribution than the IEM model. The implemented C/D algorithm is presented below.

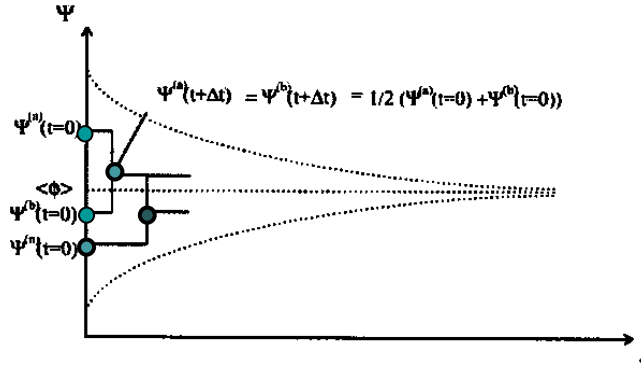


**Figure 4.5** Schematic representation of the CURL mixing model. A pair of particles mixes, both particles receiving their mean properties after mixing.

In each global time step  $t + \Delta t$  the C/D model is implemented as follow:

1. Calculate a time jump parameter.

$$t_{jp} \propto \frac{1}{\tau} \quad (4.35)$$

2. Advance a randomly calculated sub time step.

$$t_{sub} = t_{sub} + \Delta t - \frac{1}{t_{jp}} \log RN_0^1 \quad (4.36)$$

3. Select two distinct particles randomly.

4. Perform the mixing step:

$$Y_i^j(t + t_{sub}) = Y_i^k(t + t_{sub}) = \frac{w^j Y_i^j(t) + w^k Y_i^k(t)}{w^j + w^k} \quad (4.37)$$

$$h^j(t + t_{sub}) = h^k(t + t_{sub}) = \frac{w^j h^j(t) + w^k h^k(t)}{w^j + w^k} \quad (4.38)$$

5. If  $t_{sub} < \Delta t$ , then go to step 2.

For zonal models such as the two-zone SI engine model, mixing occurs only within each zone.

### 4.2.4 Chemical reaction

In the chemistry solver the PDE 4.39 is solved. For each particle a set of instationary equations that is equivalent to the set of equations describing a regular plug flow reactor (PFR) is solved. This step needs subcycling since the governing equations are highly nonlinear. A standard backward differential function (BDF) method combined with a Newton algorithm that is used to solve this system of equations. The result is the new chemical composition for the particle at the new timestep.

$$\frac{\partial}{\partial t} F_{\Phi} = \frac{\partial}{\partial \psi_{S+1}} \left( \frac{1}{c_p} \sum_{i=1}^S h_i \frac{M_i}{\rho} \omega(\Phi) F_{\Phi}(\psi, t) \right) - \sum_{i=1}^S \frac{\partial}{\partial \psi_i} \left( \frac{M_i}{\rho} \omega(\Phi) F_{\Phi}(\psi, t) \right) \quad (4.39)$$

### 4.2.5 Heat transfer

A particular strength of the SRM code is its ability to realistically model the inhomogenities inside a cylinder of a real engine. These inhomogenities have their source for SI engines in the flame movement and for DI engines through the fuel injection. In all engines, inhomogenities may also come from that the incoming gas not being homogeneous, and in all cases inhomogenities are created through heat transfer with the cylinder walls. In fact for HCCI engines heat transfer may be the only source of inhomogeneity in the cylinder gas. Accordingly, the heat transfer model is of central importance to the SRM code.

The stochastic heat transfer model [27] was extended in the present work to be able to take account of an arbitrary number of surfaces inside the combustion chamber. Since the ratio of the different surfaces inside the cylinder varies during the piston motion, the probability of interaction between the particles and the exhaust valve surface varies accordingly. This model uses the Woschni heat transfer model to determine the total amount of heat transfer [19], but a stochastic approach [27] to decide the distribution of the heat transfer over the particles. A stochastic constant  $Ch$  can be set to decide the ratio of the distribution.

A low  $C_h$  leads to a larger amount of heat transfer for each particle and to fewer particles participating, while a large  $C_h$  lead to less heat transfer for each particle and consequently to a larger number of particles participating to fulfill the total amount of heat transfer according to the Woschni model. With  $C_h$  going towards infinity the deterministic Woschni model as in the homogeneous reactor model is reproduced.

For each time step,  $t + \Delta t$

1. Calculate the area  $A^i$  of each surface that has an attributed temperature  $T_{wall}^i$  according to the current piston position.
2. For each surface  $i$  repeat 3 to 7:
3. Calculate the total heat transfer  $Q_t^i$  for surface  $i$  and the time step  $\Delta t$  according to the Woschni correlation.
4. Calculate a time jump parameter  $t_{jp}$ :

$$t_{jp} \propto \frac{c_h N_{part}}{Q_t^i} \quad (4.40)$$

6. Advance a randomly calculated sub time step.

$$t_{sub} = t_{sub} + \Delta t - \frac{1}{t_{jp}} \log R N_0^1 \quad (4.41)$$

5. Choose a random particle,  $n$ , and calculate the heat transfer through the fluctuation in heat between the particle and the wall, and give particle  $n$  the new energy:

$$h_n = \frac{T_n - T_{wall}^i}{c_h} \quad (4.42)$$

and

$$T_n = T_{wall}^i - h_n \quad (4.43)$$

6. If  $t_{sub} < \Delta t$  then go back to step 2.

### 5 The HCCI-SRM

This chapter contains several studies demonstrating the capabilities of the HCCI-SRM that was implemented here. The implementation described in the previous chapter is in fact the implementation used for the HCCI-SRM described in this chapter.

#### 5.1 Effects of modeling parameters and discretization on the HCCI-SRM

In the SRM codes implemented here, both the heat transfer model and the mixing model are stochastic. Both models contain processes that randomly select particles to participate in the heat transfer and mixing. It is obvious that these processes become more sensitive with a decreasing number of particles. If one studies the models as described in Chapter 4 one can understand that the distribution over the particles is to be maintained regardless of the number of particles. This gives as a result that with fewer particles each particle has a greater importance on the global conditions.

With an infinite number of particles, sufficiently many will be selected at each time step for the heat transfer and mixing processes that the range of the stochastic variations from Cycle-to-cycle will be the same regardless of the order of the random numbers generated (the order particles are selected). This is perfectly fine since the heat transfer and turbulence in real engines are stochastic and part of the reasons for the cyclic variations in real engines. But with a decreasing number of particles, fewer particles will be selected with the result that the evolution of the PDF over time is increasingly coarser and at some level of discretization the model starts to be increasingly more sensitive to the order of the random numbers generated. The effect is that with decreasing number of particles, at some point the cyclic variations due to insufficient discretization are introduced.

To be able to run the calculations as fast as possible, the number of particles employed is usually kept as small as possible. To overcome the cyclic variations and only obtain **one** representative result, the random number generator can be locked to produce the same sequence of random numbers at each calculation, in fact the same sequence of heat transfer and mixing processes. This is useful for instance when the effects of parametric variations are to be studied. Of course parameters that affect the random number generation should not be varied, without consideration. Such parameters are for instance particle number and time step size but also mixing time, tau, and heat transfer ratio, stocon.



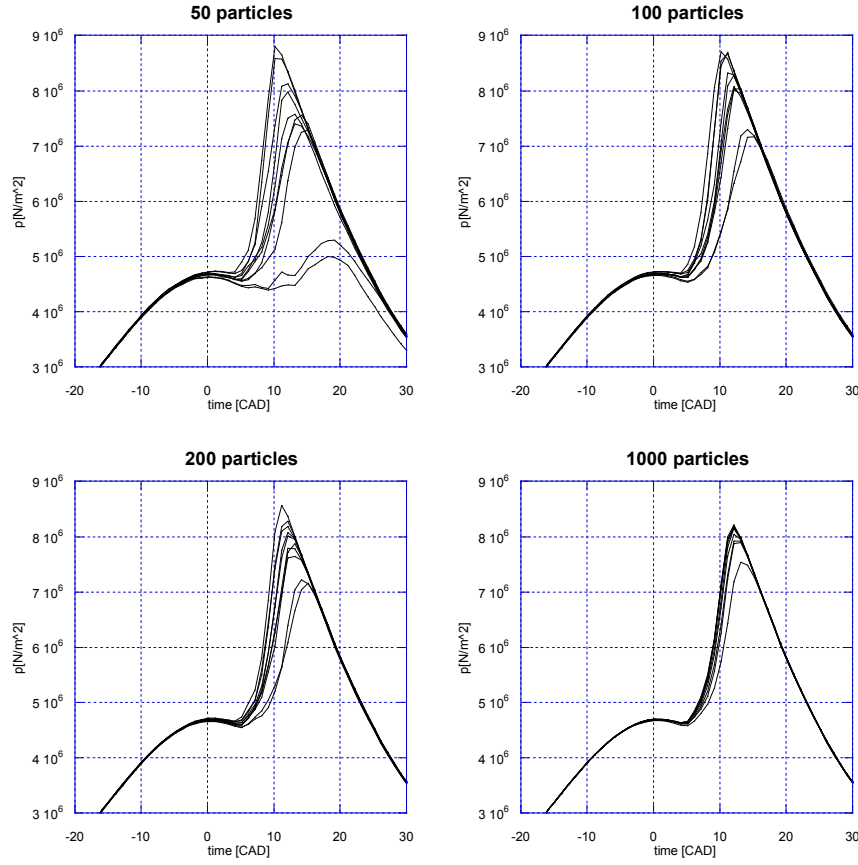


**Figure 5.1** Cycle-to-cycle variations based on 10 SRM calculations, with the same initial conditions. Decreasing number of particles increases the cyclic variations.

In the interest to minimize the calculation times and since the calculation time is basically linearly dependent on the number of particles but also on the time step size, a small number of particles and large time steps might be favored.

The number of particles, the timestep size and modeling parameters for heat transfer and mixing and their intrinsic effect on the calculations are important to understand when for instance validating an SRM to experiments and then use it for parametric and design studies.

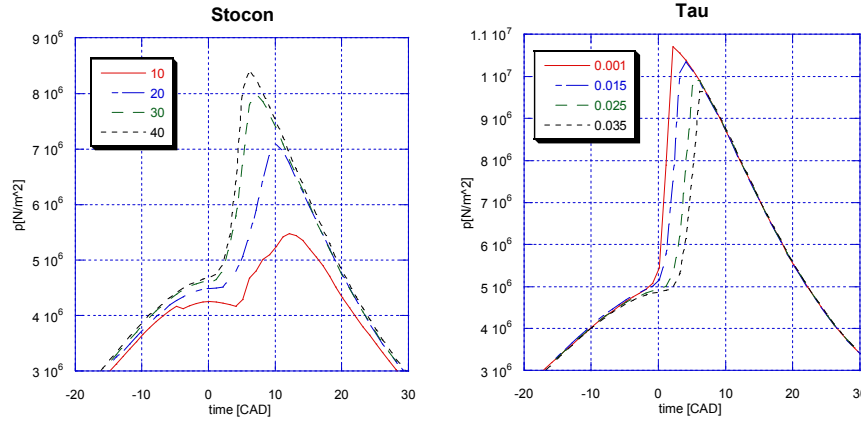


**Figure 5.2** Effects of the stochastic heat transfer parameter, *Stocon*, and of the stochastic turbulence time *Tau* on pressure. Both parameters do also affect the cyclic variations.

In validation work and parametric studies it is good practice to routinely conduct controls of the variations introduced by the stochastic models. Typical observations of the stochastic variations from particle numbers, stocon and tau can be seen in Figures 5.1-5.2 coming from one of the earlier controls done on a routine basis.

To quantify the effects of stochastic variations and to serve as guidelines for future validation work and parametric studies it was decided to set up a comprehensive study [43]. The results are intended for publication during 2008.

Section 5.1.1 contains a study of how well the **range** of cycle-to-cycle variations is captured by 10 and 100 cycle calculations. Section 5.1.2 contains investigations on the major result parameters dependencies from Stocon and Tau, using Pearson Correlations. Section 5.1.3 is an exhaustive study of results from the simultaneous variation of Stocon, Tau, number of particles and time step size.

Although in this particular study the HCCI-SRM is used, the findings are relevant to some extent as well to the TwoZone-SI-SRM and the DI-SRM, described in the chapters 6 and 7. In opposition to the real cyclic variations, the TwoZone-SI-SRM is less sensitive to cyclic variations originating from insufficient discretization since the combustion process is described by the Wiebe function, while the DI-SRM is more sensitive. This sensitivity is a direct consequence of the direct injection leading to a heterogeneous condition in the cylinder that needs to be mixed to suitable conditions for combustion. This issue becomes more critical the closer the injection

# Stochastic Reactor Models for Engine Simulations

---

gets to the combustion and for DICl combustion it is supercritical. In fact, DICl combustion is known to be mixing controlled (see more in chapter 7).

The engine and modeling settings as in Table 5.1 were used unless otherwise mentioned.

**Table 5.1** Engine and modeling settings.

Type	Four-valve HCCI engine
Engine speed	1200 rpm
Displacement (1 cylinder)	0.5 l
Bore	78 mm
Stroke	83.6 mm
Compression ratio	17.4:1
Fuel	91% isooctane 9% n-heptane
Phi	0.421
EGR	3.68 %
Wall temperature	383 K
IVC	136 BTDC
Pressure at IVC	$1.172 \cdot 10^5 \text{ N/m}^2$
Temperature at IVC	367 K
Number of particles	200
Time step size	0.5 CAD
Tau	0.002
Stocon Ch	20
Woschni C1/APO	2.28/1.2

## 5.1.1 The range of cycle-to-cycle variations in HCCI-SRM

Cycle-to-cycle variation is a phenomenon present in all engines to a greater or lesser degree. The cycle-to cycle variation has its origins in the variations concerning the in-cylinder gas motion and heat transfer interaction, the mixture preparation, the pressure fluctuations in the gas exchange processes. The cyclic variations are more pronounced in SI and HCCI engines than in DICl engines that do not have mixture preparation and is not so sensitive to in-cylinder gas motion and heat transfer since they only have basically air in the cylinder during most of these processes.

One of the major assets of the SRMs is their inherit cycle-to-cycle variation. This is a feature of the stochastic heat transfer model, with its random temporal variation and random wall surface interaction variation (if several wall temperatures are assigned) which are real physical origins for real cyclic variations in engines. It is also a feature of the stochastic mixing model which disperses the variation in accordance with the real stochastic turbulent gas motions in the cylinder.

The ability to model the cyclic variations is very useful to assess the stability of real engines, especially in operating ranges close to misfire or close to pressure rates that may be destructive for the engine.

Consequently with the SRMs, one single calculation will be somewhere in the range of the cyclic variations. Where that single calculation is in that range, is not known, unless a number of calculations is done to establish the borders of the cyclic variations.

One issue with stochastic models is that when the discretization is getting too coarse due to a too small number of particles or too long time steps, the stochastic processes get too violent and the range of the cyclic variation too big. This is not a physically correct phenomenon but a consequence of insufficient discretization. What is sufficient discretization depends on the case, where in general terms homogeneous cases as SI and HCCI are less demanding, while heterogeneous cases as DICI are more demanding. To control that, it is advisable to routinely check the current ranges of the cyclic variations to check that the discretization is sufficient. Often this control is done by running 10 calculations to define the range of the cyclic variations and to define an average cycle.

The present investigation answers the question how well 10 cycles covers the range of cyclic variations compared to 100 cycles, and if 10 cycles are enough to ensure that average values from 10 cycles are useful.

A number of cases with different settings for stocon and tau were set up. For each of the cases, 10 calculations were performed with the same initial conditions. The number of particles was set to 100 and  $\Delta CAD$  to 0.5. For this investigation one case with large cyclic variations (tau=0.001 and stocon=10) and one case with small cyclic variations were selected (tau=0.035 and stocon=40), (Figure 5.3).

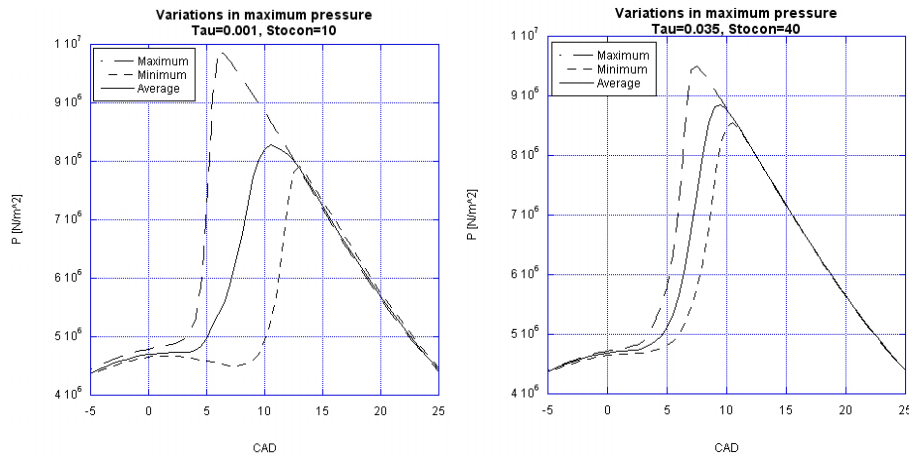


**Figure 5.3** *The two selected cases exhibiting large respectively small cycle-to-cycle variations, from 10 calculations with the same initial conditions each.*

The case with large variations was quite uncharacteristic compared to all other investigated cases that were rather similar to the case with small cyclic variations. Nevertheless it was used since  $\tau$  is within its physical bound and such setting may be applied.  $\text{Stocon}$  which has an empirical connection is also within its normal bounds.

For the two selected cases, a total of 100 calculations each were performed so that the cycle-to-cycle variation ranges and averages could be compared with those of the initial 10 calculations. All calculations for each case used the same initial conditions.

The following result parameters were compared for the calculations with 10 and 100 calculations:

- Maximum pressure
- CAD of maximum pressure
- CAD of Ignition

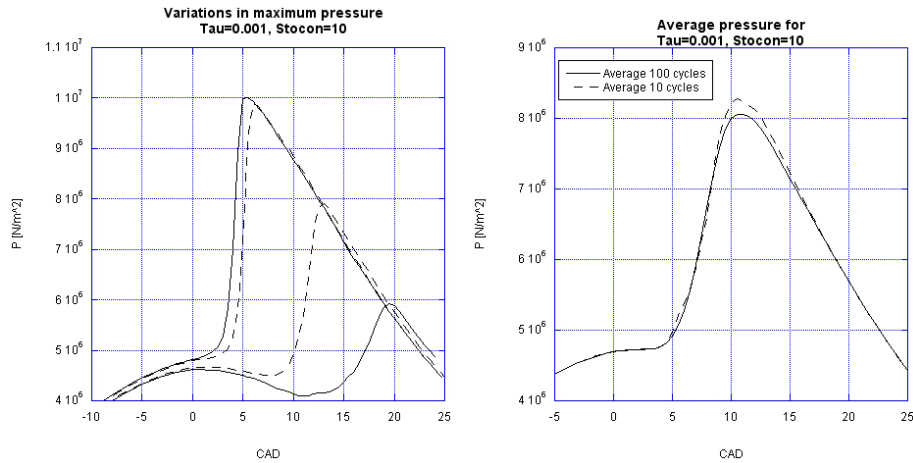


**Figure 5.4** Left: The pressure curve for the case with the highest maximum pressure and the case with the lowest maximum pressure for simulations with 100 cycles (solid) and 10 cycles (dashed). Right: The average pressure curve for simulation with 100 cycles (solid) and 10 cycles (dashed).

As can be seen in the left graph in Figure 5.4, 100 calculations gives a larger spread between maximum and minimum pressure than for 10 calculations. This is the case for the other result parameters as well and it is as expected. The averages for the 100 calculations and the 10 calculations are approximately the same.

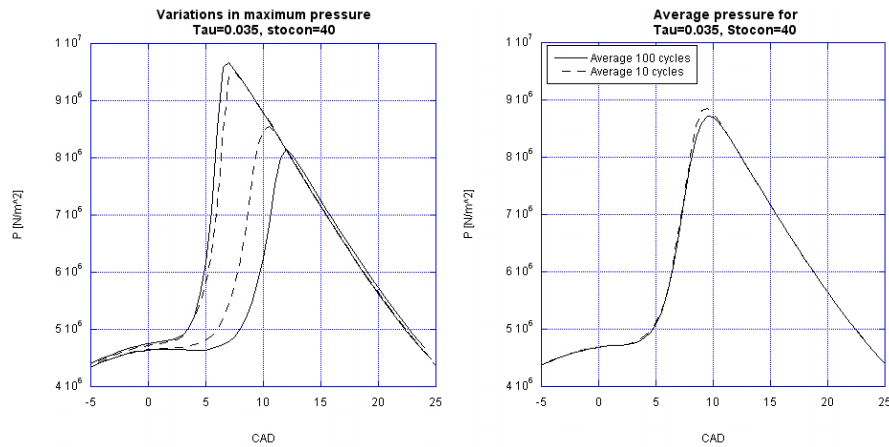


**Figure 5.5** Left: The pressure curve for the case with the highest maximum pressure and the case with the lowest maximum pressure for simulations with 100 cycles (solid) and 10 cycles (dashed). Right: The average pressure curve for simulation with 100 cycles (solid) and 10 cycles (dashed).

# Stochastic Reactor Models for Engine Simulations

---

The results for  $\tau = 0.035$  and  $\text{stocon} = 40$  are similar to the previous, although the averages are even more closely fit (Figure 5.5).

**Table 5.2** Results for 100 and 10 calculations for case with  $\tau = 0.001$  and  $\text{stocon} = 10$ .

	Maximum pressure [ $10^6 \text{ N/m}^2$ ]		CAD of maximum pressure [CAD]		CAD of Ignition [CAD]	
n Calculations	100	10	100	10	100	10
Max	10.0	9.89	19.5	13.0	9.5	6.0
Min	5.92	7.91	5.5	6.0	-1.5	-0.5
Variation	4.09	1.98	14.0	7.0	11.0	6.5
Average	8.79	8.89	9.87	9.50	3.51	3.20
Std deviation	0.71	0.54	2.34	1.90	1.62	1.70

**Table 5.3** Results for 100 and 10 calculations for case with  $\tau = 0.035$  and  $\text{stocon} = 40$ .

	Maximum Pressure [ $10^6 \text{ N/m}^2$ ]		CAD of maximum pressure [CAD]		CAD of Ignition [CAD]	
n Calculations	100	10	100	10	100	10
Max	9.66	9.50	12.0	10.5	4.0	3.0
Min	8.15	8.55	7.0	7.5	0.0	0.5
Variation	1.51	0.94	5.0	3.0	4.0	2.5
Average	8.99	9.03	9.07	8.95	1.99	1.90
Std deviation	0.30	0.28	0.99	0.86	0.76	0.67

## Conclusions

This study demonstrates that with 100 particles and a timestep of CAD 0.5 the discretization is coarse enough to give quite substantial cyclic variations for certain conditions. For the more extreme case it is obvious that one single calculation may differ from another in predicting the time of ignition with more than 11 CAD. For a study with a single calculations and using an unfortunate combination of  $\tau$  and  $\text{stocon}$  the result would be easily misinterpreted.

However, most combinations of  $\text{stocon}$ - $\tau$  do not create such large cyclic variations. Also average values from as few as 10 calculations are useful to establish the soundness of the results.

The engine case simulated in this study is according to my experience, from a physical point of view, a medium stable case. Engine operating conditions that is more unstable, verging to mis-fire, may themselves demonstrate large cyclic variations. In such circumstances the model would also experience larger cyclic variations. However the ability to predict cyclic variations is certainly useful while studying engine operating regimes. But for the SRM one should remember that this is an effect that may origin from the incorrect use of discretization, and thus not a physically correct feature.

The remedy for this is to use sufficiently many particles, and to check the cyclic variations from calculations on a regular basis.

### ***5.1.2 Effects of modeling parameters that affect mixing and heat transfer***

The aim of this investigation was to study how the HCCI-SRM behaves when tau and stocon are altered. At the start of each simulation all particles have the same chemical composition, temperature and mass. During the simulations, the properties of the particles will change due to heat transfer, mixing and chemical reactions. To model the heat transfer and the turbulent mixing two parameters are used (see chapter 4).

- Tau, the turbulence mixing time describes how fast the differences between the particles will average out. The definition of tau is the ratio between the length of the flow integral and the mean velocity of the gas.
- Stocon, the stochastic constant describes how large portion of the particles participate in the heat transfer in each time step. A smaller number gives a larger distribution of particle energies

For each set of tau and stocon 10 cycle simulations were performed, all starting with the same initial conditions and EGR mixture. For each set of 10 cycles the average, min and max cycles of the following results were collected to study the magnitude of the stochastic variations.

- variation in maximum pressure (measure of cyclic variations)
- average maximum derivative of the pressure
- average CAD of maximum pressure
- average CAD of maximum derivative of the pressure
- average CAD when the pressure starts increasing due to effects from the combustion, the time of ignition



- average duration of the combustion, time of ignition to the CAD of maximum pressure
- average amount of NO at EVO
- average amount of hydrocarbons at EVO

Values chosen for the parameters in the investigation were

- $\tau = [0.001, 0.015, 0.025, 0.035]$
- $\text{Stocon} = [10, 20, 30, 40]$

The time step size was set to 0.5 CAD and the number of particles to 200.

## Definitions of the studied result parameters

**Variation in maximum pressure** is defined as the difference in pressure between the cycle with the highest maximum pressure and the cycle with the lowest maximum pressure, see Figure 5.6. This measure is in principle a measure for the cyclic variations, discussed in the previous chapter.

$$\Delta P_{max} \equiv \text{MAX}\{P_i\} - \text{MIN}\{P_i\}$$

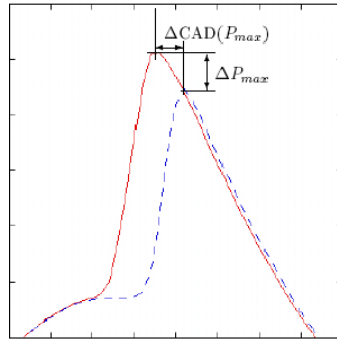


**Figure 5.6** Illustration of the difference in pressure between two cycles.

**Average maximum derivative of the pressure** is the average of the maximum pressure derivative in each cycle, see Figure 5.7. The derivative of the pressure is calculated using the *three point formula*.

$$\left. \frac{\partial P}{\partial \text{CAD}} \right|_x = \frac{1}{2 \cdot \Delta \text{CAD}} \left( -f(x+2h) + 4f(x+h) - 3f(x) \right)$$

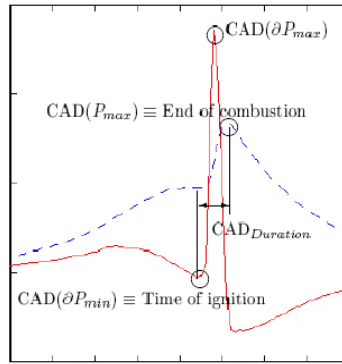


*Figure 5.7 Comparison between the pressure (dashed) and the derivative of the pressure (solid) with the important points and intervals marked.*

**Average CAD of maximum pressure** is calculated by first finding the CAD which gives the maximum pressure for each cycle then taking the average.

**Average CAD of maximum pressure derivative** is found by the same method as the average CAD of maximum pressure.

**Time of ignition** is defined as the point when the pressure starts increasing due to the combustion. This point is found by studying the derivative of the pressure and finding the minimum before the maximum pressure, see Figure 5.7. The CAD of this minimum becomes the time of ignition. This method will not work for cases where the ignition occur so early that the pressure derivate do not change sign.

**Duration of combustion** is defined as the difference in CAD between the CAD of maximum pressure and the time of ignition.

**Amount NO and hydrocarbons at EVO** is taken as the value of the specific species at the final time step.

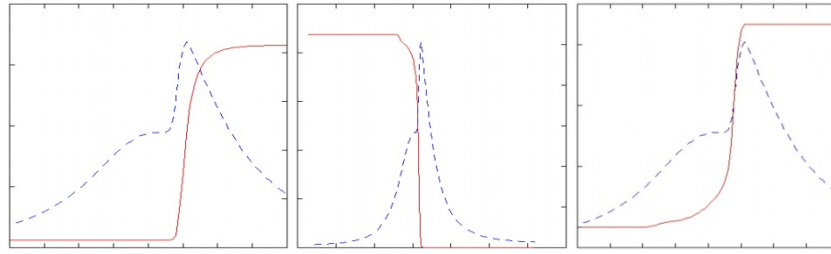


**Figure 5.8** Left: The amount of NO (solid) with the pressure (dashed). Center: The amount of hydrocarbons (solid) and the pressure (dashed). Right: The mass fraction burnt (solid) with the pressure (dashed).

### Statistical analysis methods

To characterize the influence from Tau and Stocon respectively on the different results the Pearson correlation coefficient was used.

Pearson correlation coefficient gives the linear dependency on the results from the in-parameters. The correlation coefficient can have a value between -1 and 1 where -1 is a perfect negative linear relation and 1 is perfect positive relation. For a correlation value larger than 0.5 (or smaller than -0.5) there is a large positive (negative) correlation. For values between 0.3 and 0.5 there is an average correlation, for values between 0.1 and 0.3 there is a small correlation and for values smaller than 0.1 there is no linear correlation. The coefficients are calculated by fixing one of the parameters and varying the other, giving four different coefficients for each parameter and result.

## Results

### Variation in maximum pressure

The variations in maximum pressure (Figure 5.9) are in general of the same magnitude, except for cycles with low tau where they become 3-4 times as large. The correlation coefficients for stocon are inconclusive due to the small change in the variation. For tau they are large negative.

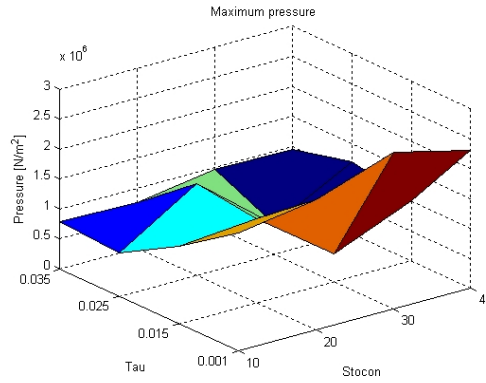


**Figure 5.9** The variations of the maximum pressure for the different values of tau and stocon.

Studying the ratio between the difference in maximum pressure and the average maximum pressure, a clear relation appears (Figure 5.10). The correlation coefficients are large negative for tau and large positive for stocon.

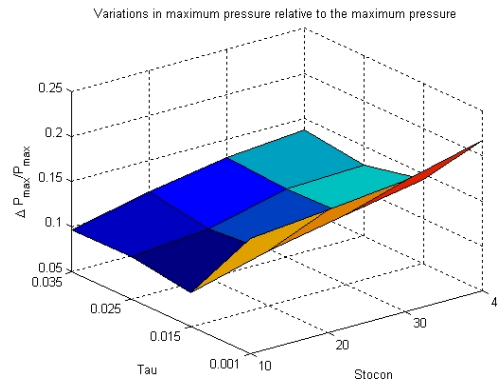


**Figure 5.10** The variations of the maximum pressure relative to the average maximum pressure.

## CAD of maximum pressure

The CAD of maximum pressure gets clearly delayed with decreasing tau and increasing stocon (Figure 5.11). The correlation coefficients are large positive for tau and large negative for stocon.

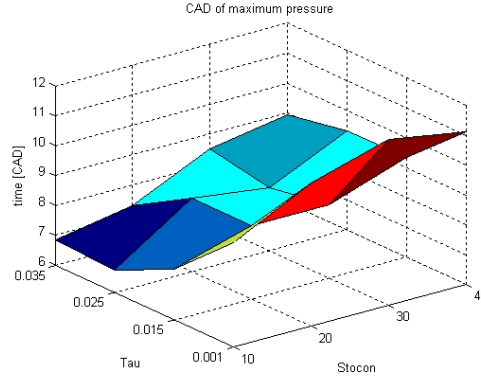


*Figure 5.11 The CAD for the maximum pressure for the different tau and stocon.*

## Maximum derivative of the pressure

Clear trends are seen in Figure 5.12. Large stocon and small tau gives a high derivative in the pressure. In the other end, small stocon and large tau, gives small pressure derivative. These trends are also seen in the correlation coefficients. For tau the correlation is large negative and for stocon it is large positive.

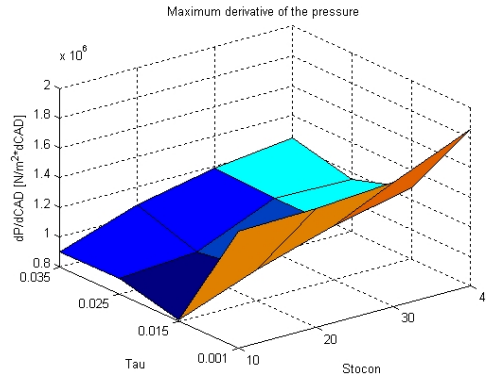


*Figure 5.12 The maximum derivative of the pressure for the different tau and stocon.*

### CAD of maximum derivative of the pressure

Studying the CAD of the maximum derivative of the pressure in Figure 5.13 the dependence on stocon is stronger than on tau. For larger stocon the CAD for maximum derivative of the pressure becomes later. The correlation is large positive for stocon and large negative for tau.

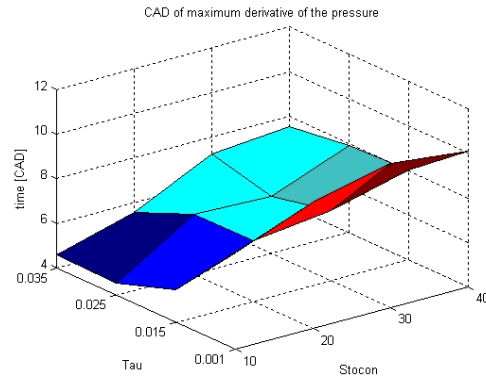


*Figure 5.13 The CAD for the maximum derivative of the pressure for the different tau and stocon.*

### Time of ignition

From the time of ignition in Figure 5.14 it is clear that it becomes later for homogenous mixing. The correlation coefficients are large positive for stocon and large negative for tau.

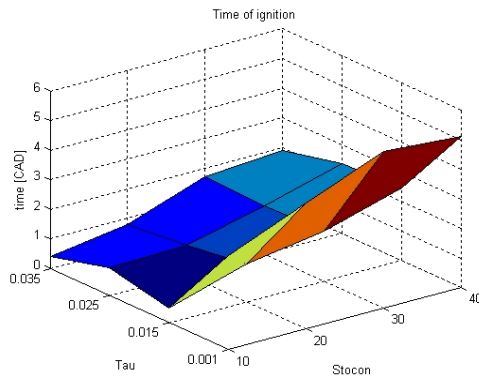


*Figure 5.14 The time of ignition for the different tau and stocon.*

## Duration of combustion

The dependencies for the duration of combustion are not clear. It is quite chaotic as seen in Figure 5.15. The correlation coefficient for tau is average positive and inconclusive for stocon.

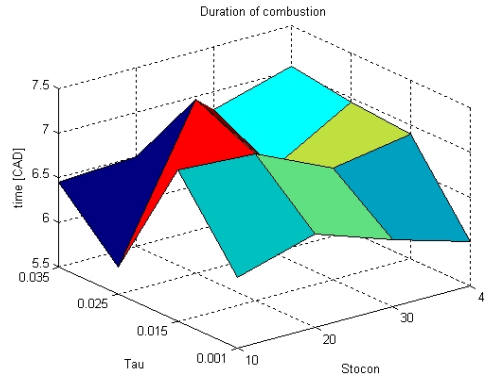


*Figure 5.15 The duration of combustion for the different tau and stocon.*

## Amount of NO at EVO

With increasing stocon and decreasing tau the amount of NO in the exhaust decreases. The effect from stocon is stronger. For the correlation coefficients it is large positive for tau and large negative for stocon.

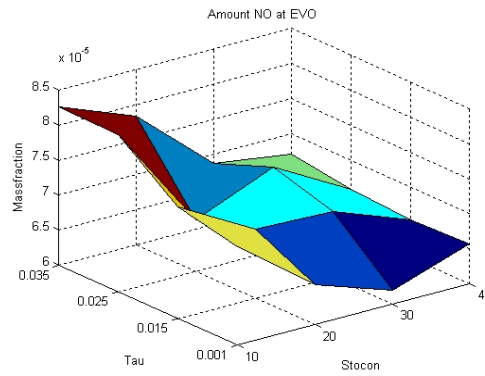


*Figure 5.16 The amount of NO for different tau and stocon*

### **Amount hydrocarbons at EVO**

The amount of hydrocarbons at EVO is basically insensitive to changes in  $\tau$  and  $\text{stocon}$ .

### **Conclusions**

With low  $\tau$  the in-cylinder conditions become homogeneous faster. High  $\text{stocon}$  spreads the heat transfer over a larger portion of the in-cylinder gas, leading to less inhomogeneous conditions. The results indicate that inhomogeneities promote earlier ignition and thus a more stable operating condition and less cyclic variations (defined as pressure variations). The pressure derivative is in general terms decreased with inhomogeneous conditions. The value of  $\tau$  or  $\text{stocon}$  does not have any major impact on the duration of combustion or the amount of hydrocarbons and NO at EVO.

The reason to do several cycles for each value of  $\tau$  and  $\text{stocon}$ , is to be able to get the average of the stochastic variations and also to be able to study range of the stochastic variations. Here one assumption was made: 10 cycles will give the statistical distribution of the variations. With the combinations of  $\tau$  and  $\text{stocon}$  that give large variations 10 cycles may not be enough to give the statistical distribution. More cycles may be needed to give the necessary statistics.

In the cases where there was an impact on the result from varying the parameters the correlation was large, for  $\text{stocon}$  often larger than 0.9. For  $\tau$  it was more in the range of 0.7. The sign of the coefficients in all cases were opposite to each other. One interesting note is that even for results with little dependence on the value of the parameter, the coefficients become quite large. In these cases the variations between each coefficient is also large. If the simulations would have been done with more closely spaced values for the parameters, thus giving a larger amount of data to work with, the correlations in these cases would probably have been lower and more coherent.

The main disadvantage of the Pearson correlation coefficient is that it only gives information on how linear the dependency between the variables is.



## Stochastic Reactor Models for Engine Simulations

---

### Correlation coefficients

*Table 5.4 Correlation coefficients.*

Stocon 10 Tau 0.035	Stocon 20 Tau 0.025	Stocon 30 Tau 0.015	Stocon 40 Tau 0.001
Variations of maximum pressure			
0.67	-0.55	0.10	0.82
-0.94	-0.93	-0.69	-0.84
Variations of maximum pressure relative the average pressure			
0.97	1.00	0.96	0.98
-0.78	-0.80	-0.80	-0.85
CAD of maximum pressure			
0.81	0.95	0.89	0.98
-0.93	-0.95	-0.81	-0.91
Maximum derivative of the pressure			
0.87	0.99	0.91	0.97
-0.76	-0.76	-0.80	-0.84
CAD of the maximum derivative of the pressure			
0.84	0.98	0.92	0.97
-0.91	-0.94	-0.80	-0.91
Time of ignition			
0.91	0.99	0.95	0.97
-0.83	-0.89	-0.83	-0.90
Duration of combustion			
-0.69	-0.79	0.45	0.97
-0.17	0.11	0.71	0.89
Amount NO at EVO			
-0.73	-0.95	-0.78	-0.97
0.93	0.80	0.74	0.72
Amount HC at EVO			
0.80	-0.77	0.90	-0.77
0.24	-0.92	-0.82	-0.91

How to read the table:

For each upper row stocon is fixed at a value and tau is varied. The first column gives the coefficient when stocon is set to 10, second column when stocon is 20 and so forth. For each lower row tau is fixed and stocon is varied. Each point represents the correlation coefficient of 40 calculations.

### ***5.1.3 Effects of discretization; time step size and number of particles***

In the previous section, the effects of different heat transfer and mixing on cyclic variations and other important result parameters were examined. Cyclic variation is a natural phenomenon in engines which can be assessed with the SRM. But when the discretization is too coarse, the cyclic variation in the SRM may be promoted in an unnatural way. To determine the level of sufficient discretization the length of the time step and the number of particles are changed. Since both of these parameters have a major impact on the calculation time it is desirable to choose these such that the calculation time is minimized but still not to lose any accuracy in the model. It has to be assumed that a low time step and large number of particles gives higher accuracy in the model.

#### **Method**

When studying the effect of different time steps and number of particles it was chosen to be done for 5 pairs, points, of tau and stocon. These were chosen to be the four corners and the center (in the tau/stocon parameter investigation):

- Corners (tau, stocon): (0.001, 10); (0.001, 40); (0.035, 10); (0.035,40)
- Center: (0.020, 25)

The length of the time step ( $\Delta CAD$ ) was given the values [0.1, 0.2, 0.5, and 1.0] and the number of particles was chosen as [100, 200, 500, and 1000]. The time for a run of 10 simulations was also studied.

For each choice of  $\Delta CAD$  and the number of particles, 10 simulations will be run and the results presented are the average in that set. So for each point there will be a total of 160 simulations and total in this investigation 800 simulations.

## Results

### Variations in maximum pressure

The variations in maximum pressure have a similar dependence for all 5 points. It increases with approximately  $10^6 \text{ N/m}^2$  when the number of particles is decreased and is independent on  $\Delta\text{CAD}$ . The size of the variations is in the order of  $10^6 \text{ N/m}^2$  for the points with low tau or stocon and in the order of  $10^6 \text{ N/m}^2$  for the other 2 (Figure 5.17).

Studying the variations in maximum pressure relative to the average maximum pressure gives another uniform behavior. It is slightly dependent on the number of particles, decreases with larger number of particles, and decreases slightly with the longer time step. The size of the decrease is higher for low tau and high stocon, where it is 0.18 (between 0.29 and 0.47), and smaller for high tau and low stocon, about 0.1 (between 0.14 and 0.24)

### Maximum derivative of the pressure

The maximum derivative of the pressure behaves as the difference in maximum pressure relative to the maximum pressure, the main dependence is on the length of the time step. When the length of the time step is decreases from 1.0 to 0.1 the maximum derivative of the pressure increases with approximately  $10^6 \text{ N/(m}^2 \cdot \text{CAD)}$

### CAD of maximum pressure

The CAD of maximum pressure is mainly dependent on  $\Delta\text{CAD}$  and the dependence on the number of particles is irregular. As  $\Delta\text{CAD}$  decreases the CAD of maximum pressure is delayed up to 1.5 CAD for every point, except for tau=0.001 and stocon=10 where there are no dependencies at all.

### CAD of maximum derivative of the pressure

The results are inconclusive, since in every point the CAD for maximum derivative of the pressure behaves differently. However, the variations are sufficiently small,  $<1 \text{ CAD}$ , to be considered constant.

### Time of ignition

For the lower tau the time of ignition increases with both the number of particles and the time step. The increase from  $\Delta\text{CAD}$  is twice as large as the increase from the number of particles. Total increase for tau=0.001 is 4CAD. For higher tau the result becomes more irregular and should be considered constant. The variations for these points are between 1CAD and 3CAD.

### Duration of combustion

Do to the complex definition of the duration of combustion ( $\text{CAD}_{\text{Pmax}} - \text{CAD}_{\text{Ign}}$ ) the result becomes complex as well. For tau=0.001 there is a very small influence on the number of particles,

the duration of combustion becomes shorter for larger particle numbers. The dependence on  $\Delta CAD$  is far more dominant since for shorter time steps the duration of combustion becomes longer. The variation is quite large, 3CAD. When  $\tau$  increases the behavior shifts. For the time step it reverses, being almost independent for  $\tau=0.020$ , so the duration of combustion increases with larger  $\Delta CAD$ . The influence from the number of particles becomes larger but the result in general more chaotic. For the point  $\tau=0.035$  and  $stocon=10$  the variations is again 3CAD but for the other two less than 1CAD.

### **Amount NO at EVO**

The mass fraction of NO decreases by  $10^{-5}$  with longer time steps for all points. Changing the number of particles alters the result only very slightly.

### **Amount hydrocarbons at EVO**

The amount of hydrocarbons at EVO is independent of both the length of the time step and the number of particles. Only a very slight decrease in hydrocarbons with smaller time step can be detected, but it is in the order of 1-2% of the value. With these small values the amount of hydrocarbons at EVO will be taken as constant. Also some simulations with abnormal high values were found, mostly because the amount of hydrocarbons in one of the cycles became much larger due to misfire.

### **Conclusions**

If one assess the range of cyclic variation in pressure, the variation decreases with the number of particles to level out in the range of 500 to 1000 particles. To really decide if this is true a range of simulations with 400, 600, 800 and 1200 particles could be needed to perform. Judging from the other result parameters it feels safe to say that for this HCCI-SRM configuration a reasonable number of particles should be 500. Regarding the timestep size the results are not so clear. For many of the parameters a time step size of 0.5 CAD seem to be sufficient, but for some, notably time of ignition and combustion duration, results for 0.2 CAD show slightly different results compared to both 0.5 CAD and 0.1 CAD time step size. Still the conclusion is that a time step size of 0.5 CAD seems to be a sufficient choice. Nevertheless, studying the average values, the variations due to coarse discretization is smaller than the changes of the heat transfer and mixing parameters. Thus it feels safe to conclude that even with such coarse discretization the trends from the HCCI-SRM are correct. For studies of cyclic variations the discretization need to be of higher resolution, 500 particles and 0.5 CAD time step size, to give trustworthy results.

The trends observed in the previous section are also confirmed in the section. More homogeneous conditions, through lower  $\tau$  and higher  $stocon$ , lead to increasing cyclic variations, delayed ignition timing and higher pressure rates. Values of HC and NO are in principle not much

## Stochastic Reactor Models for Engine Simulations

---

affected, except for HC that rocket when individual cycles misfire and affect the mean values (Figure 5.24).

All graphs and tables are ordered as in the figure below.

Tau	=	0.035
Stocon	=	10

Tau	=	0.035
Stocon	=	40

Tau	=	0.020
Stocon	=	25

Tau	=	0.001
Stocon	=	10

Tau	=	0.001
Stocon	=	40

## Chapter 5 The HCCI-SRM

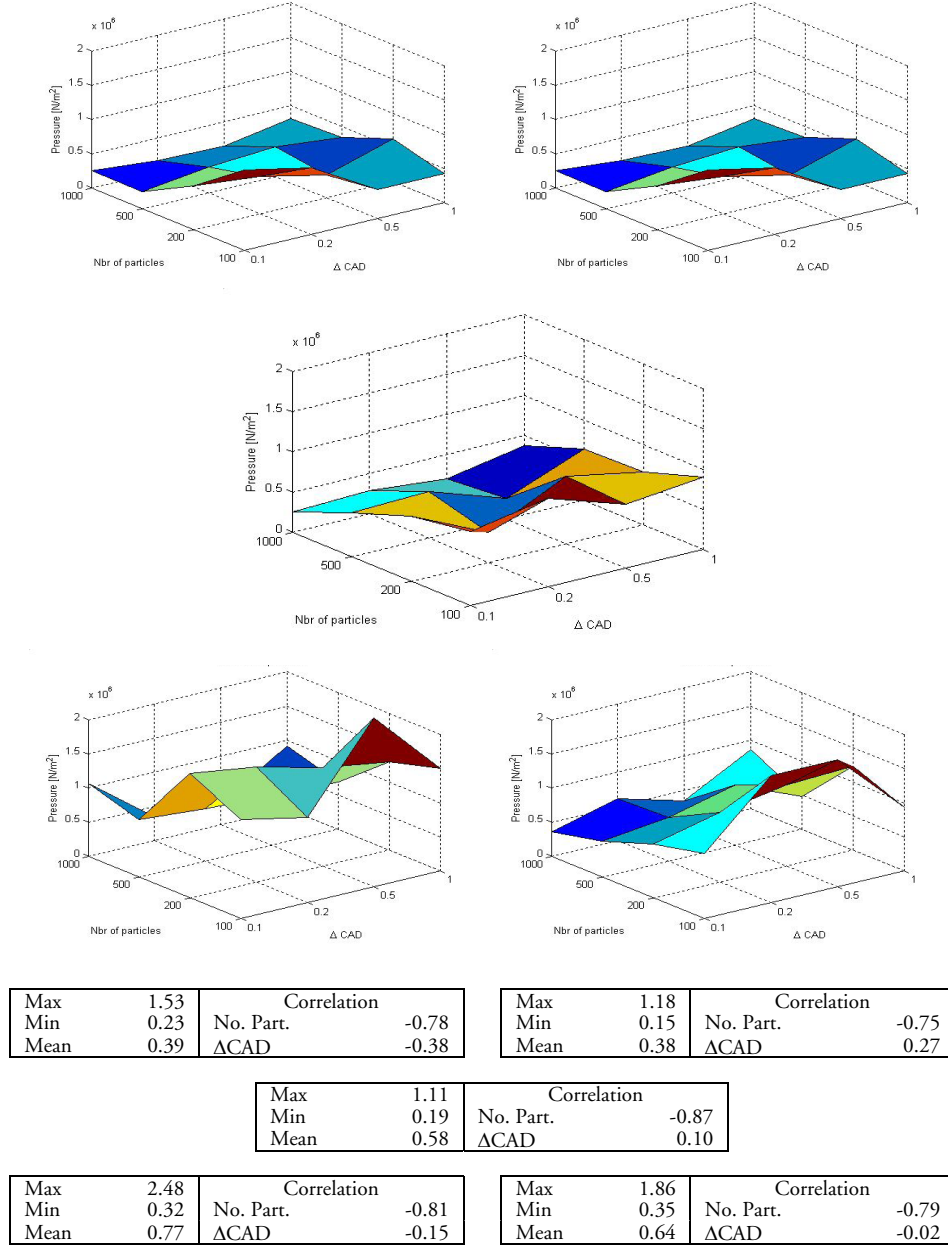
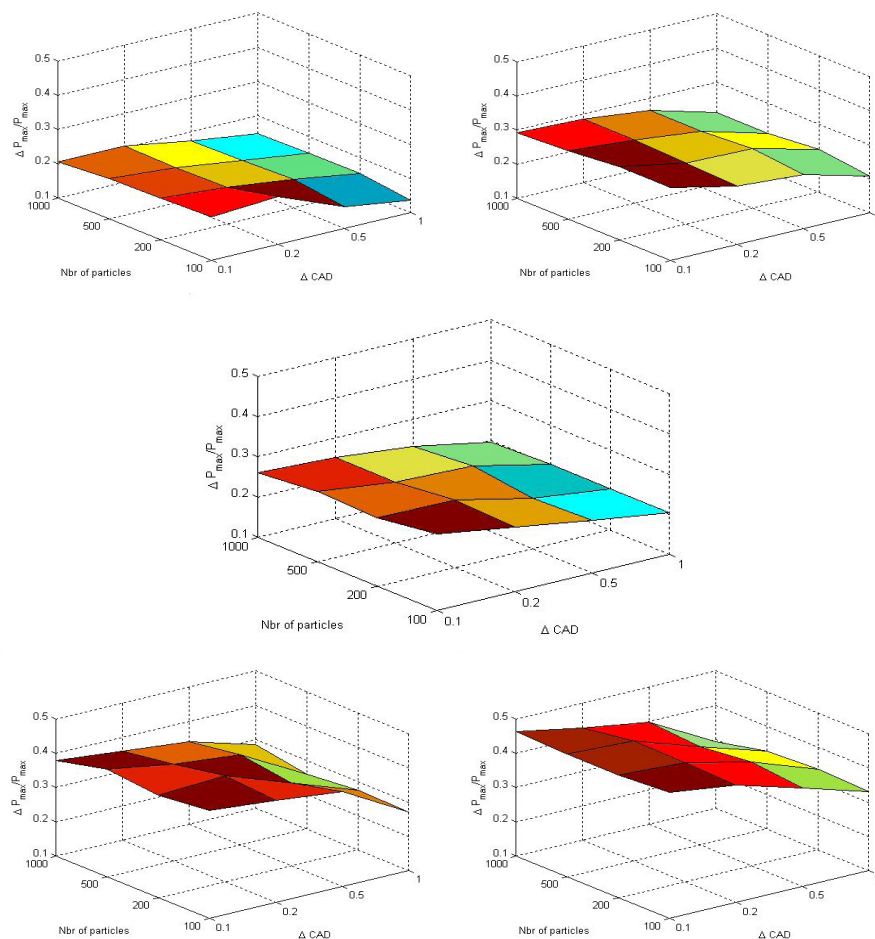


*Figure 5.17 Variations in maximum pressure. Values are in  $10^6$  N/m<sup>2</sup>.*

# Stochastic Reactor Models for Engine Simulations



Max	0.24	Correlation	
Min	0.13	No. Part.	-0.46
Mean	0.20	$\Delta CAD$	-0.98

Max	0.31	Correlation	
Min	0.20	No. Part.	-0.44
Mean	0.23	$\Delta CAD$	-0.99

Max	0.29	Correlation	
Min	0.20	No. Part.	-0.58
Mean	0.25	$\Delta CAD$	-0.97

Max	0.42	Correlation	
Min	0.26	No. Part.	-0.32
Mean	0.38	$\Delta CAD$	-0.97

Max	0.47	Correlation	
Min	0.29	No. Part.	-0.13
Mean	0.45	$\Delta CAD$	-0.97

**Figure 5.18** Variations in maximum pressure relative to the average pressure. A Value of 1 corresponds to variations in pressure equal to the average maximum pressure. Higher than 1 then the variations is larger than the average.

## Chapter 5 The HCCI-SRM

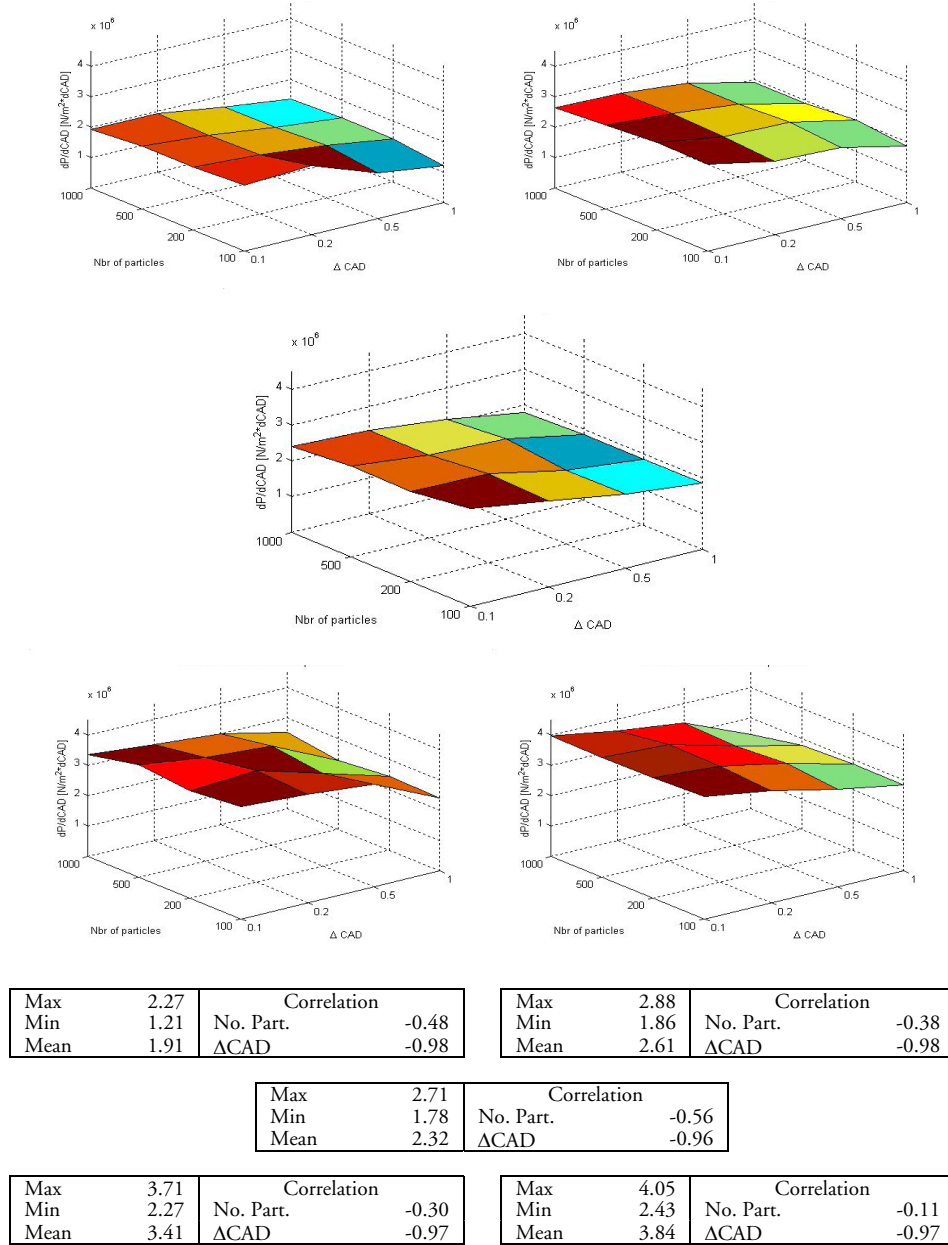


*Figure 5.19 Maximum derivative of the pressure. Values are in  $10^6 \text{ (N/m}^2\text{CAD)}$ .*



# Stochastic Reactor Models for Engine Simulations

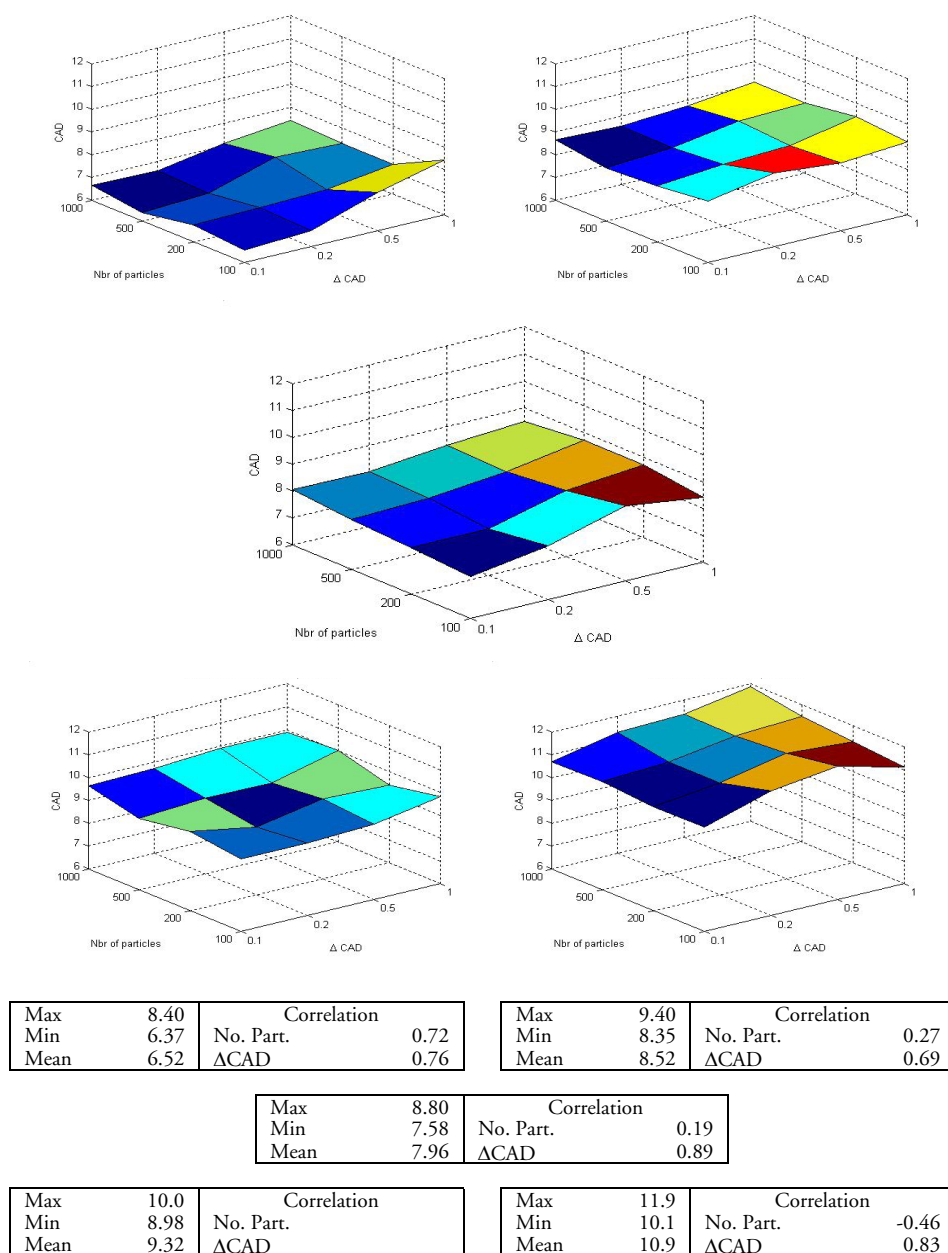


**Figure 5.20** CAD of the maximum pressure. Values are in CAD, where 0 CAD equals TDC.

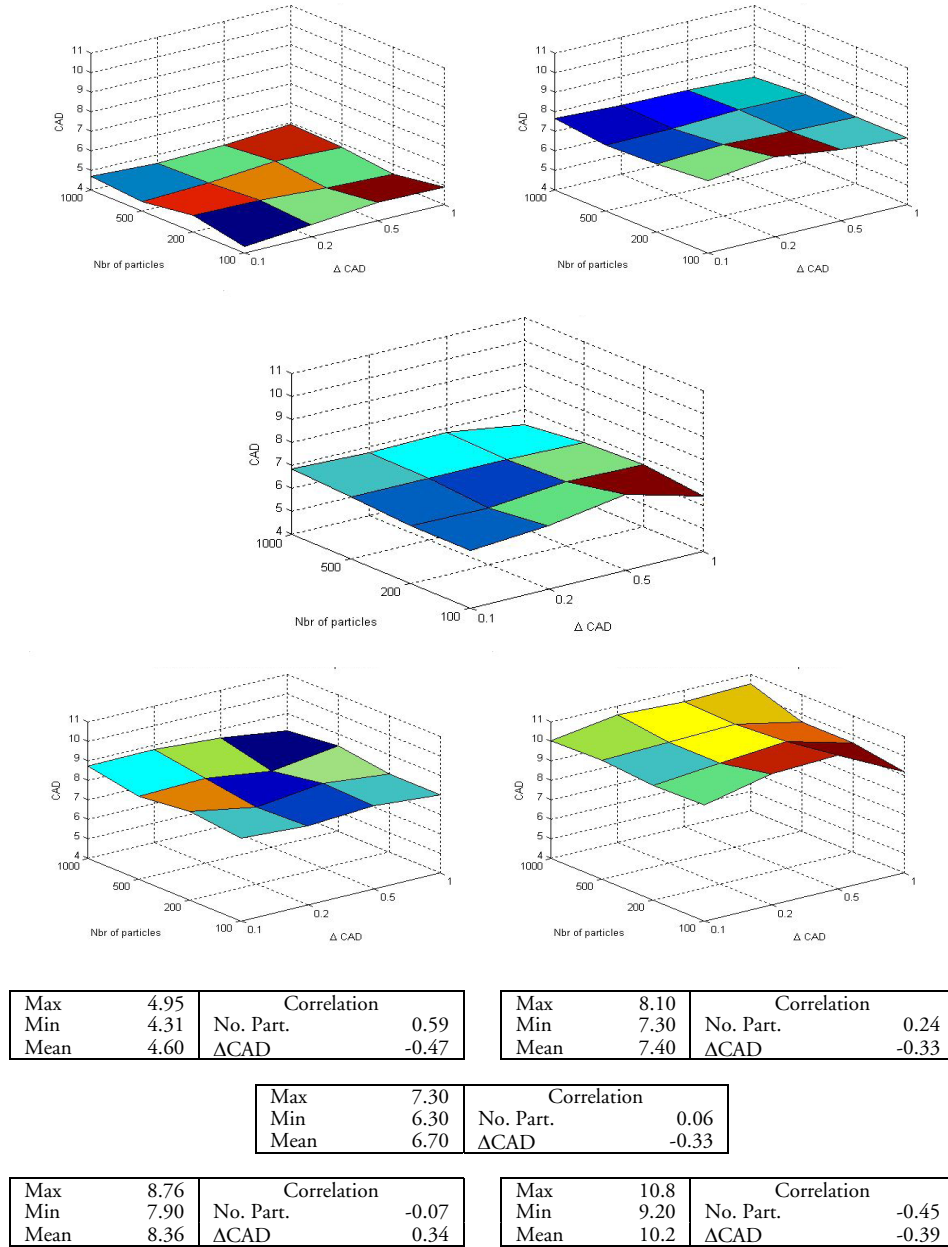


**Figure 5.21** CAD of the maximum derivative of the pressure. Values are in CAD, where 0 CAD equals TDC.

# Stochastic Reactor Models for Engine Simulations

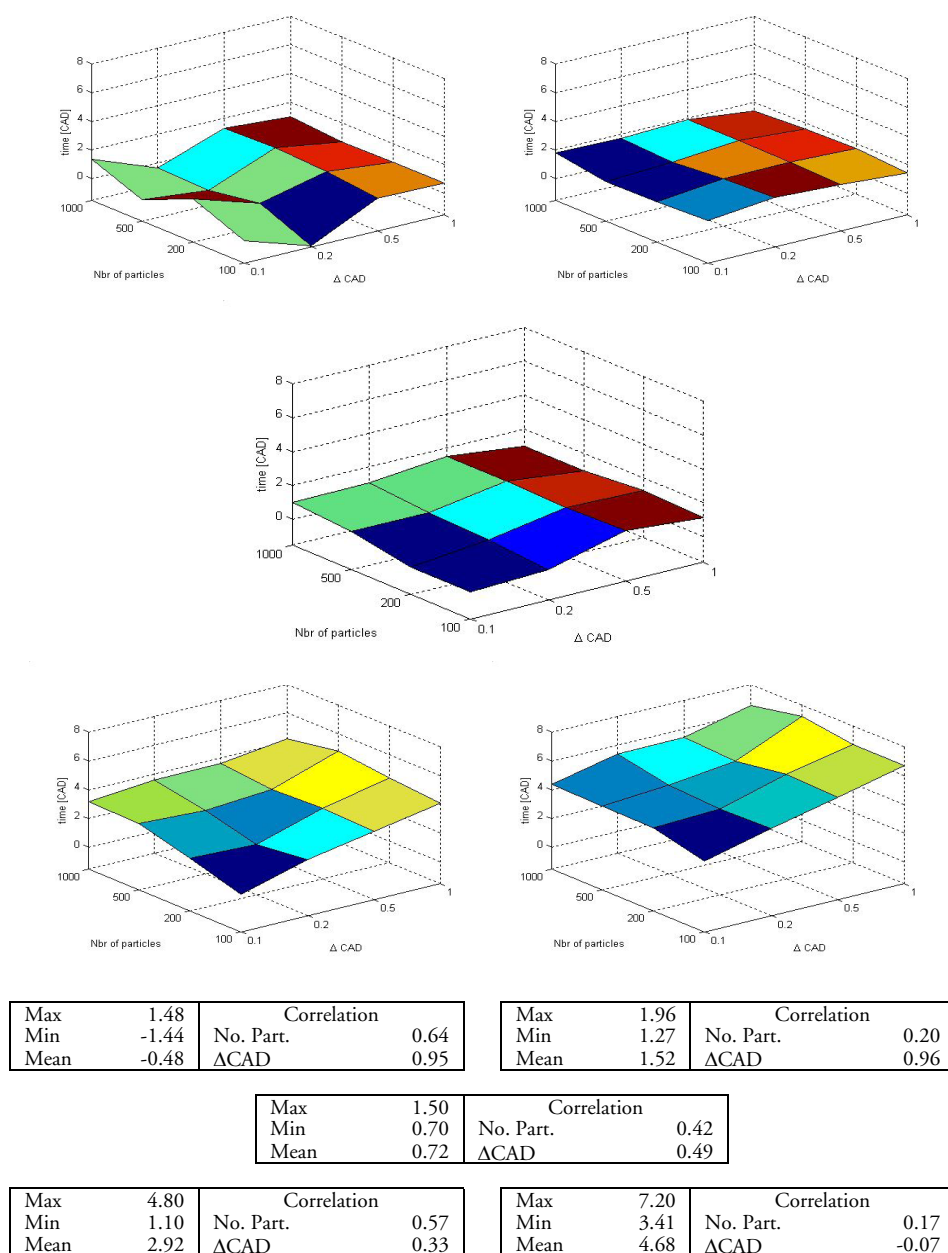


**Figure 5.22** Time of ignition. Values are in CAD, where 0 CAD equals TDC.

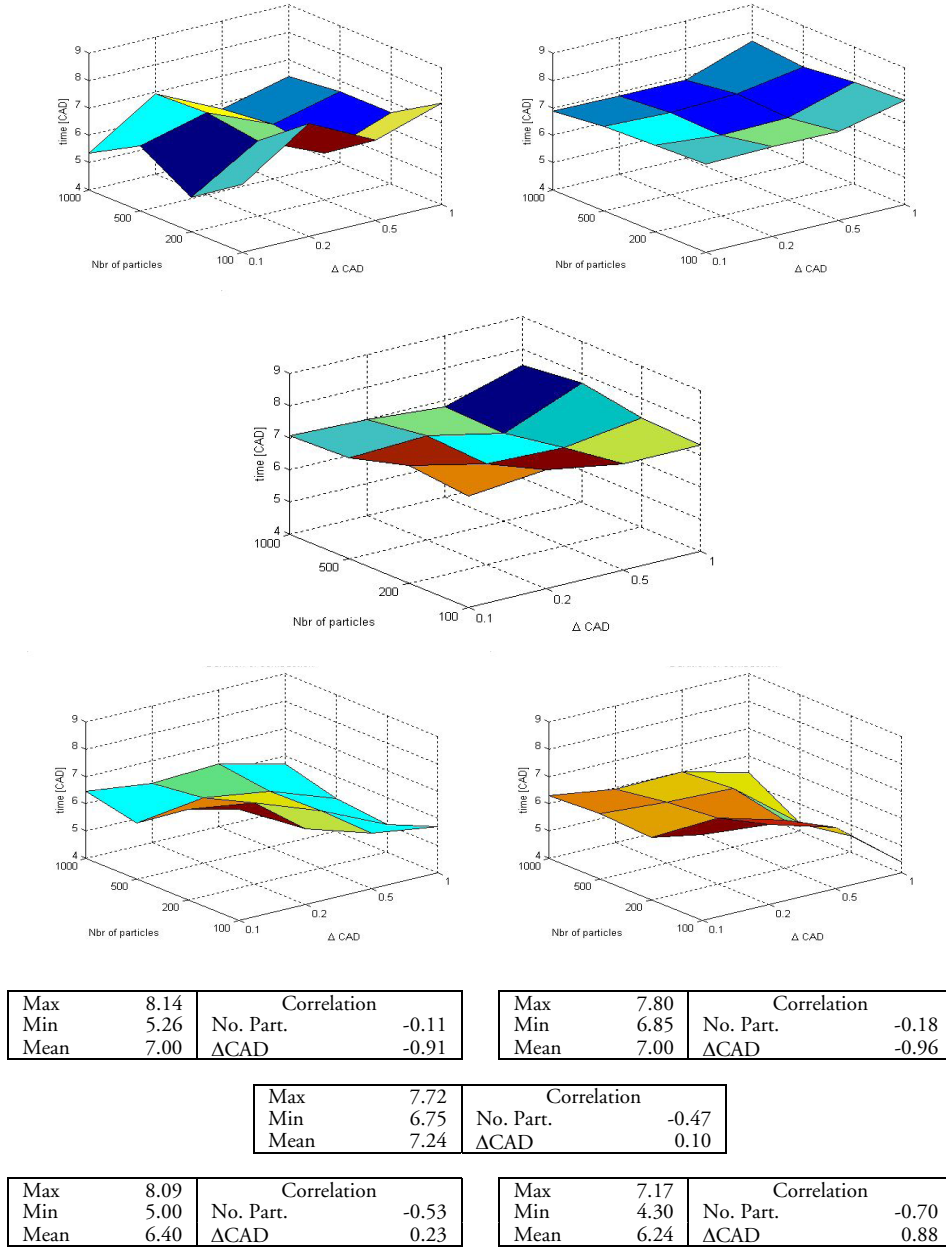


**Figure 5.23** Duration of combustion. Values are in CAD, where 0 CAD equals instantaneous combustion.

# Stochastic Reactor Models for Engine Simulations

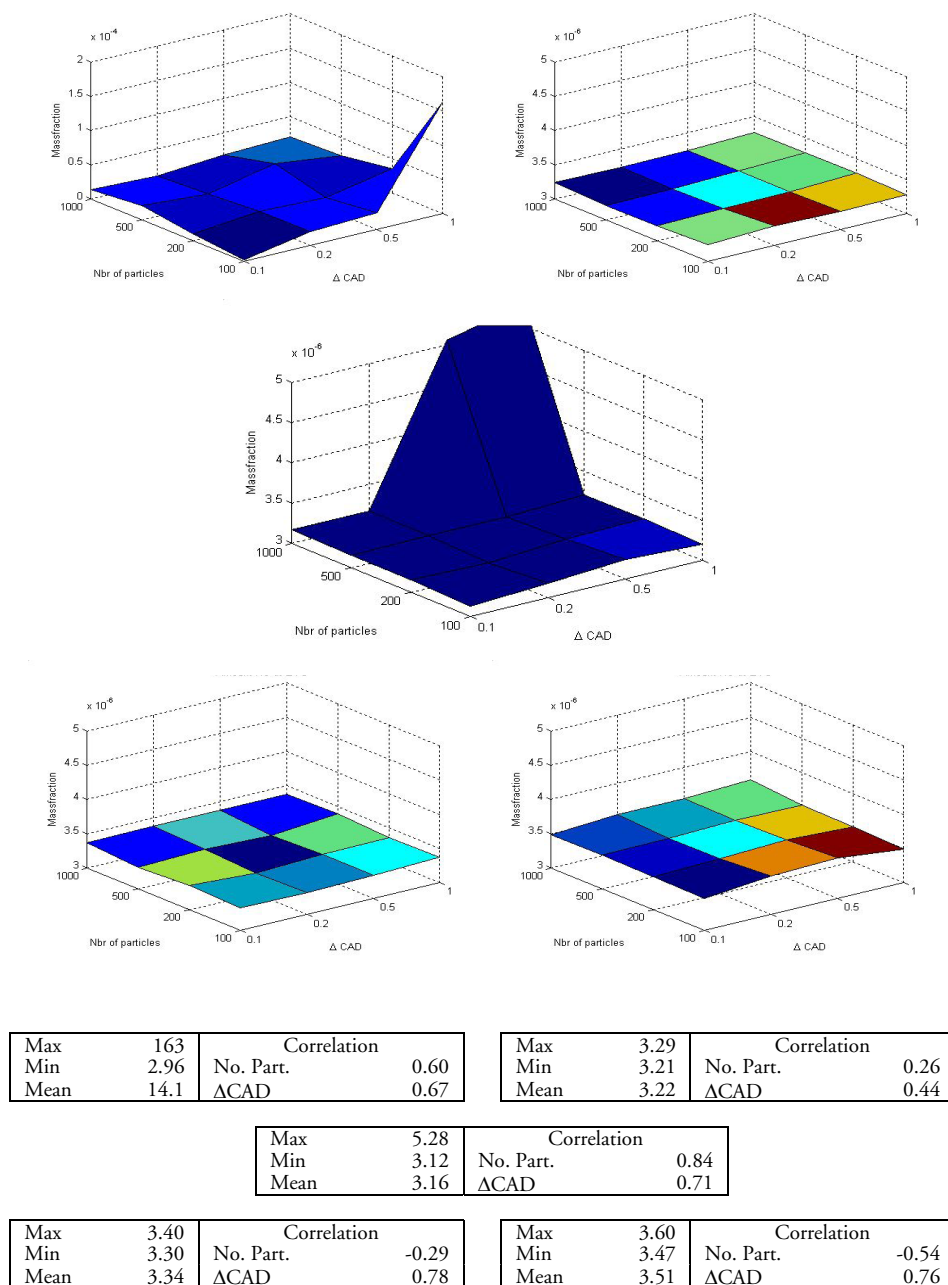
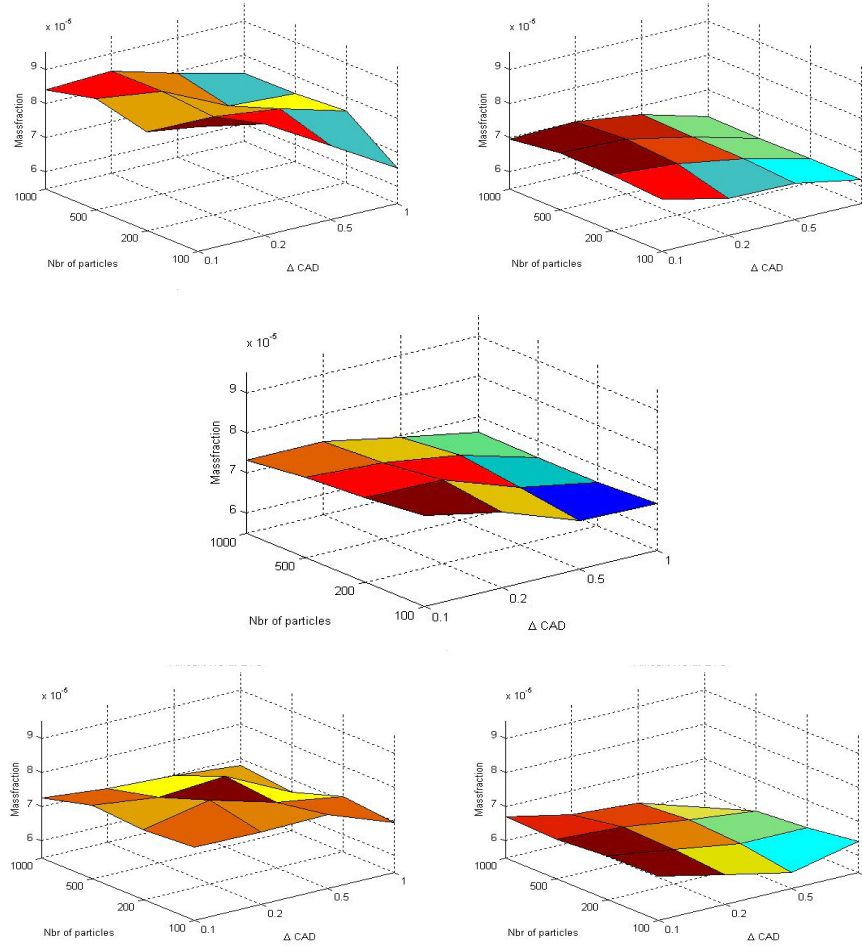


**Figure 5.24** Amount of hydrocarbons at EVC. Values are in  $10^{-6}$  mass fractions. Note that the scale of the upper left figure has values in  $10^{-4}$  mass fractions, two orders of magnitude greater.

## Chapter 5 The HCCI-SRM



Max	9.16	Correlation	
Min	6.53	No. Part.	-0.79
Mean	8.50	$\Delta$ CAD	-0.89

Max	7.17	Correlation	
Min	6.18	No. Part.	-0.45
Mean	7.09	$\Delta$ CAD	-0.79

Max	7.77	Correlation	
Min	6.58	No. Part.	-0.34
Mean	7.39	$\Delta$ CAD	-0.96

Max	7.39	Correlation	
Min	6.62	No. Part.	-0.08
Mean	7.42	$\Delta$ CAD	-0.97

Max	6.80	Correlation	
Min	5.58	No. Part.	0.31
Mean	6.56	$\Delta$ CAD	-0.97

**Figure 5.25** Amount of NO at EVC. Values are in  $10^5$  mass fractions.

# Stochastic Reactor Models for Engine Simulations

## Computational times

The simulations were performed on one of the cores of a Pentium 4 3.2GHz dual core, with 1GB of RAM running Windows XP Professional.

**Table 5.5** Computational times for different number of particles and time step sizes.

No. particles	Time step size CAD			
	0.1	0.2	0.5	1.0
100	28min	16min	7min	4 min
200	54 min	26min	14min	8min
500	1h 54min	51min	21min	12min
1000	3h 56 min	2h 6min	1h 6 min	41min

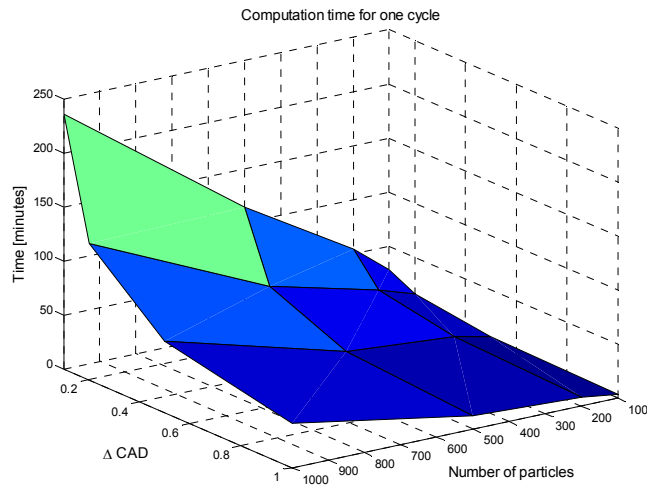


**Figure 5.26** Computational time for different number of particles and different time steps using a 3.2GHz Pentium 4 with 1GB RAM running Windows XP Professional.

### 5.2 Formaldehyde and hydroxyl in HCCI combustion

The investigation in this section is important in the sense that it demonstrates the validity of SRM codes to make predictions of individual species. Although the study is related to the species formaldehyde and hydroxyl, which were the species measured, the conclusions can be extended to cover other species related to emissions, as hydrocarbons and nitric oxides. The work described in this section is included in [28].

#### 5.2.1 Introduction

Formaldehyde ( $\text{CH}_2\text{O}$ ) and hydroxyl ( $\text{OH}$ ) radicals are known as two key species for tracing the occurrence of ignition and combustion development in engines. The knowledge on formaldehydes importance for auto-ignition goes back to Withrow and Rassweiler's engine experiments from the 1930's [44], where several investigations on knocking SI-engines were performed using a variety of optical techniques. In one of the papers, absorption spectra were measured in the end-gas, and it was concluded that absorption occurred prior to knock in a region where several groups of species, such as aldehydes, ketones and olefins absorb. In [44] the absorbing species was identified as formaldehyde. In yet another publication it was concluded that formaldehyde is seldom seen in the end-gas when no knock occurs, and also that some of the fuel-additives that inhibit or promote knock also change the amounts of formaldehyde in the end-gas, while others (actually just one, tetraethyl lead) does not. Addition of formaldehyde in the end-gas does not encourage knock either [45].

Today it is well-known that formaldehyde is formed by the decomposition of peroxyalkyls formed from slow oxygen-addition reactions at low temperatures. Formaldehyde in itself does not promote auto-ignition, rather it is a spin-off from reactions that supply initial heat and a radical pool that initiates a further development into faster reactions [46]. A number of publications cover the chemical kinetic aspects of formaldehyde formation from low-temperature reactions in knocking engines [47-52], others plunge more deeply into optical diagnostics of formaldehyde in the end-gas of knocking engines [53,54], while yet other papers describe the occurrence of hot-spots in the end-gas and aim at developing an understanding for the development of engine knock [55,57].

Currently there are not many publications yet that deal with formaldehyde and its relation to auto ignition in HCCI engines [58,59]. Conditions for auto ignition of methane in HCCI engine by adding improvers (DME or Hydrogen), have been recently investigated experimentally and by using detailed chemical mechanisms in [60] and [61] thus providing useful information about formaldehyde and hydroxyl.



Hydroxyl radicals are formed during combustion of all hydrocarbons species. The most important reaction pathways for hydroxyl formation differ with fuel, fuel-air ratio and temperature regime. For fuel species containing an OH-group, such as alcohols, some of the hydroxyl is formed directly through decomposition, but for most hydrocarbon species hydroxyl is formed from reactions in the H<sub>2</sub>-O<sub>2</sub> regime. As such, the OH can be used as indicator of the radical pool, which is by itself influenced by chain branching and chain determining reactions. This, and of course the fact that OH for some time exists in rather large concentrations, combined with beneficial spectroscopic properties, has led to that the OH radical is an often used tracer for combustion in SI-engines, when detecting the development of the flame front [62-65], as well as for gain information on the flame zones in the fuel sprays of CI-engines [66].

### 5.2.2 Engine configuration and experimental procedures

#### Experimental setup

The engine used in the experiments is a 0.5 l single-cylinder optical HCCI engine. The engine was equipped with a port-fuel injection system, which generates a mainly homogeneous charge. The fuel used was a blend of equal mass percentages of iso-octane and n-heptane, and the air-fuel ratio for all engine runs was roughly  $\lambda = 3.0$ -3.1.

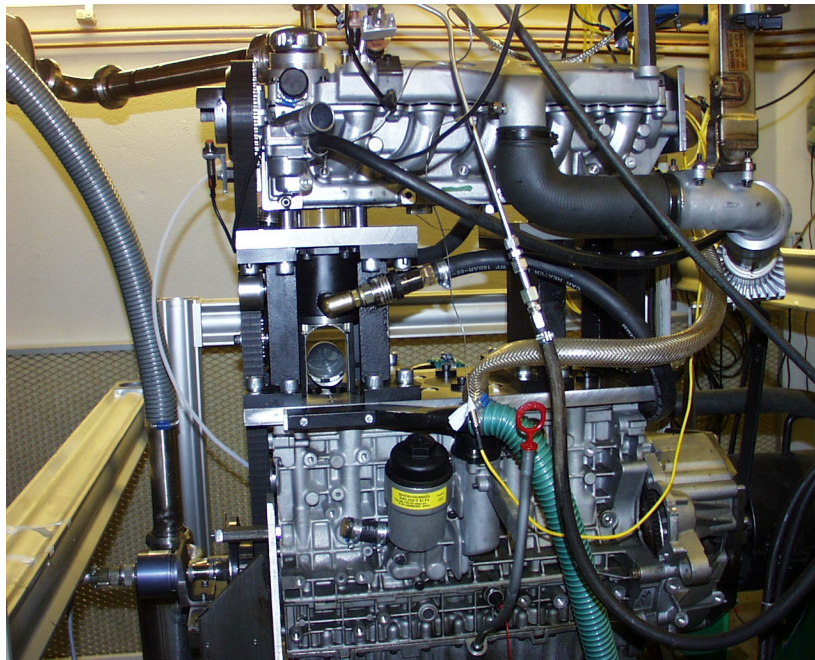


*Figure 5.27 The optical engine used for the experiment.*

## Chapter 5 The HCCI-SRM

A wide-band lambda sensor was used to measure the air/fuel ratio. In order to maintain 50% heat released at 5-6 CAD ATDC, the inlet air temperature was governed. This temperature was 120°C at startup and was decreased to 80-90°C at the end of the measurement, as more and more heat was accumulated in engine inlet and cylinder walls.

*Table 5.6 Engine specifications.*

Type	Four-valve one-cylinder optical HCCI
Engine speed	1200 rpm
Displacement (1 cylinder)	0.5 l
Bore	81 mm
Stroke	93 mm
Compression ratio	12:1
Fuel	50% isooctane 50% n-heptane

To provide optical access from below, the piston was elongated, equipped with a quartz window, and a 45° mirror was mounted beneath the transparent piston. Horizontal access to the upper part of the cylinder liner was provided through a quartz cylinder liner. Thus, the laser sheet was sent horizontally through the quartz cylinder liner, and the measured signal was detected from below through the window in the piston. The path of the laser sheet through the cylinder is as shown in Figure 5.28.

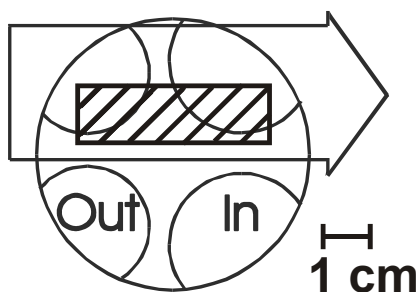


*Figure 5.28 The path of the laser beam through the cylinder.*

Two laser sources, firing in sequence with a pulse separation of 1 micro-second, are used for the two LIF measurements. The laser used for OH-LIF is working at 283 nm wavelength with 30

mJ pulse energy. The laser used for formaldehyde LIF is working at 355 nm with 75 mJ pulse energy. The two laser pulses are superimposed on top of each other and formed to horizontal laser sheets with a width of 40 mm covering half the cylinder bore. The LIF signals from the two probed species are separated before they are collected on two ICCD camera systems equipped with filters appropriate for formaldehyde- and OH LIF signal, respectively. The optical set-up of the LIF system and the engine are presented in detail in an earlier paper [67]. In that work and in references there-in additional information about the formaldehyde- and OH LIF technique can also be found.

### Experimental procedures and results

LIF measurements were performed in a time range starting well before the onset of low-temperature reactions and continuing beyond the major, high temperature heat release (HTHR). For every measured crank angle position 20 image-pair of LIF signals from formaldehyde and hydroxyl radicals were collected, and the corresponding pressure trace was recorded.

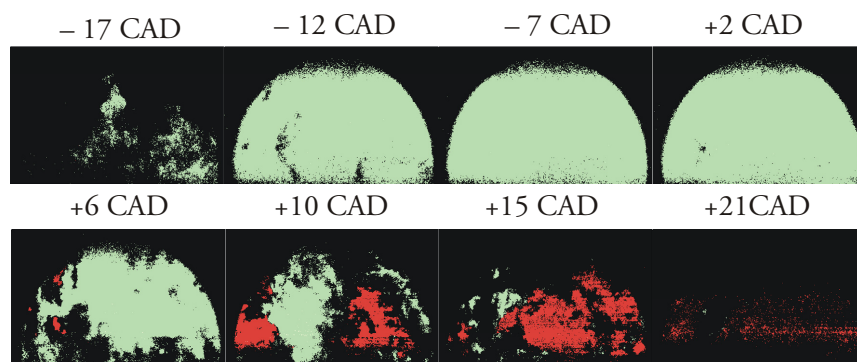


**Figure 5.29** Superpositioned LIF-images from start of low-temperature combustion till the end of high temperature regime. Formaldehyde is shown in green and hydroxyl in red. The images were digitized in order to clearly show the instantaneous structure of each species.

In order to compensate for background signals, e.g. from lubricant oil and scattered light, background images were obtained from motored cycles. This background was then subtracted from the measured signal before the data was evaluated. For clarity, the presented image-pairs of hydroxyl and formaldehyde signals were color-coded and superimposed to one single image showing the simultaneous signals of both OH and  $\text{CH}_2\text{O}$ . This allows gaining knowledge on the spatial structures of the combustion progress. In these combined images, LIF signals corresponding to formaldehyde are colored green (light-grey) while OH signals are colored red (dark-grey).

Examples of superimposed LIF images are found in Figure 5.29 and of averaged cycle resolved signals in Figure 5.30.

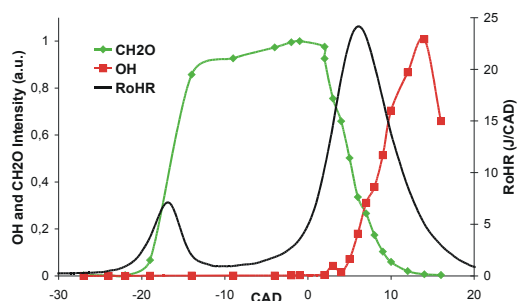


**Figure 5.30** Averaged experimental formaldehyde and hydroxyl signals, and heat release. Formaldehyde and hydroxyl signals are normalized (a.u. = arbitrary units).

### Conditional filtering of LIF-images

The maximum peaks in the measurement noise are well above 10 % of the maximum measured signal at any measurement, whereas the average noise levels are below that. A large portion of the noise found in these images origin from the CCD and amplifier in the camera used in the measurements. This noise is white noise, meaning that it is non-periodical; no specific frequency can be associated with it.

In order to generate joint probability density plots (PDP) (see “Calculation results – relative distributions of hydroxyl radicals and formaldehyde from SRM calculations” and “Calculations results – comparison of particle/pixel distributions” for more information about joint PDPs) from the LIF data, it was necessary to remove noise from the raw images. Otherwise the joint PDPs would contain information that is not useful, and the joint PDPs would display stochastic variations in the noise rather than demonstrating systematic changes in the combustion process.

Since substantial parts of the noise is white, no periodicity could be associated with it and thus signal processing through Fourier transformation is not an adequate method. Instead conditional filtering was used, a straight-forward method that could easily be implemented in Matlab. If correctly implemented there are with this method only minor and less critical distortions for these images of the remaining signal. Caution must be taken however that the threshold levels are carefully distributed and set, otherwise the filtering will give substantial impact on the PDPs. The best way to determine whether the filtering was correctly implemented is to compare filtered PDPs with unfiltered.

## Stochastic Reactor Models for Engine Simulations

---

In this method, a number of preset threshold levels for OH-signal and  $\text{CH}_2\text{O}$ -signal were set up. The threshold levels were investigated in descending order. The pixels in the LIF-images were systematically investigated and compared to surrounding pixels 2 positions away. If a pixel exceeding a certain threshold level was surrounded by two pixels in either direction also exceeding the same threshold, it was considered a signal and left retaining in the image. Otherwise the pixel signal was cropped down to the nearest lower threshold level and then again compared to its surrounding pixels.

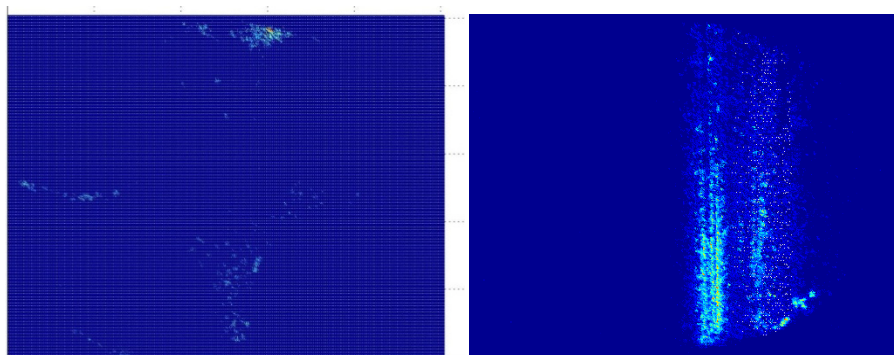


**Figure 5.31** *Left: Remaining signal from valves in  $\text{CH}_2\text{O}$ -signal at -27 CAD TDC after filtering. Right: Signal (after filtering) in the OH frequency area during the growth phase of  $\text{CH}_2\text{O}$  (-14 CAD) and thus long before the occurrence of the major heat release. Shown is a trace that was not possible to filter, remaining throughout most parts of the combustion. This signal is believed to origin from broadband dispersing ketones.*

A lowest threshold level was also set, below which no signals were considered. This lowest threshold level supposedly filters the background noise, not really related to the act of measuring but rather to the signal independent noise in the measurement equipment; CCD thermal noise, CCD on-chip electronic noise, and amplifier noise. In this case the cut-off level was set to 4% of the maximum concentration of either species.

The conditional filtering method is quite efficient, and what are only partially filtered are reflections from the contour of the valves as seen in Figure 5.31. Luckily this contribution does not affect to any noticeable degree the joint PDPs. Moreover there was also found some faint but clearly visible signal in the OH frequencies when the presence of OH was not expected (Figure 5.31). This signal occurs in the region crossed by the laser beam and starts almost where the first signs of low-temperature oxidation is found, and disappears during the main heat release. It is

believed that this signal comes from broad dispersing ketones. This signal could not be filtered away, and a visible imprint from this signal was found in the joint PDPs.

### 5.2.3 Chemical model used

The chemical kinetic model used in this work was the PLANET 2.2 kinetic mechanism [68, 69], consisting of 240 species and 2403 reactions including NO<sub>x</sub> reactions [70]. This is a semi-detailed mechanism initially designed as a decently accurate and calculation efficient kinetic model, specially developed with HCCI engine calculations in mind [71]. The mechanism uses an updated version [72] of the well-known Chevalier mechanism as a base up to the C<sub>4</sub> regime [73] whereas the C<sub>5</sub>-C<sub>8</sub> chemistry is in-house developed according to a method described by Curran et al. [74], though frequent lumping limited the total number of reactions [75].

### 5.2.4 Results and discussion

#### Results LIF-measurements

In Figure 5.29, a series of single-shot image-pairs obtained from different crank-angle positions are shown to exemplify the formation and consumption of formaldehyde and OH. In Figure 5.34 the average rate of heat-release for the case shown in figure 5.29 is presented together with the averaged and normalized LIF signals from formaldehyde and OH. It can be seen that formaldehyde is formed rapidly during the low temperature heat release (LTHR) regime. After LTHR formaldehyde signal is uniformly distributed and remains so until HTHR starts. At this point formaldehyde is consumed and holes with no signal start to appear. In places from where formaldehyde has disappeared OH start to form and as the averaged formaldehyde signal decreases, the average OH signal increases.

The formaldehyde signal was spectrally investigated in order to confirm that the detected signal originated from formaldehyde. The result from this investigation is presented in Figure 5.32 where spectrally resolved formaldehyde signal, recorded between LTHR and HTHR, is shown. The peaks that build the spectra strongly indicate that the signal originates from formaldehyde. However the spectrum has a broad structure compared to other spectra obtained at lower pressures and temperatures. This can be explained by conventional pressure broadening in combination with a temperature effect, where more energy levels get populated at higher temperatures, which lead to the broadened structure [76]. The broadened structure can also originate from the possible existence of other fluorescent species. Plausible species in this case are other aldehydes and ketones.

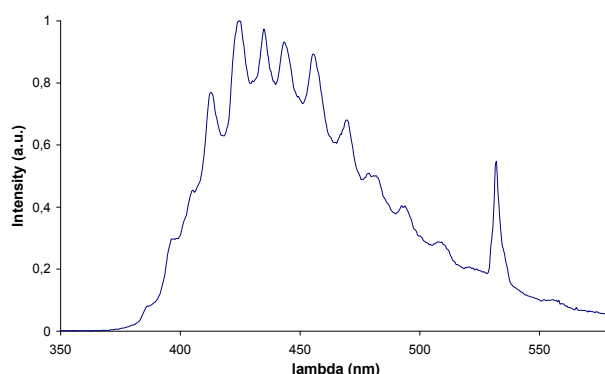


**Figure 5.32** Spectrally resolved formaldehyde signal from the HCCI cycle.

Calculations (see Figure 5.33) show that the concentrations of ketones and aldehydes are fairly low but far from negligible compared to that of formaldehyde, except for one species, acetaldehyde, whose concentration approaches that of formaldehyde. Therefore the broad structure, seen in Figure 5.32 can be explained by the pressure and temperature broadening in combination with the existence of aldehydes other than formaldehyde. However, formaldehyde is used as a tracer for intermediate species, formed from low temperature reactions in the HCCI process. Since the other acetaldehydes are also intermediate species, formed in the same process, their possible mix-up is not a problem for the investigation of the low-temperature combustion processes.

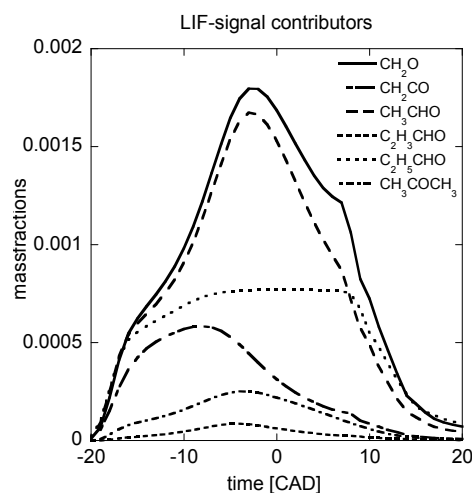


**Figure 5.33** SRM Calculated concentrations of various aldehydes and di-methyl-ketone in comparison with formaldehyde.

### Calculation results – comparison of averaged LIF-signals and calculated concentrations

Initial conditions and calculation parameters were set as in Table 5.7 unless otherwise mentioned.

*Table 5.7 Initial conditions and calculation parameters*

Initial CAD	-140 CAD
Initial pressure	0.97 bar
Initial temperature	380 K
Total number of particles	200
EGR	0 %
Mixing time $\tau$	0.015 s
Stochastic Heat Transfer Const. $C_p$	12
Compression Ratio	12.0
$T_{\text{wall}}$	475 K
Time step size	1 CAD

A direct comparison of calculation results from the stochastic reactor model calculations and measurements (see Figure 5.34) show that the calculations are correct in their general description of the combustion process and that formaldehyde and hydroxyl radical profile are in resemblance of the measurements.

Here it must be noted that in order to gain a good agreement to experiment, it was quite important to make sure that the calculations really resembles the experiments. It was found throughout the work that the better the calculations agreed to the heat release trace (Figure 5.34) the better they agreed to the averaged LIF signals.

Regarding the actual concentrations, a direct comparison is not possible to make, since the measurements are not quantified. Assuming the concentrations to be in direct proportion to the LIF signal of both species, there appears to be an error in the calculations of formaldehyde, since the shapes of the calculations and the LIF signals do not conform. Although LIF is a linear technique, the relation between signal and concentration is not necessarily linearly proportional. Temperature and pressure broadening in combination with quenching introduce deviations from the linear relation, especially at higher pressures. This together with a possible structural error in the kinetic mechanism gives an unavoidable discrepancy between the LIF measurements



and the calculations. The error in the kinetic mechanism is not easily dealt with, since experiments to which to correlate the formaldehyde profile for heptane-isooctane mixtures scarcely exist.

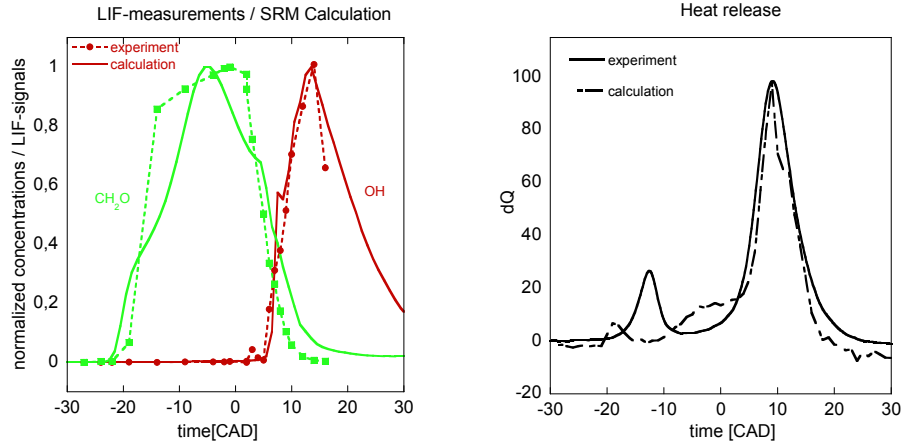


**Figure 5.34** Experimental LIF-signals of formaldehyde and hydroxyl compared to SRM calculated concentration. Heat release profiles to the right.

Further, in Figure 5.34, a discrepancy is visible also for the hydroxyl radical peak. We suspect this difference is mainly dependent on physical modeling, a suspicion that is partly confirmed by a comparison of formaldehyde and hydroxyl profiles using different mixing parameters and inlet temperature.

As seen in Figures 5.35 and 5.36, the levels of hydroxyl are very sensitive both to mixing intensity as well as inlet temperature. The formaldehyde peak on the other hand is hardly altered with these parameter changes.

As for all the SRM calculations in this work, the initial temperature distribution is set uniformly. In lack of turbulence data from the experiments the mixing intensity is adjusted. The best fit with the experimental heat release was achieved with a mixing level of 0.015 s, corresponding to full mixing in 108 CAD. The mixing intensity is sensitive, as can be seen in Figure 5.35, where the more intense mixing corresponds to 0.01 s and 72 CAD.

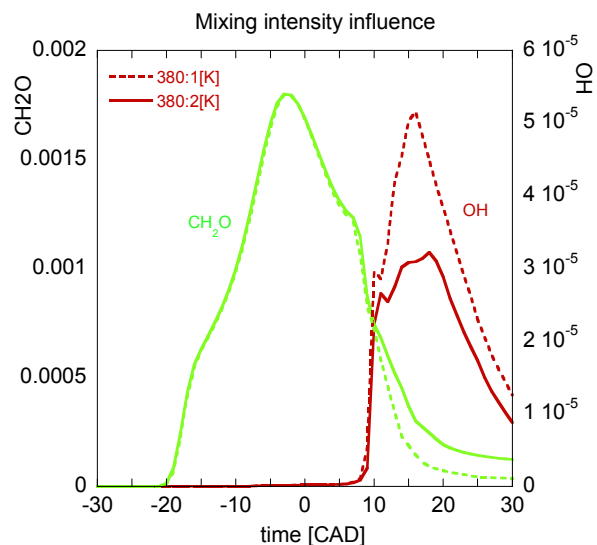


**Figure 5.35** SRM calculated formaldehyde and hydroxyl profiles for two cases using different mixing intensities. Intense mixing (380:2) leads to lower levels of hydroxyl.

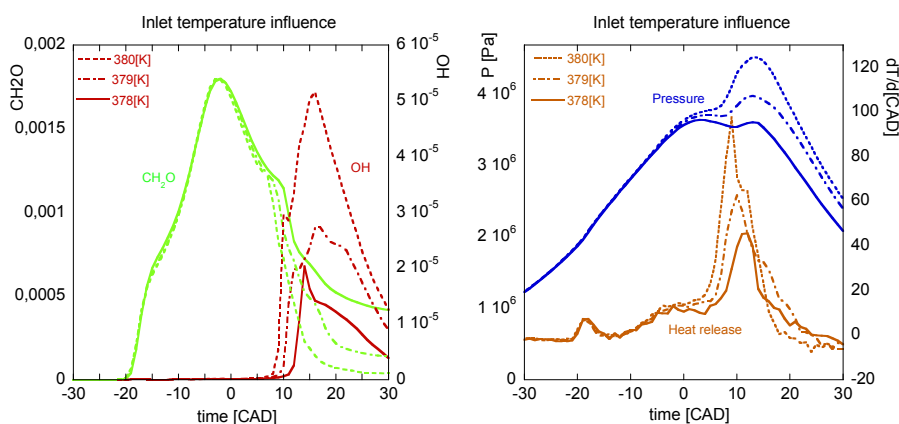


**Figure 5.36** SRM calculated formaldehyde and hydroxyl profiles for three cases using different inlet temperatures. Apparently temperature has some effect on consumption rate of formaldehyde, and a huge effect on both formation and consumption of hydroxyl. Pressure and heat release profiles for the three cases are shown to the right.

Alternative contributors to the formaldehyde LIF signal were also investigated, namely other species containing a carboxyl group ( $C=O$ ). This group of species includes different ketones and aldehydes, and a comparison of the species concentrations profiles of aldehydes are shown in Figure 5.33. It is found here that a highly probable contributor to the formaldehyde LIF is acetaldehyde, but since both species occur simultaneously in the combustion process, it will not change the outcome of attempts to characterize combustion through formaldehyde LIF.

## Calculation results – temperature dependence of species profiles

Figure 5.37 shows a series of calculations performed using the homogeneous reactor model code. Here the same set of inlet data are used for each calculations, except the calculation inlet temperature at 60 CAD before TDC, which was varied in the range 400-470 K. All three plots here represent the same data but plotted from different angles. Studied carefully, these plots show some interesting characteristics, giving valuable information of the self ignition processes in HCCI engines.

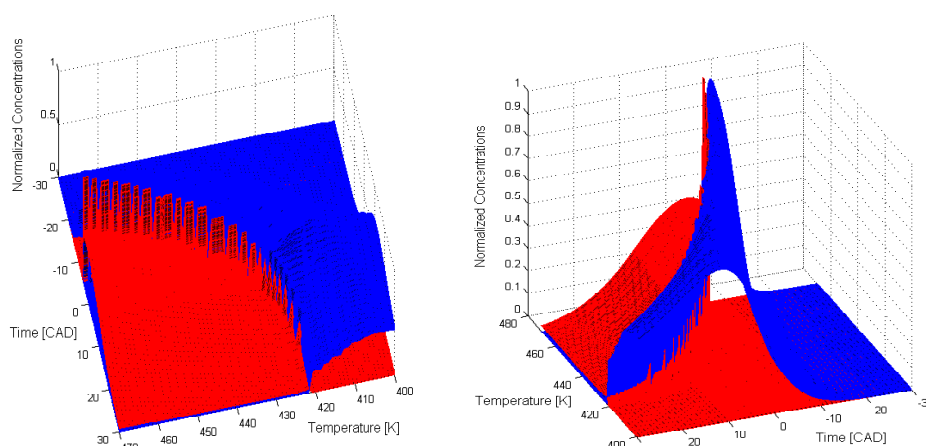


**Figure 5.37** HRM calculated concentrations of formaldehyde (dark) and hydroxyl radicals (light) plotted as function of CAD and different inlet temperatures. The spiky hydroxyl profile is a feature from the image processing, in reality this should be continuous.

First, it is noticed that the formaldehyde concentration drops meanwhile the hydroxyl radical concentration rises. If the OH-concentration curve never rises (which, of course, is the same thing as that no high temperature ignition ever occurs, and subsequently the cylinder never reaches the stage of full combustion), the formaldehyde concentrations never really drops till the temperature has decreased enough for the equilibrium concentration of the semi-unstable formaldehyde to be substantially decreased. Seen from above, the OH-concentration forms a half half-moon shape, as the ignition timing advances with start temperature. Visible is also that the

maximum concentration of OH-radicals increases substantially with raising starting temperature, whereas the concentrations of  $\text{CH}_2\text{O}$  show only minor increases with temperature.

Another interesting feature is that the rate of combustion is speeded up as the inlet temperature increases. This is expected for the OH-curve; the high-temperature ignition and the heat release from CO to  $\text{CO}_2$  conversion is known to increase with temperature, but given the negative temperature regime for low-temperature oxidation, this not obvious for the formaldehyde curve. However, Figure 5.37 clearly shows that the curve is narrowed as the inlet temperature increases. Most possibly this is due to a combined effect from low-temperature and high-temperature oxidation; the formation of formaldehyde may in some cases be punished by an increased temperature, but the consumption of formaldehyde will always be faster as the temperature rises, and thus the overall effect will be that the formaldehyde curve is narrowed with temperature.

### Calculation results – relative distributions of hydroxyl radicals and formaldehyde from SRM calculations

Figure 5.38 visualizes how the joint PDP of formaldehyde and hydroxyl works.

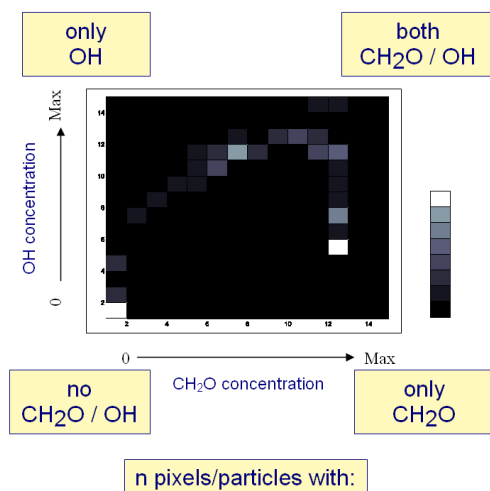


**Figure 5.38** Joint PDPs of formaldehyde concentration on the x-axis and hydroxyl concentration on the y-axis. The lighter the color of the cell relates to a higher number of particles or pixels within a specific range of concentrations of the two species.

A 14x14 array for sorting the output data from each particle is constructed, where the cells reflect the particle's distribution of OH and  $\text{CH}_2\text{O}$ , arranged in order of increasing concentration:

## Stochastic Reactor Models for Engine Simulations

The cell closest to 0 holds the particles of near zero concentration of OH and  $\text{CH}_2\text{O}$ . On the right of the x-axis we find the particles with increasing formaldehyde concentrations, and upwards on the y-axis we find cells holding particles with increasing hydroxyl concentrations. The cell limits  $C_{S,cl}$  are determined by:

$$C_{S,cl} = \frac{1.2^n}{1.2^{N_{\max}}} \cdot C_{S,\max}$$

Here S is any of the two species considered,  $N_{\max}$  is the array size, n is the cell number and  $C_{S,\max}$  is the maximum concentration of species S found in any cell during any time during the ignition.

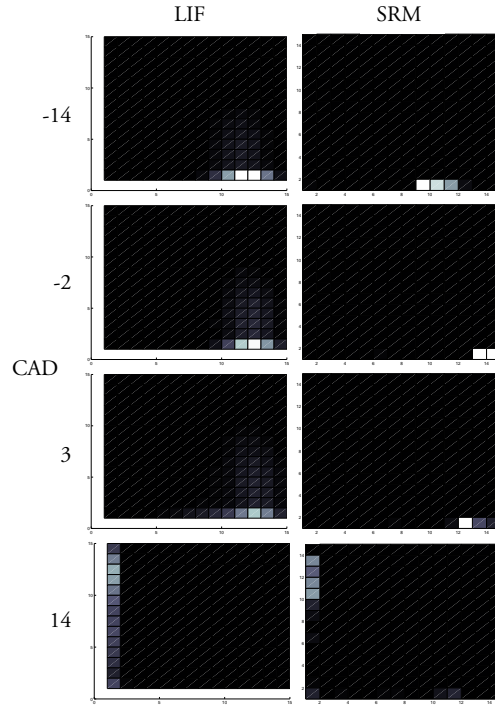


**Figure 5.39** Joint PDPs of LIF measurements on the left hand side pictures and SRM calculations on the right hand side pictures.

The resulting PDPs from the SRM calculations are showed on the right hand side of Figure 5.39. These images show how the combustion evolves over time, how the formaldehyde gradually builds up and reaches a maximum. Further we see how, during a couple of time steps, a transition stage is reached where some particles have virtually no formaldehyde at all but substantial amounts of OH, whereas other particles remain with substantial amounts of formaldehyde but

no hydroxyl radicals. We can see throughout the calculations some particles will continue having  $\text{CH}_2\text{O}$  but no OH; most likely we have partial misfire in these particles, with resulting emissions of CO and hydrocarbons. It should also be noted that the images do not show any example particles having concentrations of both OH and  $\text{CH}_2\text{O}$  beyond the lowest interval cell. This is in accordance with previous experimental findings [67]. If a more detailed mesh is used for sorting the particles, thus giving lower lowest threshold values, we will actually find a certain overlap in the lowest concentration regions.

### **Calculations results – comparison of particle/pixel distributions**

Joint PDPs of formaldehyde LIF and hydroxyl LIF pixel distributions were created in a similar way as the joint PDPs of SRM-calculations, after the image processing method described in 'Conditional filtering of LIF-images' was applied. These joint PDPs are shown in Figure 5.39, left hand side pictures.

Considering the delicate and sensitive nature of the joint PDPs, the respective PDPs show a very good resemblance, if compared step by step in the combustion build up and excluding the contribution from the broad dispersing ketones. This proves not just the validity of the SRM calculations, and also that any conclusions from joint-PDPs of SRM-calculations will be in quite good accordance with reality as long as the kinetic model used is valid and the physical modeling is carefully considered. This is important since calculation joint PDPs does not contain any noise and thus the conclusions are possible to extend beyond detection level of images. Further this is important since the approach may also be extended to other species pairs, species pairs that may be difficult to measure through optical techniques.

### **Calculations results – Temporal maximum joint PDPs**

In calculated joint PDPs in Figure 5.39 there is not one single example of a particle in the calculations with both  $\text{CH}_2\text{O}$  and OH concentrations above the lowest interval. The same holds for the measured joint PDPs where there is not one example of an image containing a detectable number of pixels with both OH and  $\text{CH}_2\text{O}$  signals above the lowest interval.

This is however a matter of PDP resolution limits. In Figure 5.34 it is clear that the intersection point between  $\text{CH}_2\text{O}$  and OH in both the measurements and the calculations contain reasonable amounts of both species. Since the average value is used from both calculations and measurements we cannot conclude from this that these high amounts are present at the same time and place; merely that they are present at the same time. The homogeneous calculations in Figure 5.37 show that the concentrations in the intersection point are lower than Figure 5.34 would indicate.

## Stochastic Reactor Models for Engine Simulations

---

Since we have proven that the calculated joint PDPs give the same results as PDPs attained through LIF measurements, it is interesting to raise the resolution of these PDPs by using temporal maximum concentrations rather than global. This investigation was made in order to study in detail the nature of this overlap. These images are shown in Figure 5.40.

If we start at the very onset of ignition, at the growth phase of  $\text{CH}_2\text{O}$ , we find that the particles having the highest concentrations of  $\text{CH}_2\text{O}$  also have the highest concentrations of OH. This pattern becomes less clear as the peak of the low-temperature heat release approaches, since particles having these (for the stage of ignition) relatively high concentrations of OH become fewer, and just beyond that peak, the highest levels of OH seem to disappear.

During the following stage, the transition stage between low-temperature and high-temperature ignition, characterized by high levels of formaldehyde, seemingly all particles have the same high levels of  $\text{CH}_2\text{O}$ , whereas the OH-levels are low but the concentration proportions unevenly distributed. The distribution patterns vary over time, but reveal little over the nature of the combustion evolution.

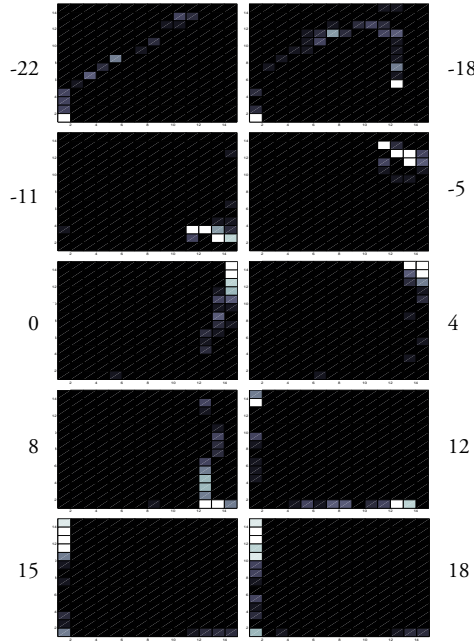


**Figure 5.40** SRM calculated joint PDPs using total maximum concentration as maximum plot value, at various CADs during the ignition process

A logarithmic averaged concentration plot helps us understand what we see. As seen in Figure 5.41 the average concentration of OH drops after the peak of low-temperature heat release. Slightly beyond top dead center the heat release starts raising again, and with that the OH concentrations. It is right where the heat release begins to rise that we find again (for the ignition phase relative) high peak concentrations of OH and  $\text{CH}_2\text{O}$  situated in the same particles. Slightly beyond, where the absolute concentrations of OH are substantially higher, the connection that high concentrations of  $\text{CH}_2\text{O}$  are connected to high concentrations of OH is no longer valid. At that point we can say that the high-temperature ignition has begun.

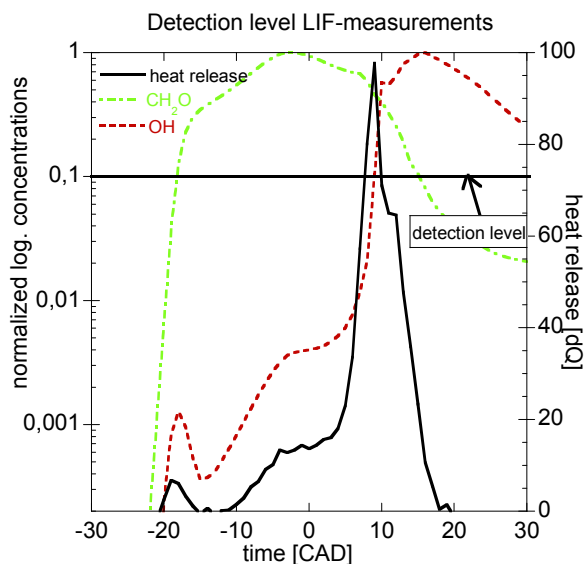


*Figure 5.41 SRM calculated OH and  $\text{CH}_2\text{O}$  concentrations on a logarithmic scale and the heat release curve on a linear scale, also showing the detection level of the LIF measurements. Apparently well verified SRM calculations can be used to extend the analyzed region below the signal-to-noise threshold level in the calculations*

### 5.2.5 Conclusions

Concentrations of hydroxyl radicals and formaldehyde were calculated using homogeneous (HRM) and stochastic reactor models (SRM), and the result was compared to LIF-measurements from an optically accessed iso-octane / n-heptane fuelled homogeneous charge compression ignition (HCCI) engine.



## Stochastic Reactor Models for Engine Simulations

---

The main heat release was well predicted, but the low temperature heat release in the cool flame region was less well predicted.

The profiles of averaged concentrations of  $\text{CH}_2\text{O}$  and  $\text{OH}$  were quite well predicted by the SRM, when compared to averaged LIF-signals of the respective species. A moderate deviation in  $\text{CH}_2\text{O}$  was attributed to the chemical model, giving a too slow growth of formaldehyde in the low-temperature regime. A minor deviation in hydroxyl radicals were most likely due to a minor deviation in the physical model, a belief that was supported by investigations using different mixing times, and thus resulting in different rates of heat release, a property that gave direct impact on the shape of the hydroxyl radical concentration profile.

The good agreement between SRM and LIF PDPs clearly proves the validity of the stochastic reactor model. Further it shows that a well-performed SRM calculation using a good detailed kinetic model is a valid method of gaining insight into the ignition characteristics for homogeneous ignition. Further the method is possible to extend to other species, species that are difficult to measure but still give important information on the combustion and the information sought.

Of significance is also that the SRM may be used to extend the concentration range of the investigated species to go far beyond the LIF detection limit.

The interrelation between  $\text{OH}$  and  $\text{CH}_2\text{O}$  during HCCI combustion was investigated. It was found that at the very onset of ignition, during the growth phase of  $\text{CH}_2\text{O}$ , the particles having the highest concentrations of  $\text{CH}_2\text{O}$  also have the highest concentrations of  $\text{OH}$ . At the peak of the low-temperature heat release particles having the (for the stage of ignition) relatively high concentrations of  $\text{OH}$  becomes fewer, and just beyond that peak the highest  $\text{OH}$  levels disappears and that during the transition stage between low-temperature and high-temperature ignition, seemingly all particles have the same high levels of  $\text{CH}_2\text{O}$ , while the  $\text{OH}$ -concentrations are low but unevenly distributed. It was also observed that during the growth phase of  $\text{CH}_2\text{O}$  there is a temporal peak of  $\text{OH}$ , coinciding with the first heat release peak.

### 5.3 Modeling and investigation of Exothermic Centers in HCCI-combustion

Whereas in section 5.2 the ability of the SRM codes to simulate and track individual species was demonstrated, the investigation in this section shows how the SRM code can be used to study the effects of the temperature inhomogeneities and distribution. Parts of the results were presented at the Competence Center for Combustion Processes (KCFP) in Lund in 2004, although experimental data that could confirm the findings were not available at that time. Recent and planned experiments at the department of Combustion Engines at Lund University can be useful for an extended investigation and to confirm the findings in this work.

#### 5.3.1 Introduction

Exothermic centers are described as small hot kernels of reactive gas that begin to burn earlier than the surrounding mixture. In SI-engines exothermic centers can lead to pre-ignition or knock [77] and consequently to impaired engine efficiency and even engine damage [78]. Exothermic centers are thus unwanted phenomena in SI combustion where the ignition is supposed to be controlled by the timing of the ignition spark. Exothermic centers may nevertheless be formed if particular surfaces inside the combustion chamber reach temperature a high enough to affect the ignition process. The surfaces often involved are the exhaust valves and the sharp corners on the upper surface of the piston. This problem is generally solved by appropriate design, by seeing to that there are no sharp corners on the top of the piston, that the exhaust valves are sodium cooled, and that the valves only have short parts of the stems exposed in the exhaust port. Another measure is to use camshaft profiles that are sufficiently quick lifting to avoid excessive heating of the exhaust valves.

In the HCCI engines, however, exothermic centers are part of the combustion and in fact the process that initiates the combustion and thus a needed phenomenon [79]. Since HCCI engines are difficult to regulate due to the fact that they do not have a physical process that starts the combustion, like the occurrence of a spark (SI engine) or the injection of fuel (CI engine), the formation of exothermic centers are interesting to investigate. Since the combustion process in an HCCI engine is supposed to commence simultaneously throughout the combustion chamber, variations within the chamber are also of interest to investigate.

The idea behind the present investigation is to take what is a problem in an SI engine and examine the effect it has on combustion in the HCCI engine, namely the temperature of the hot exhaust valves. In order to be able to calculate the formation of exothermic centers, one cannot regard the combustion chamber as a single entity as with the Homogeneous Reactor Model (HRM). In this investigation a Stochastic Reactor Model (SRM) with 200 particles is used, were

each particle can be considered as a small homogeneous reactor interacting with any other particle or any in cylinder surface.

Since there are no experiments performed, involving variation of the surface temperatures inside the combustion chamber, the model was validated only for a single case. The validation was performed to ensure that the physical model was correct.

### The Chemical Model

The chemical kinetic mechanism employed is an in-house developed n-heptane mechanism [80]. The complete mechanism is reduced, and contains 151 species and 1402 reactions.

### 5.3.2 Experiment

A Scania DSC12 DI diesel engine converted to HCCI operation was used for the experiment, performed by the Department of Combustion Engines at Lund University. The engine is an in-line six-cylinder 12 liter turbocharged, one normally used as a heavy-duty truck engine. In converting it to HCCI, the injectors in the engine head were replaced by pressure transducers, and low-pressure injectors were placed in the intake instead. Major mechanical parts of the engine, such as pistons, cylinder heads and camshafts, were left unchanged.

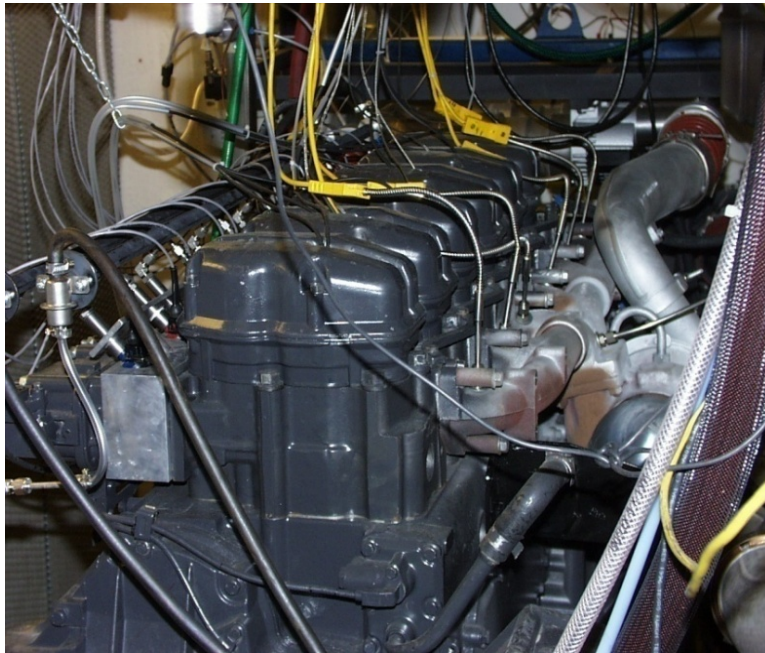


*Figure 5.42 The six cylinder HCCI engine used for the experiment.*

The original turbocharger turbine, however, was replaced by a smaller one, since otherwise the turbocharger would have obstructed the gas flows rather than supplying over-charge, due to the low temperatures of the exhaust gas and the consequently low energy content of the exhausts. The most important engine parameters are presented in Table 5.8.

**Table 5.8** Basic engine parameters.

Total displacement [cm <sup>3</sup> ]	11,705
Compression ratio	11,5:1
Bore [mm]	126.6
Stroke [mm]	154
Connecting rod [mm]	255
Engine Speed	1000 rpm
Intake Valve Opening	54° BTDC
Intake Valve Closing	78° ABDC
Exhaust Valve Opening	96° BBDC
Exhaust Valve Closing	52° ATDC

The engine has 4 valves per cylinder with the two intake ports characterized by different geometries: the first one goes straight into the cylinder in order to have low fluid-dynamic losses; the second is designed with a helicoidally shape to enhance the in-cylinder swirl. One injector for each intake port permits bi-fuel operation, using one injector for n-heptane and one for iso-octane. The mixtures for each cylinder can be individually tested and adjusted from a controlling computer. An electrical heater was placed between the compressor and the inlet manifold in order to be able to adjust the engine inlet temperature, which contributes to controlling the ignition timing. In the experiment carried out the fuel was 100 % n-heptane with mixture strength of  $\lambda = 3.49$ .

### 5.3.3 Calculation and results

#### Validation

First, calculations were made to validate the model. The basic engine parameters were set as indicated in Table 5.8. The experimental data was provided from -90 CAD BTDC to 90 CAD ATDC, so the calculation was set to the same timing as used for the initial pressure and temperature in the experiment. The fuel employed, its mixture strength and the EGR rate was set as in the experiment. Since no data was available regarding wall temperatures and turbulence, these parameters were set to typical values (Table 5.9).

**Table 5.9** Initial conditions and calculation parameters

Initial CAD	-90 CAD
Initial pressure	1.75 bar
Initial temperature	493 K
Total number of particles	200
EGR	0 %
Mixing time $\tau$	0.02 s
Stochastic Heat Transfer Const. $C_h$	35
Compression Ratio	12.1 (tuned)
Fuel	n-heptane
$T_{\text{wall}}$	502 K
Time step size	1 CAD

The compression ratio, which was rated to 11.5:1, was adjusted to 12.1:1 to provide a closer fit with the experimental maximum and the expansion cycle pressure. Since the mixing and heat transfer processes vary stochastically from calculation to calculation, ten consecutive calculations under the same initial conditions were performed. The mean pressure obtained in these calculations was compared with the measured pressure (Figure 5.43).

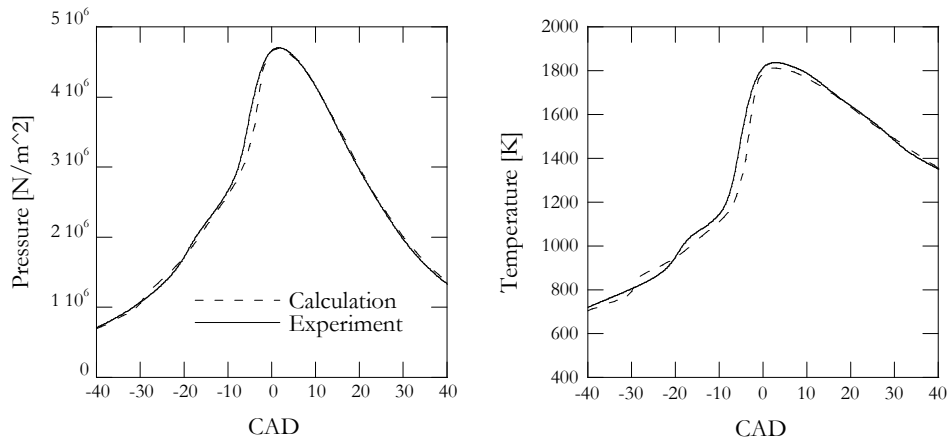


**Figure 5.43** Measured pressure (left) and temperatures (right) compared to the mean of 10 calculated pressures and temperatures.

Reasonable agreement was obtained, except for certain slight deviations in the cool-flame region and a somewhat greater deviation in the main ignition region. The main ignition timing was underpredicted, by some 2-3 CAD in the calculations. The maximum pressure as well as the expansion pressure were almost perfectly matched.

### Assigning wall temperatures

A second case was set up in order to investigate the impact of assigning different temperatures, to different parts of the combustion chamber walls. The base case was the one used for validation, in which a single wall temperature of 502 K was assigned to all the surfaces. For the second case, the surface temperature of the exhaust valves was raised to 875 K, whereas the temperature of the remaining surfaces was lowered to 475 K. The average wall temperature in both cases was the same.

For this second case ten calculations were performed, the results of these being compared with those of the calculations used for the earlier validation.

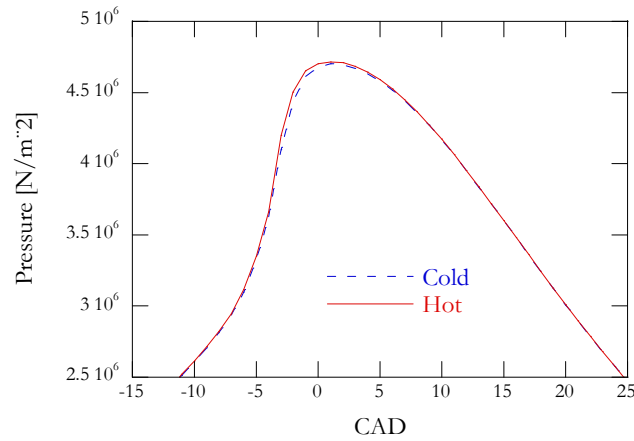


**Figure 5.44** Mean pressures for the two cases considered, showing there to be only negligible differences in timing.

In studying Figure 5.44 one can note that the difference in timing between the two cases is only negligible, less than 1 CAD. This is a difference that was smaller than expected.

Since only very small differences between results of any of the 20 separate calculations were noticed, it was concluded that the running conditions were very stable. At the same time, the

experimental running conditions did not represent a typical HCCI case, since the combustion phasing would normally come much (approx. 10 or so CAD) later. Thus it was decided to lower the initial temperature to 468 K, so as to create an HCCI case with a later and thus more typical combustion phasing (Figures 5.45-5.46).

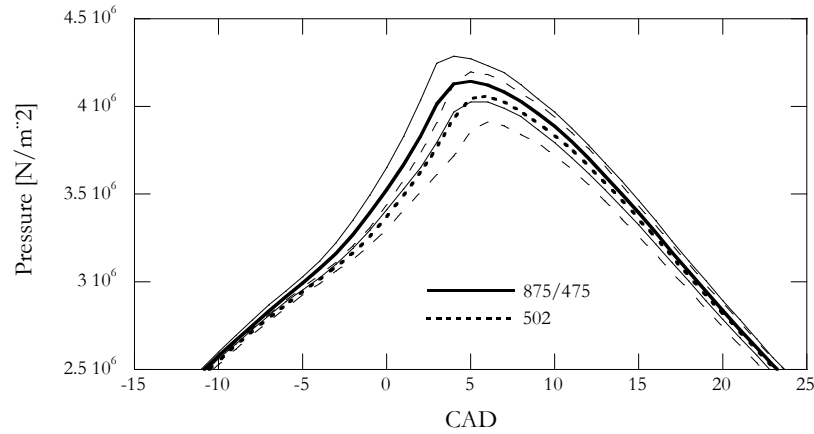


**Figure 5.45** Mean pressures for the two cases with obvious differences in timing and also in maximum pressure. The thin lines show the maximum and minimum of the 10 calculations for each of the two cases.

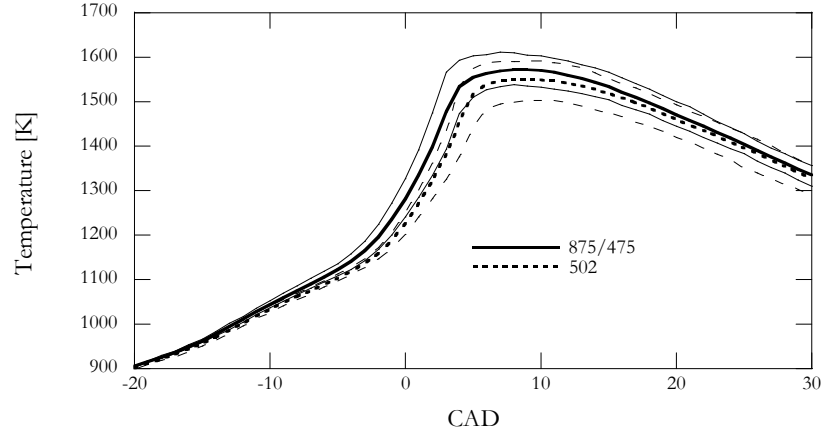


**Figure 5.46** Mean temperatures for the two cases with obvious differences in timing and also on maximum temperature. The thin lines show the maximum and minimum of the 10 calculations for each of the two cases.

With use of this later combustion phasing, the difference in timing becomes more obvious, in the order of 2-3 CAD. The variation between the calculations also becomes greater, implying the combustion to be less stable.

Not only has the timing changed, but also, as can be seen in Figure 5.45 the differences in maximum pressure are quite obvious. The mean pressures for the two cases differ by slightly more than 1 bar, while for each of the two single cases, the variation between the minimum and the maximum of the 10 calculations is nearly 3 bar.

The same trends, regarding the temperature, can be observed in Figure 5.46. The mean temperatures differ by 15 K, while for each of the single cases the variation between the minimum and the maximum of the 10 calculations is nearly 80 K.

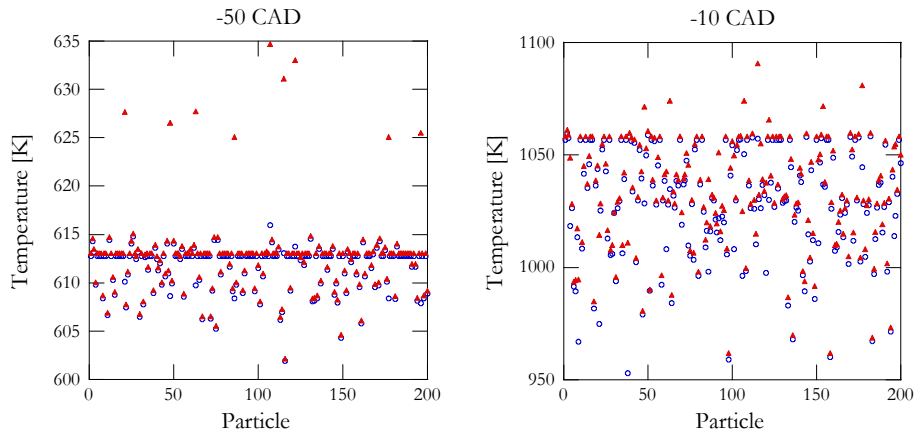


**Figure 5.47** Scatter plots of individual particle temperatures in the SRM during compression phase in the case of uniform wall temperature (circles) and of a cylinder wall area containing hotter regions (triangles).

The individual particle temperatures can be studied in Figure 5.47. At -50 CAD a number of particles have a quite much higher temperature than most of the others. These hotter particles shown in the figures as triangles are the ones from the calculations in which the walls are assigned two temperatures. In the case of this more realistic wall temperature distribution, particles that exchange heat with the hotter walls will get a higher temperature than that of the mean particles (or mass) in the cylinder, since some portions of the wall surface are higher in temperature. For the case of a uniform wall temperature, the wall temperature is almost all of the time, during compression, combustion and expansion, lower than that of the gas temperature in the cylinder, meaning that no heating of the particles occurs. Since the SRM do not contain any



spatial information concerning the position of the particles, the plots in Figure 5.47 have the particles spread in their modeling number, effectively a random distribution. Although the Scatter Plots do provide some information concerning the process they do not give a good measure of the differences in the distribution of the particles or a measure of the effect these differences have. The standard deviation (Figure 5.48) provides at a quick glance a reasonably good idea of the distribution of the particles and the inhomogeneties present, over time.

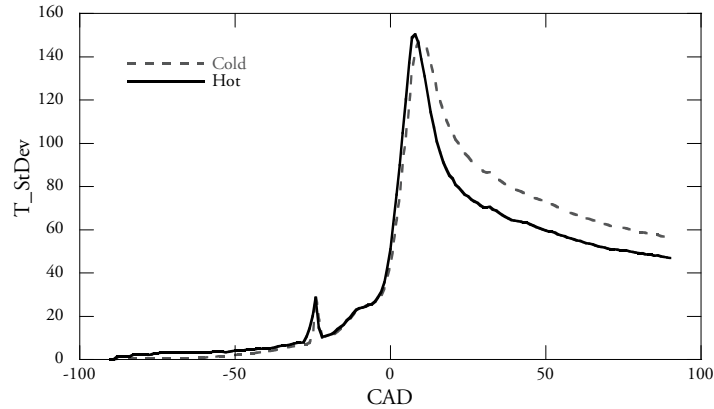


**Figure 5.48** Standard deviations of the particle temperatures in the 2 cases.

It is very interesting to see how the standard deviation captures periods of high chemical activity such as the cool flame period or the main combustion period, in which the temperature distribution shows a greater spread. Up to the point where the main combustion period begins, the standard deviation was found to be about of the same magnitude, a result that was not in line with initial expectations. The expectations initially were to find earlier and larger standard deviations of the temperature, for the case with distributed wall temperatures. In fact, just the opposite appears after the main combustion period, where the case with homogeneous wall temperature contains larger variations in temperature. This might suggest that combustion for this case is not as complete and that the variations of species mass fractions are larger as well. If this is the case than it would most likely show itself in higher amounts of different emissions.

**Table 5.10** Emissions of CO and HC for the two cases calculated.

	Hot valve	Cold valve
CO ppm	2870	3380
HC ppm	2340	2860

Since the chemical model used in the investigation does not contain any NO<sub>x</sub> chemistry, only CO and HC emissions were studied. It was found that in the case of a homogenous wall temperature the emissions of CO and HC were 20% higher, as can be seen in Table 5.10. The standard deviation of the temperature does provide some additional insight to what is happening. Yet adequate conclusions cannot be drawn on the basis of only the standard deviation. The case with homogenous wall temperatures had higher amount of emissions and higher spread of the particles, but in fact a lower mean temperature. Further the standard deviation can have the same value from several different sets of data. So the standard deviation is good in giving a rough assumption of the results but less useful for a detailed study.

Investigating the PDF directly provides certain insight into the complexity of the combustion process. For each of the variables associated with the particles, the PDF can be studied. These variables are for instance the temperature, but also all of the species mass fractions defined by the chemical model that was employed in the calculation. Apart from the detailed information the PDFs provide, they have the useful characteristic that they can be constructed either on the basis of measurements made in real engines or through CFD calculations, where the spatial distribution of some property can be transformed into a PDF which can then be readily compared with a PDF based on a calculation of a SRM. Figure 5.40, in the previous investigation, for example, allows a comparison to be made of a joint PDF based on pixel counts from a camera with calculations performed using the SRM.

Figures 5.49-5.52 contains PDFs of the temperatures found at -50 CAD, -10 CAD, 10 CAD and 50 CAD in the two cases that were calculated. Note that the temperature range is quite different for each of the figures.

## Stochastic Reactor Models for Engine Simulations

---

At the start of the calculations, at -90 CAD, all the particles have the same temperature, with the result that the PDF is only a single line. As the calculation evolves over time, heat transfer induces inhomogeneties in temperature, the mixing model (turbulence) spreading and diffusing them.

Already at -50 CAD, the two PDF's look different. Although their general shape is rather similar, the hot case has a marked bump in which a number of hotter particles are evident. So far, all particles have temperatures within the range of 30 K.

At -10 CAD the range of temperatures has expanded to almost 250 K, but the same trend is still visible, the general shape of the PDFs being similar and there being a clear group of hotter particles in the hot case. The hot surface has a temperature of 875 K, so at this point the hot particles have all a higher temperature and can only be cooled by the surface, and are thus only being maintained here through compression work and chemical reactions. At this point, they are very close to igniting. This small and clearly visible group of particles (Figure 5.49 and 5.50) can be described as exothermic centers and do contribute to earlier ignition in the hot case.

At 10 CAD the main combustion is well developed, and the shapes of the PDFs are now different with a shift towards the hot region in the hot case, and a more even temperature distribution in the cold case. The range of temperatures at that point is around 700 K, which implies that the particles are in several different stages of combustion. This is confirmed by the standard deviation of the temperature as shown in Figure 5.48. The small group of hotter particles that can be noted at -10 CAD has now disappeared and is part of the main bulk.

After combustion, during expansion the PDFs relax to create more coherent distributions, yet the differences persist until the exhaust valve opens, and results in different emission levels (Figure 5.52 and Table 5.10).

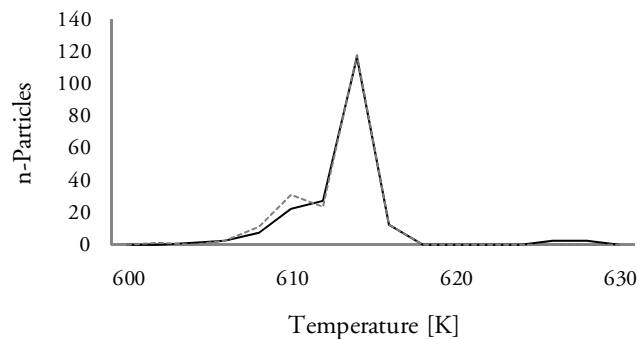


**Figure 5.49** PDF of the particle temperatures at -50 CAD.

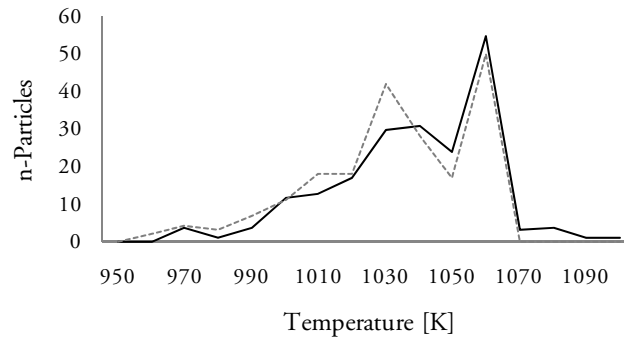


**Figure 5.50** PDF of the particle temperatures at -10 CAD.

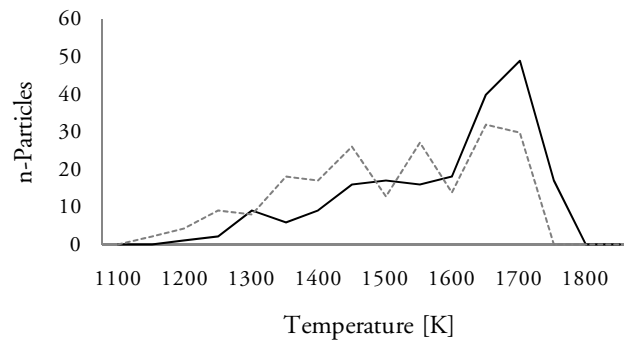


**Figure 5.51** PDF of the particle temperatures at 10 CAD.

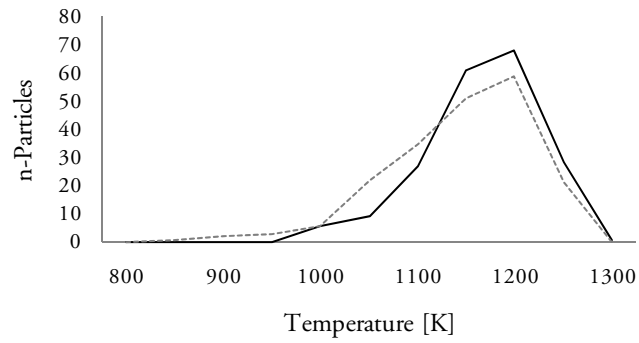


**Figure 5.52** PDF of the particle temperatures at 50 CAD.

### 5.3.4 Conclusions

The formation of exothermic centers was modeled with the SRM to investigate their impact on HCCI combustion. By varying the exhaust valve temperature, and thus assigning more realistic wall temperatures, the formation of exothermic centers and the ignition timing was shifted in time.

To be able to study the exothermic centers, their formation and their distribution, Scatter plots, standard deviation plots and PDF plots were constructed on the basis of the data the SRM calculations provided. The standard deviation for the particle temperatures was found to be an excellent indicator of the degree of homogeneity within the combustion chamber, and thus of how efficient the combustion process was. It was observed that when the standard deviation of the temperature was higher, the emissions of CO and of hydrocarbons present at the end of the closed cycle were higher. It was thus concluded that the standard deviation of the temperature, provided some indication of such emissions as those of hydrocarbons and CO. Since no NO<sub>x</sub> model was used for the calculations, no conclusions can be made on the relation of NO<sub>x</sub> formation and the standard deviation of temperature.

The standard deviation does not provide any absolute levels concerning the parameter in question. PDF plots do just this, while at the same time providing a detailed picture of the spread of the parameters being studied. According to the PDF results obtained, higher absolute temperature implies more NO<sub>x</sub> to be present in the “hot” case. Still, the temperatures were so low that the typically very low levels of NO<sub>x</sub> in HCCI engines could be expected to be maintained.

It was shown that promoting exothermic centers could be one way of counteracting emissions of hydrocarbons and CO which are a problem in HCCI engines.

## 5.4 Coupling to GT-Power

Part of the thesis work included the construction of a new interface between the newly developed HCCI-SRM code and the 1-D-EST, GT-Power [81]. The new coupled model, although having extended capabilities, has substantial better performance compared to older interfaces [82,83]. Calculation times were reduced 80-95 % thanks to better implementation of chemistry routines and a new solver. At the same time memory allocation/usage was reduced with 90% due to stricter handling of parameters and new fundamental structure of the SRM code. The Interface which is termed DARS-ESM is continuously developed and includes today several SRMs for HCCI, SI, DI and CI engines. For more information on different models and simulation strategies, consult the DARS-ESM/GT-Power manual [84].

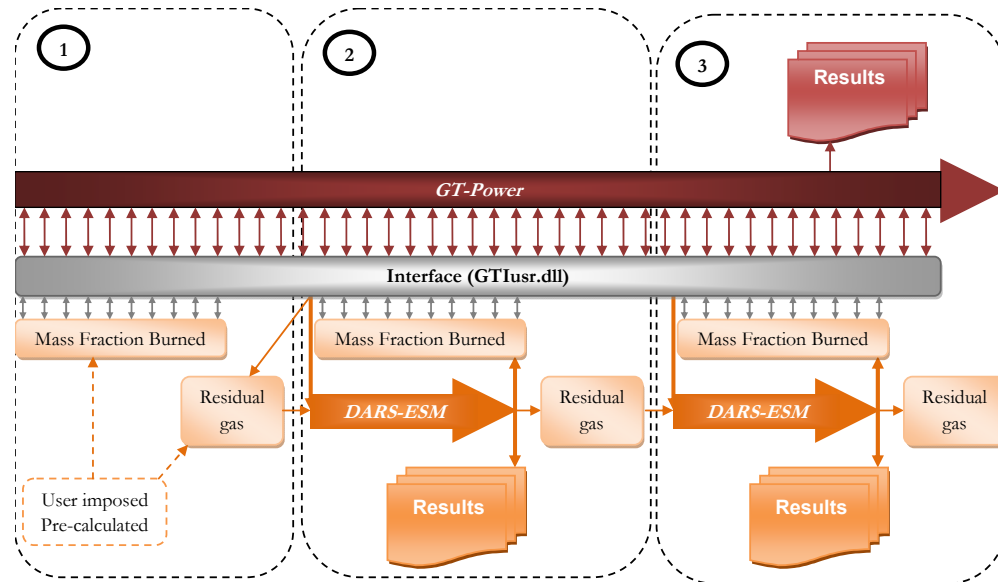


**Figure 5.53** Temporal representation of the Coupling between HCCI-SRM (DARS-ESM) and GT-Power.

Figure 5.53 describes the temporal coupling between the 1-D-EST and DARS-ESM. The 1-D-EST, which contains the full engine model (Figure 5.54-5.55), calculates the flow dynamics in each location of the engine, all the basic engine parameters as well as the engine performance, while DARS-ESM predicts the in-cylinder combustion.

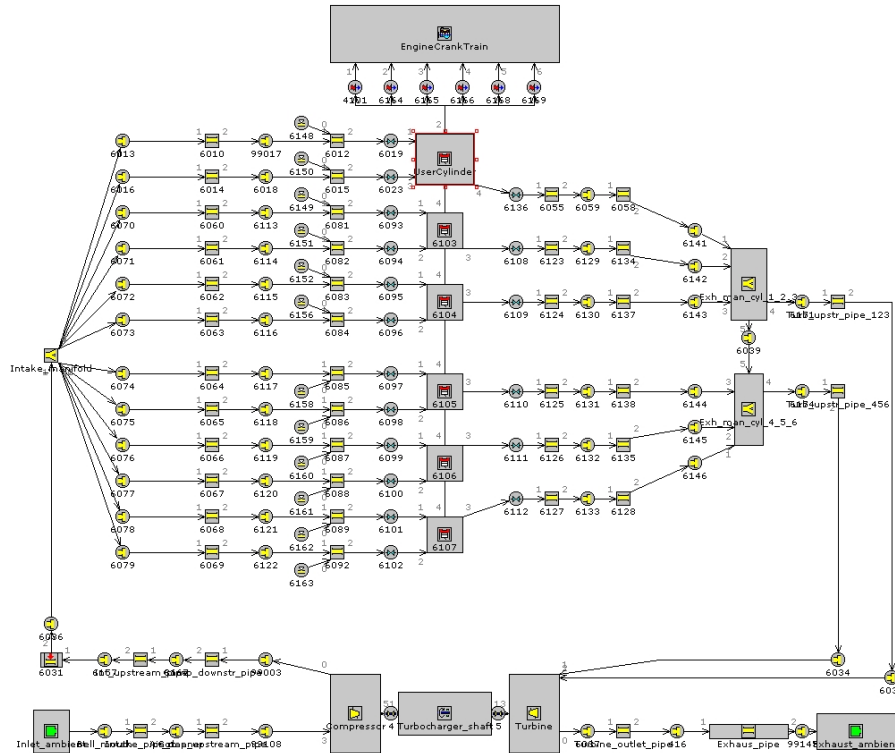
The fundament of the coupling is that the 1-D-EST provides information about the initial conditions at IVC as cylinder temperature, pressure and amount of residual gases. DARS-ESM

## Stochastic Reactor Models for Engine Simulations

returns a cumulative mass fraction burned (MFB) curve that the 1-D-EST then uses to evaluate the cylinder properties during combustion.

If we look closer at Figure 5.53, the steps of the coupling are:

1. Initial cycles are calculated to obtain flow convergence in the 1-D-EST model. For each 1-D-EST time step the 1-D-EST interrogates DARS-ESM regarding the cumulative MFB. Since the combustion event has an immediate effect on the flow conditions in the engine a pre-calculated and for the conditions appropriate MFB should be used.



mass fraction list for the residual gases may be provided by the user. DARS-ESM will perform the complete calculation while the 1-D-EST waits. DARS-ESM updates the MFB and outputs result data for this cycle. The 1-D-EST continues its calculations and collects the updated MFB data.

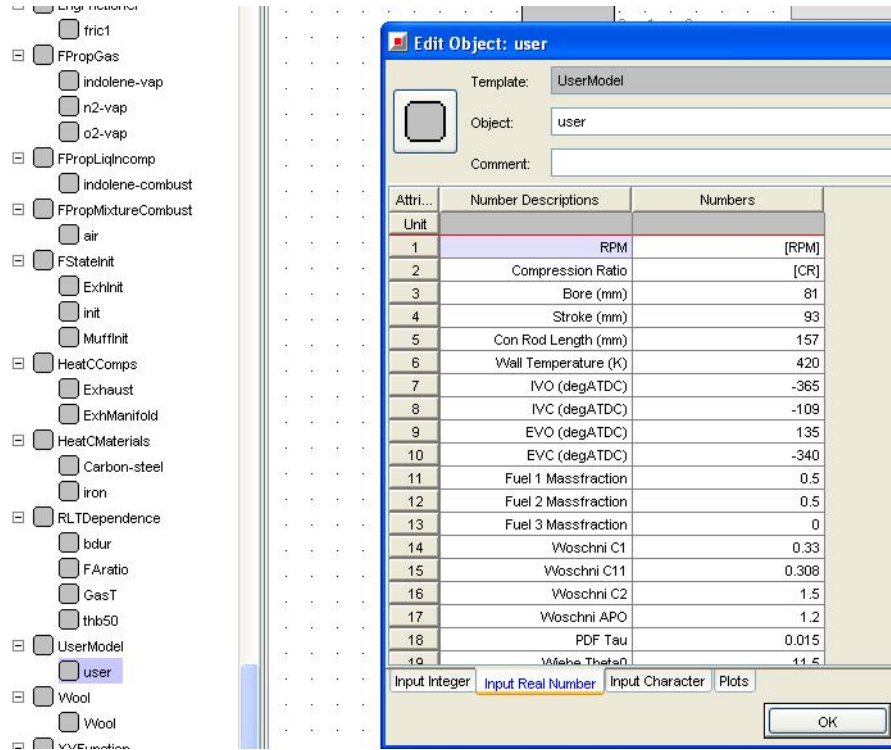


**Figure 5.55** Data needed for the coupling of DARS-ESM with GT-Power can be included in the user object.

3. All following calculated DARS-ESM cycles take as initial conditions the cylinder temperature, pressure and amount of residual gases from the 1-D-EST. But for all these cycles DARS-ESM uses the final species mass fractions from the previous calculated DARS-ESM cycle as residual gas species. As before DARS-ESM will perform the complete calculation while the 1-D-EST waits. DARS-ESM will update the MFB and output result data for each individual cycle. The 1-D-EST continues its calculations and collects the updated MFB data. When all cycles are completed the 1-D-EST results data can be accessed.



## Calculation of MFB in DARS-ESM

For the 1-D-EST to establish the heat release from the combustion and thereby the cylinder pressure, temperature and species properties, the main parameter containing the key for this information is the mass fraction burned (MFB). In DARS-ESM the MFB is calculated by using the change of the molar specific enthalpy  $H$ .

At the start of the combustion calculation with DARS-ESM the enthalpy  $H(t_0)$  for the initial condition of the species, including the fuel to be injected, is calculated. For the same conditions the adiabatic or burned enthalpy  $H_{ad}(t_0)$  is calculated. For each following time step the current enthalpy  $H(t)$  is calculated, considering any fuel still to be injected, giving a MFB between 0 to 1 in the relative borders of  $H(t_0)$  and  $H_{ad}(t_0)$ .

The expression for the MFB in this model is:

$$MFB = \frac{H(t) - H(t_0)}{H_{ad}(t_0) - H(t_0)} \quad (5.10)$$

$$H(t) = \frac{m_{cyl}Y_{i,cyl} + m_{tbi}Y_{i,tbi}}{m_{cyl} + m_{tbi}}(t)h_i(298.0) \quad (5.11)$$

$$H(t_0) = \frac{m_{cyl}Y_{i,cyl} + m_{tbi}Y_{i,tbi}}{m_{cyl} + m_{tbi}}(t_0)h_i(298.0) \quad (5.12)$$

$$H_{ad}(t_0) = \frac{m_{cyl}Y_{i,cyl,ad} + m_{tbi}Y_{i,tbi,ad}}{m_{cyl} + m_{tbi}}(t_0)h_i(298.0) \quad (5.13)$$

The denotation  $tbi$  stands for “to be injected”.

### 6 The Two Zone SI-SRM

The investigation reported in this chapter concerns the important question of how detailed kinetics calculations can be performed faster. A two-zone detailed kinetic code involving use of adaptive chemistry was developed to investigate this. Implementation of the code follows the basic idea proposed in [32] but with use of a more efficient chemistry solver that reduces the calculation times 80-90 %. Further gains are achieved through use of the adaptive chemistry described in this chapter. Part of the work described here is included in [85].

#### 6.1 Flame propagation model

The SI-SRM TwoZone is based on the PaSPFR, just as the HCCI-SRM described in chapter 4, but with the extension of having two zones in the classical Wiebe approach, the one an unburned and the other a burned zone[17]. There is no interaction between the zones except for the transfer of mass from the unburned to the burned zone, as dictated by the Wiebe function, yet particles within each zone are free to mix with each other and to transfer heat to the walls. In effect, the model is deterministic on the basis of the Wiebe function, but pre-ignition and knock are solved by means of kinetics. It has been shown that the SI-SRM TwoZone can be used to predict knock and emissions when correctly tuned parameters are employed [32].

The SI-SRM TwoZone is an extension of Equation 4.17. The operator split loop in Figure 6.1 contains an added flame propagation step. For each zone in the TwoZone model, the mixing, chemistry and heat transfer steps are solved separately. This means that the zones are effectively sealed off from each other, except for the transfer of mass in terms of the Wiebe function.

##### Flame propagation

The effect of flame propagation is modeled by the Wiebe function [17], which specifies the relation between the mass fraction which is burned and the crank angle degree:

$$m_b = m_{total} \left( 1 - \exp \left[ -b \left( \frac{\theta - \theta_0}{\Delta\theta} \right)^{n+1} \right] \right) \quad (6.1)$$

In Equation 6.1,  $\theta$  is the current crank angle,  $\theta_0$  the crank angle at the start of combustion and  $\Delta\theta$  the duration of the combustion period where the mass fraction burned varies from 0.0 to 0.9. The Wiebe parameters  $b$  and  $n$  have adjustable values. The values, if unknown, can be found by fitting the calculated pressure trace to the experimental pressure, yet the values only apply under these conditions. An advantage of the Wiebe model is its simplicity in modeling and the short time required for the determination of the fitting parameters.

## Stochastic Reactor Models for Engine Simulations

---

At the start of the calculations a preset number of particles are given the initial conditions of fuel, oxidizer and residual gases masses, temperature and pressure. During combustion a new particle is created in the burned zone from the mass determined by the Wiebe function at each time step. This mass is taken equally from the particles in the unburned zone.

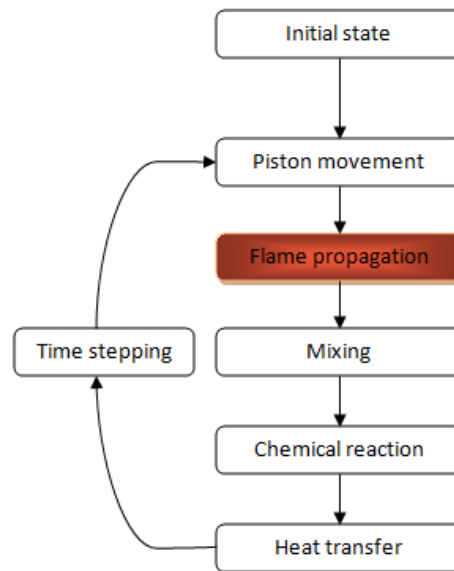


*Figure 6.1 The operator split loop in the SI-SRM TwoZone model*

### 6.2 Phase Optimized Skeletal Models

Several investigations were carried out to demonstrate a novel approach to reducing calculation times without a loss in accuracy. Although the investigations involved use of the TwoZone-SI-SRM, the POSM approach can also be used with any of the reactors described here.

#### 6.2.1 Introduction

For use in engine simulations, chemical models can only be reduced to a certain point since the combustion processes takes place under quite an extensive range of pressure and temperature. A decrease in computation time is not always guaranteed. In solving the system numerically, use of a reduced chemical model can lead under some conditions to "stiff" problems that can result in computational times being still higher than the use of a detailed model would require.

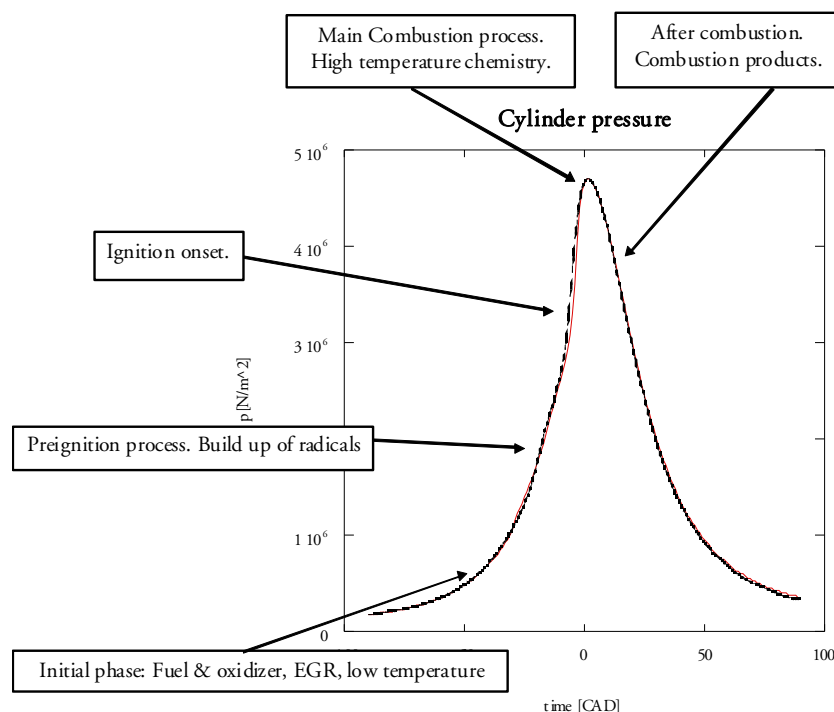


**Figure 6.2** The engine combustion process intuitively divided up into phases.

Although use of skeletal mechanisms generally provides faster calculations, one can do even better yet than “simply” using a skeletal mechanism. It is known that the combustion process can be divided up into several distinct events or phases (Figure 6.2). In engines, combustion calculations typically start with the fuel and the oxidizer and certain residual gases, and eventually end with only residual gases, which mean that in the course of the calculations certain species are more important than others at particular phases. If one can effectively divide the combustion process into phases, then for each phase one can use a skeletal mechanism that is smaller than a mechanism applying to the combustion process in its entirety. Instead of simply using one’s intuitive knowledge, one can also use statistical and machine learning techniques to find the optimal phases. For each phase, a specific, reduced and optimized chemical model (POSM) can be employed.

### **The skeletal mechanism**

There are a number of techniques that can be employed for the reduction of chemical models as was demonstrated in chapter 3. The technique used in the present investigation is that of ‘skeletal mechanisms’. The approach to create skeletal mechanisms is to omit species that play no significant role in the chemistry under the conditions that apply. The species that are omitted can thus be said to be unnecessary. The ‘necessity’ of a species, meaning that it should be retained in the mechanism is a single parameter based on a combination of reaction flow analysis and sensitivity analysis [86]. Sensitivity analysis determines which species need to be calculated accurately for the complete mechanism to provide the accuracy desired. Species of high sensitivity need to be retained in the combustion process, whereas species of low sensitivity can be omitted. Sensitivity analysis only indicates the necessity of a given species on the basis of its local reactive properties, however. Species of low sensitivity, which thus are candidates for being omitted, may nevertheless be important for the formation of highly sensitive species. The addition of reaction flow analysis includes species that are necessary for the formation of sensitive species.

The basis for producing a skeletal mechanism is typically a set of zero-dimensional constant volume calculations over a set of such physical conditions as starting temperatures, pressures and species concentrations [86]. During these calculations sensitivity analysis and reaction-flow analysis are conducted simultaneously so as to provide a ranked list of the species in terms of their necessity. Species with a degree of necessity below some cutoff value are eliminated, while the species that remain form the new skeletal mechanism. The skeletal mechanism produced is compared finally with the original detailed mechanism that has been validated.

### **6.2.2 The POSM strategy**

If the set of conditions is relaxed, meaning that it is only for a reduced set of conditions that a given species is required to have a high necessity value, then a smaller and more reduced mechanism can be constructed. Only species having a high degree of necessity at some point in the

mechanism are included in the base mechanism then, whereas if under a given set of conditions there is no point at which a particular species has a high degree of necessity, the species can be eliminated. One way to relax the set of conditions that necessity involves is to only consider a small part of the combustion process, meaning a particular phase of it. For example, one can say that the presence of some set of species is only necessary in the pre-ignition phase. This means for example, that all of the species that are necessary during the ignition phase might perfectly well be unnecessary in the pre-ignition phase. In this smaller phase considered, a smaller skeletal mechanism could be made use of.

If a mechanism is divided up into several submechanisms, each representing a particular phase, then within each phase the conditions for necessity can be relaxed. A given species needs only to be unnecessary in the smaller region which is considered in order for it to be eliminated there. From this point of view, any division into phases would result in a smaller overall mechanism. Wherever the divisions may be located, the necessity conditions are relaxed, providing the possibility for the elimination of a given species. If the phases are chosen such that they mimic the phases of the known chemistry, however, a more optimal reduction can be achieved. The intuitive notion is that the best phase choices are made when each phase reflects a similar type of chemistry. What is considered similar chemistry, however, is a matter of interpretation. In the determination of POSM phases, useful criteria for similarity of this sort should include the concept of necessity. Necessity not only reflects the type of similar chemistry, but is also the criteria for producing the phase skeletal mechanism. Thus, the phases produced would have a similar set of necessary and unnecessary species.

Clustering is an automated way of detecting a set of similar objects [87,88]. If the objects are the individual time steps in an ignition process, then phases of similar chemistry translate to sets of consecutive time steps. For clustering a set of objects, a description of each of the objects is needed. These descriptions determine which objects are to be considered similar and which are not. In earlier studies [87,88], clustering was used to determine the phases of zero-dimensional constant volume processes. In those studies, a description of the process was given as a vector of the parameters applying to each time step. The process can be described in terms of the matrix of time steps versus parameters. Similar time steps were clustered together to form the phases of the process. These phases were shown to be physically justifiable. In addition, the phase descriptions were extrapolated to predict the phases in other processes having similar, but somewhat different starting conditions.

If the set of time step descriptions used in combustion calculations is the relative necessity parameter of the species, then the clustered time steps represent phases in which the set of necessary and of unnecessary species involved are similar. Thus, each phase represents a distinct skeletal mechanism. Since the same parameter is used for both clustering and reduction, an optimal

skeletal phase mechanism is created. To produce the skeletal mechanism from the necessity measure, a cutoff value is used to determine whether a species is unnecessary and can thus be eliminated. All species below this cutoff value for the phase considered are candidates for being eliminated. Thus, if the time step description reflects whether the necessity value of a given species is above or is below the cutoff, then the phases created reflect still more the optimal phases for the phase skeletal mechanisms. The set of species remaining in the skeletal mechanism of a given phase all have a necessity value above a given cutoff value for each of the time steps within that phase.

In order to use the phases that have been established and the skeletal mechanisms they represent at a given time step in ignition calculations, the algorithm must be able to determine which phase skeletal mechanism should be employed at any given point. This is important since the phase optimized mechanisms in question are only valid for their specific phase and could introduce large errors if used elsewhere. In principle, the descriptions used in determining the cluster descriptions themselves could be used for determining the phase. However, if a given description is not available, as can be the case in POSM because of necessity measures being too expensive to calculate, some other description must be found. In ignition calculations the mass fraction of the species is information that is readily available. Using the concentration of each species, a function must be found then giving as output the phase that the set of mass fractions represents.

There is another machine learning method that can accomplish this task, that of 'decision tree' production. This method takes as its input a set of objects and their descriptions. In this case, the set of time steps and the mass fractions of each species at any given time step, is employed. In addition, for each time step, the phase that the time step is in (as determined by a clustering procedure) is needed. The output of this method is a decision tree, one that is similar to a set of nested IF-THEN-ELSE statements. The conditions of the IF statement are questions concerning the mass fractions. At the end of the chain of IF's is the decision as to which phase to select. The method aims at finding the most efficient set of questions for determining the phases to be employed. This translates to automatically finding a minimal set of progress variables that effectively determine the phases. In the final POSM module, the decision tree is coded so as to determine which skeletal mechanism to employ. From the user's point of view, for example the CFD code, the input is the same as if the call was to the full mechanism. The use of the different mechanisms is transparent.

### Creating a POSM mechanism

The process of producing the POSM consists of five parts:

**Tabulation:** A set of zero-dimensional combustion process calculations representing a range of physical parameters, usually temperature, pressure and stoichiometry, are run. The necessity

measure is calculated for each time step of each of the runs. The result is a tabulation of time step vectors of the necessity values and of the concentration values of the different species.

**Discovery:** The entire set of time step vectors is used then as input to the clustering algorithm so as to determine the phases of the ignition processes. This results in a set of time step vectors, each of which is supplemented by its phase assignment.

**Recognition:** The set of time step vectors together with the species concentration values and the phase assignments is employed here. A decision algorithm in the form of a decision tree is created using these vectors. The resulting algorithm takes as input the set of species concentrations and provides as output the combination it belongs to.

**Reduction:** The phase identification algorithm is used to identify the time step a given phase belongs to. The maximum necessity value of each species within each phase is then determined. If the maximum necessity value for a particular species falls below a predetermined cutoff point within a given phase, that species can be eliminated from the mechanism in that phase. The result is a set of phase optimized skeletal mechanisms.

**Implementation:** Each phase optimized skeletal mechanism is converted then to a FORTRAN module and the phase recognition algorithm (the FORTRAN code is generated by the analysis procedure) is designed so as to call the appropriate phase optimized skeletal mechanism module.

The set of POSM FORTRAN modules representing the set of skeletal mechanisms selected is formed in the preprocessing stages outlined above. These modules are then incorporated into codes requiring the calculation of the chemical source terms. The input to this process (Tabulation) is a set of calculations spanning the chemical space needed. Earlier studies [87] have shown that, due to the consistency of the ignition process, relatively few starting conditions are needed in order to encompass a relatively large set of conditions. The output of this preprocessing is a set of FORTRAN modules that can be incorporated into the external model, in this case the SRM engine model. The preprocessing steps are relatively automatic, meaning that minimal user interaction is required. Automation of these preprocessing steps facilitates further optimization of the set of skeletal mechanisms. Once created, the POSM mechanisms can replace the standard mechanism under all conditions where the latter was applicable. This means that for any standard mechanism the POSM mechanisms only need to be created once. The creation of a POSM mechanism from any given standard mechanism takes less than a day.

In terms of the external codes that make use of POSM, there is relatively no difference between the POSM interface and the single mechanism interface. The overhead for POSM during the calculations is limited to the nested IF-THEN-ELSE statements of the decision tree and certain



vector copies. This takes much less time than an LU-decomposition of the system of differential equations would take for example. The number of phases employed has no practical implications for the calculation time.

### Implementing POSM in the two-zone SRM

In this part of the work the POSM was implemented in the two-zone SRM software. POSM can, of course, be implemented in any type of software that uses chemical kinetics. As described earlier, most of the two-zone SRM code and all of its functionality are retained when POSM are implemented. However, in the time marching algorithm an extra layer is added on top of the solver (Chemical reactions in Figure 6.1). At the top level in the SRM the chemical model always is viewed as the original one, which in this case includes the total number of 125 species and 1066 reactions. This mechanism is only used for bookkeeping, however, and never by the solver. The solver always uses POSM.

During the solving at a given time step, each particle in each of the zones calls the solver. As can be seen in Figure 6.3, in the POSM version the following takes place:

1. The particle phase is decided in terms of the state and the mass fraction values of the particle in question.
2. The full set of properties of the particle is translated into the POSM of the current phase.
3. The particle's chemical reaction is solved by POSM.
4. The POSM mass fractions for the particle are translated back to the full set of species. Any mass fraction that has not been updated, i.e. which has not been included in the POSM mechanism during this time step, retains its properties from the previous time step.

In the implementation here, the phase decision is made outside the solver, although it would have been perfectly feasible for the phase decision to be made within the solver instead during subcycling. The time-step used for the call to the solver calculations (Solve POSM) was kept small so as to avoid the need of phase changes being made in sub-cycling of the solver.

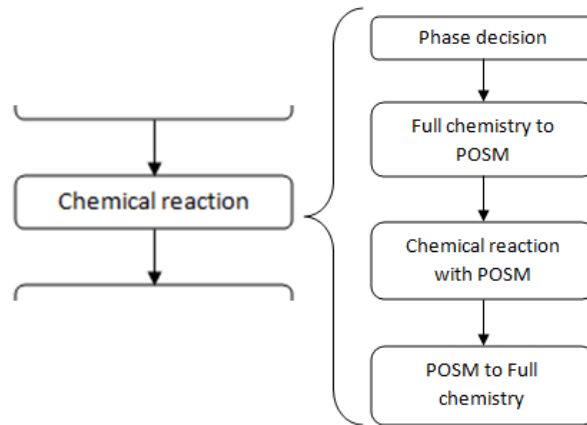


*Figure 6.3 POSM steps for the solver.*

### 6.2.3 Investigation 1

Comparative calculations were made for the two-zone SRM, one set of calculations for the POSM and the other for the standard mechanism. The calculations were limited to the closed cycle of the engine. The conditions for both sets of calculations are specified in Tables 6.1 to 6.3. Despite the calculations applying to a fictive engine, all the input data are realistic and are typical for an automotive engine. A somewhat high compression ratio is used so as to force knocking conditions. This makes the calculations more complicated, but is aimed of examining eventual deviations.

*Table 6.1 Initial conditions and calculation parameters.*

Initial CAD	-137 BTDC
Initial pressure	0.74 bar
Initial temperature	350 K
No. of particles in unburned zone at IVC	5
No. of particles with residual gas at IVC	1
Internal residual gas fraction (vol.)	6%
Mixing time $\tau$	0.01 s
Stochastic Heat Transfer constant $C_p$	30
Time step size	1 CAD

**Table 6.2** Engine parameters and boundary conditions.

Bore/ Stroke/ Rod	85 / 88 / 135 mm
Displaced Volume	500 cm <sup>3</sup>
Compression Ratio	14.5
IVC	-137 CAD
EVO	137 CAD
Crankshaft rotational speed	2500 rev/min
Fuel	n-heptane 70% toluene 30
Wall temperature	450 K

**Table 6.3** Parameters specific to the mixture.

Mixture	$\lambda = 1.0$
Timing of Ignition (CAD)	-11.5
Combustion duration (CAD)	50
Wiebe – a / Wiebe – m	3.2 / 1

## The Chemical Model

The chemical kinetic mechanism employed, both for the standard two-zone SRM calculations and as a base mechanism for creating the POSM, is a skeletal n-heptane / toluene mechanism. This skeletal mechanism had already undergone the necessity analysis with respect to the entire calculation to form an optimally reduced mechanism. The toluene mechanism developed in our group is based on the original mechanism [89]. It is combined with the skeletal mechanism of n-heptane oxidation [80, 11]. The n-heptane / toluene mechanism contains 125 species and 1066 reactions.

## The POSM Created

For this investigation a very conservative level of reduction was employed. Using the original skeletal mechanism, a set of zero-dimensional constant volume calculations were made at five different starting temperatures, ranging from 800 to 1600 degrees Kelvin. All the calculations were made for a starting pressure of 40 bars. This resulted in five different phases consisting of one phase optimized skeletal mechanism in each phase (Table 6.4). The phases represent a further reduction in size from the original already reduced skeletal mechanism.

## Chapter 6 The Two Zone SI-SRM

**Table 6.4** Numbers of species and reactions used by the different mechanisms.

Original mechanism	125 species / 1066 reactions
Phase 1	79 species / 604 reactions
Phase 2	89 species / 774 reactions
Phase 3	92 species / 818 reactions
Phase 4	110 species / 995 reactions
Phase 5	72 species / 537 reactions

In the constant volume ignition calculations carried out the phases can be readily identified. Phases 1 and 2 are basically initiation phases. Phase 1 is more important at low starting temperatures. Phase 3 is a pre-ignition phase for the initial buildup of radicals. Phase 4 is an ignition phase in which the upper boundary is essentially the auto-ignition point. Phase 5 is the phase following ignition, marked by the buildup of combustion products.

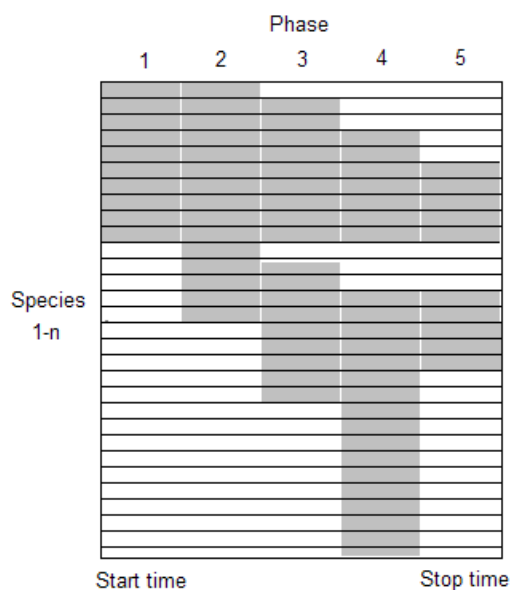


**Figure 6.4** Representation of the basic idea of involving calculations using POSM. The species used by the different phases are shown in gray while the total number of species in the standard mechanism is both gray and white. The calculations start with phase 1, which has only a few species, and continue on through the phases with differing number of species.

The decision tree created uses mass fractions of only certain species for deciding which phase to employ. Essentially, the questions were whether the mass fraction values were very low or not. Temperature and pressure could be considered at an intuitive level, in the questions. However, since the tabulations made involved constant volume calculations where the temperature and pressure do not go down after combustion, unlike an engine calculation with its expansion, these were consciously ruled out.

### Results

The aim of this study was to compare the POSM approach with the standard mechanism in terms of accuracy and computational time. The case considered involved simulations of an SI engine under knocking conditions, using a mixture of n-heptane and toluene as fuel.

#### Calculation Accuracy

Pressure and temperature profiles, together with mass fractions over time for the species CO, OH and CH<sub>2</sub>O are presented. These three species were chosen since they are commonly measured and for the highly reactive OH also could provide some differences [28].

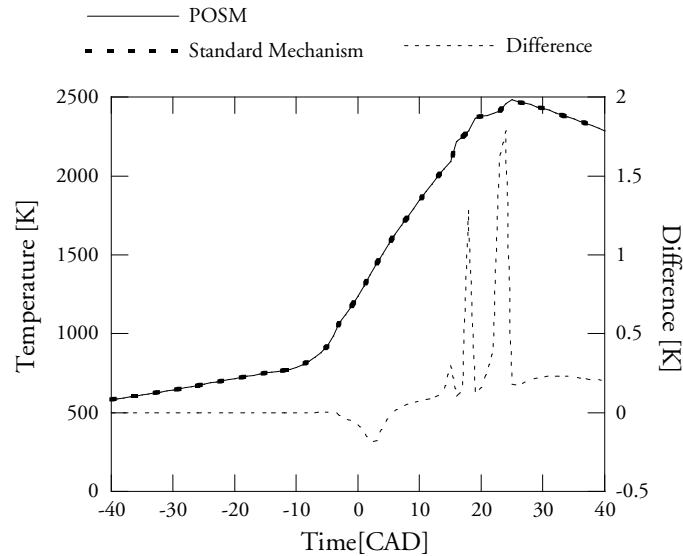


**Figure 6.5** Calculated temperatures as a function of time (left axis) and of absolute differences between the calculations (right axis).

As can be seen in Figures 6.5-6.9, the differences between the calculations are small. For more precise comparison purposes, the absolute differences between the calculations are also given. For each figure, the thin line is for POSM calculations, the thick dots are for standard mechanism calculations and the thin dotted line shows the absolute differences between the two sets of calculations. The differences in temperature between the standard calculations and POSM, shown in Figure 6.5 are too small for it to be possible to distinguish between them. As the difference curve indicates, the differences are well below 0.1% or 2 K throughout the calculations. The maximum differences are found at the autoignition points or roughly at 16, 18 and 24 CAD. The differences are so small that they can be neglected.

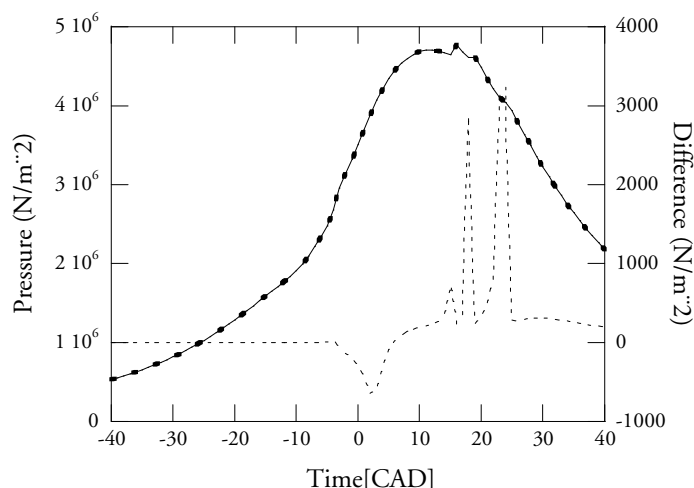


**Figure 6.6** *Calculated pressures as a function of time (left axis) and of absolute differences between the calculations (right axis).*

The pressure curves in Figure 6.6 show exactly the same type of behavior as that for the temperature curves. The capabilities of the two-zone SRM are clearly demonstrated by the smoothly rounded pressure peak and the jagged edges of knock. Just as in Figure 6.5, the differences are very small, less than 0.1 % or 4000 N/m<sup>2</sup>, and they also peak at the same time as the temperature curves in Figure 6.5 do.

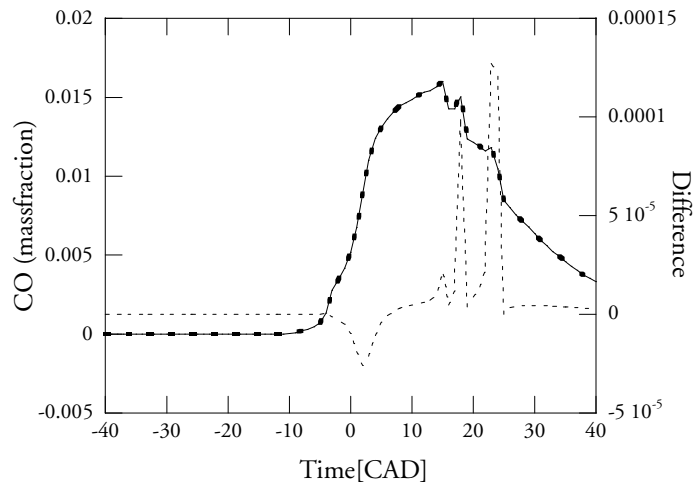


**Figure 6.7** Calculated mass fractions of CO as a function of time (left axis) and of absolute differences between the calculations (right axis).

Regarding the mass fractions calculated for the species CO, OH and CH<sub>2</sub>O (Figures 6.7-6.9) one can note the same very small differences. In terms of accuracy, it is obvious that the POSM performs almost as well as the standard mechanism. For CO the largest difference, in the order of 1 %, occurs at 24 CAD.

The largest deviation in the calculations occurs for CH<sub>2</sub>O at 24 CAD and is in the order of 7 %. However this happens at a point at which nearly all of the CH<sub>2</sub>O is already consumed and thus not of any significance. Most of the time, the difference is well below 0.1 %. Finally for OH which was suspected to be hard to match, actually shows a very good agreement for the calculations. The largest difference is less than 0.1 %.

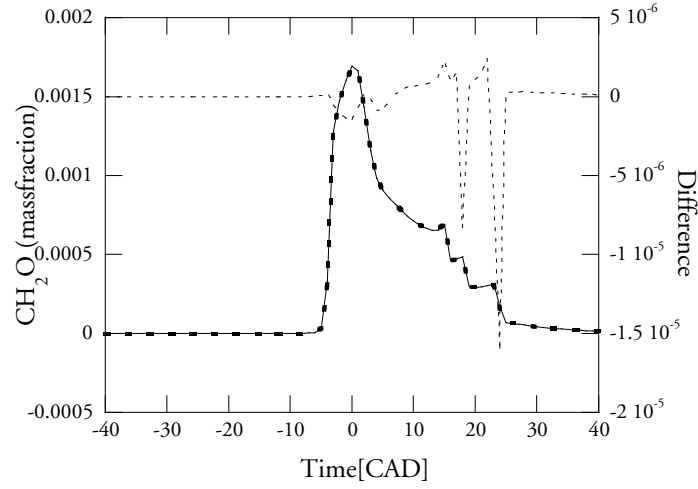


**Figure 6.8** Calculated mass fractions of  $\text{CH}_2\text{O}$  as a function of time (left axis) and of absolute differences between the calculations (right axis).

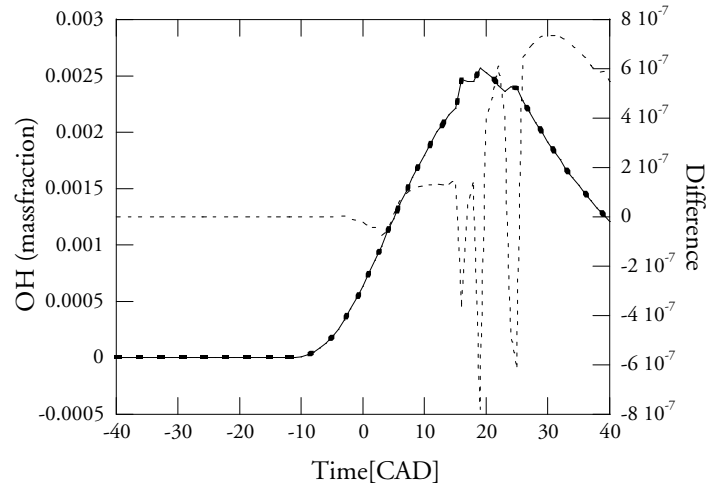


**Figure 6.9** Calculated mass fractions of  $\text{OH}$  as a function of time (left axis) and of absolute differences between the calculations (right axis).



## Reduction in calculation time

As been shown, POSM shows excellent agreement with the standard mechanism, at the same time as it is roughly three times as fast. On a laptop having a 3.2 GHz Pentium processor the calculations using the standard mechanism required 318 s to be completed, while the POSM calculations were completed in 114 s. This translates to a factor of about 3 in terms of computational savings.

## Discussion

This part of the work shows that the POSM technique meets the major objectives for calculations making us of a two-zone SRM code, namely retention of accuracy together with improved calculation efficiency. The current investigation showed good results. No extra effort was made to optimize the phase mechanisms, through the elimination of further species. A conservative necessity cutoff was chosen to ensure accuracy. In view of the level of accuracy achieved, the computational efficiency could be expected to improve significantly with optimization.

There appears to be considerable potential for much faster calculations being achieved with retention of accuracy, through further development of the POSM generation technique and greater emphasis being placed on reduction. Further computational efficiency can be gained through the accuracy criteria being relaxed in comparison with the stringent results currently being obtained. Examination of Figures 6.5-6.9 shows there to be distinct deviations at 16, 18 and 24 CAD coinciding with the auto-ignition events. These deviations are so small, however, that they can be neglected.

In the present study, the POSM phases were based on zero-dimensional constant-volume calculations at given pressures and temperatures. It is likely that using calculations closer to engine conditions would improve POSM, such as through using a set of points obtained from actual SRM engine calculations. Even when using data that was not tuned to engine calculations, a speed-up was achieved, however. With use of more realistic starting data, more realistic phases can be expected to be found and still greater speed-up to be obtained. Finally, just as POSM can be used to improve the calculation speed it can also be used to improve the accuracy of the calculations. In that case the approach would be to have a number of optimized yet not reduced mechanisms for each phase. For numerical reasons, it would still be faster than a single mechanism would be.

## Conclusions

An already reduced skeletal standard mechanism was divided into five sub mechanisms, each representing a phase in the combustion events. These Phase Optimized Skeletal Mechanisms, POSM, together with the establishing of the phases, were achieved by use of an automated tool employing machine-learning, clustering and decision tree algorithms. The phases were established on the basis of constant-volume calculations. The POSM model created was implemented

in the two-zone SRM code, comparative calculations being made for the standard mechanism and for the POSM, respectively, with the aim of determining the accuracy and the calculation speed of this novel technique. POSM shows excellent agreement with the standard mechanism, in terms of pressure, temperature and species mass fractions. The deviations are generally less than 0.1 %. POSM is three times as fast as the standard mechanism.

### 6.2.4 Investigation 2

A second investigation using the POSM approach was performed to confirm that the findings of investigation 1 could be repeated with use of another chemical model. The engine and calculation parameters were the same as in investigation 1. These can be found in Tables 6.1-6.3. The fuel employed in the present investigation was a mixture of n-heptane and isooctane.

#### The Chemical Model

The chemical kinetic mechanism employed, both for the standard two-zone SRM calculations and as a base mechanism for the POSM, is a skeletal n-heptane / isooctane mechanism. This skeletal mechanism had already undergone the necessity analysis with respect to the entire calculation, required to create an optimally reduced mechanism. The n-heptane / isooctane mechanism contains 96 species and 647 reactions [80].

#### The POSM Created

In this investigation the same conservative level of reduction was employed as in investigation 1. Instead of using multiple zero dimensional constant volume calculations, a single engine calculation with the two-zone SRM using the original standard skeletal mechanism, was carried out to provide the statistics needed for phase creation. The POSM creation process performed resulted in six different phases with one phase optimized skeletal mechanism for each phase (Table 6.5). The phases represent a further reduction in size as compared with the standard reduced skeletal mechanism.

**Table 6.5** *Number of species and reactions for the mechanisms employed.*

Original mechanism	96 species / 647 reactions
Phase 0	20 species / 117 reactions
Phase 1	95 species / 646 reactions
Phase 2	80 species / 428 reactions
Phase 3	46 species / 275 reactions
Phase 4	43 species / 275 reactions
Phase 5	47 species / 277 reactions

The phase decision model created for these mechanisms makes use of the massfractions of the following species: the *hydrogen radical*  $H$ , the *hydroperoxy radical*  $HO_2$ , the *oxygen radical*  $O$ , the *hydrogen-peroxide*  $H_2O_2$ , the *formyl radical*  $HCO$ , *carbon-monoxide*  $CO$ , *methanol*  $CH_3OH$ , *propene*  $C_3H_6$  and *iso-octene*  $I-C_8H_{16}$ . Generally speaking, *iso-octene* can be formed by oxidation of the fuel *iso-octane* by hydrogen atom abstraction, for example, which can also yield the *hydroperoxy radical*. Yet, this is only one way species are formed or disappear. Describing the processes applying to the involved species adequately would require a whole textbook, to which the interested reader is referred [90]. On an intuitive level, temperature and pressure could both be taken into account in deciding which phase to use. During the POSM process, however, these were found to not be as efficient as the species massfractions, for the division or the selection of phases.

## Results

The aim of this study was to compare the POSM approach with the standard mechanism in terms of accuracy and computational time and also determine whether the performance of the POSM demonstrated in investigation 1 could be reproduced.

### Calculation Accuracy

Pressure and temperature profiles, together with mass fractions over time for the species  $OH$  and  $CH_2O$  are presented. These two species were chosen since they are commonly measured and for the highly reactive  $OH$  also could provide some differences [28].

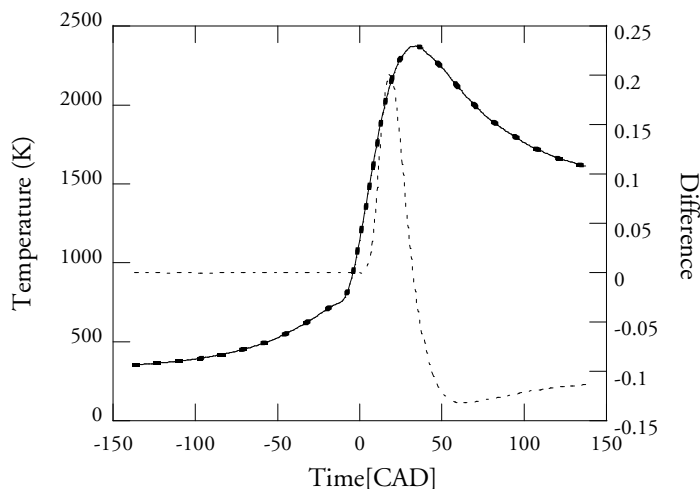


**Figure 6.10** Calculated temperatures as a function of time (left axis) and of absolute differences between the calculations (right axis).

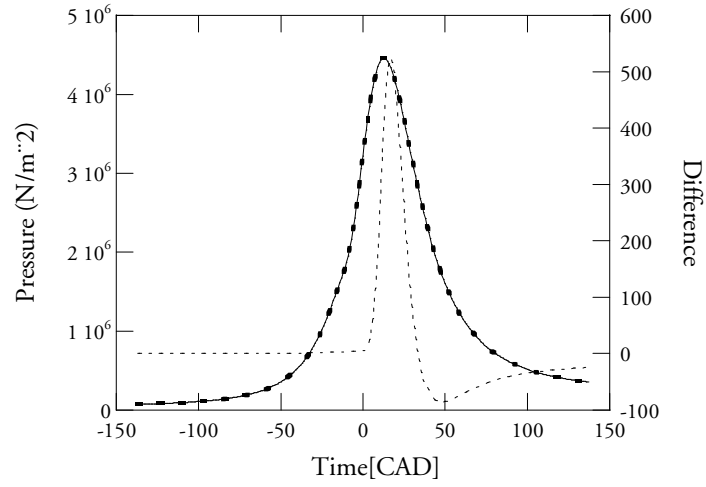


**Figure 6.11** Calculated pressures as a function of time (left axis) and of absolute differences between the calculations (right axis).

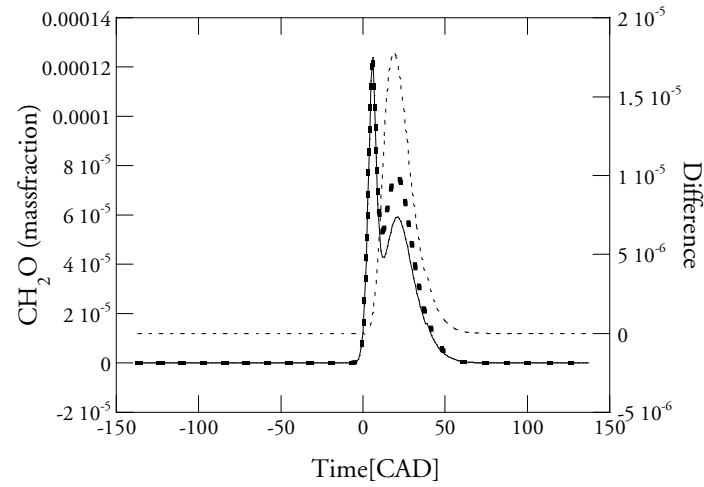


**Figure 6.12** Calculated mass fractions of  $\text{CH}_2\text{O}$  as a function of time (left axis) and of absolute differences between the calculations (right axis).

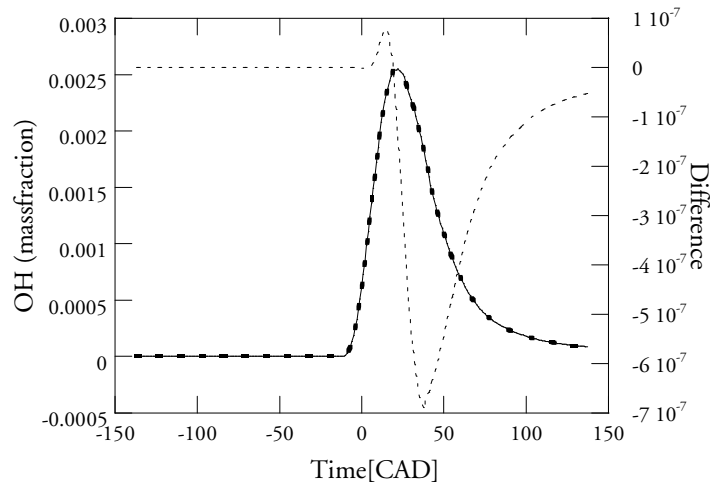


**Figure 6.13** Calculated mass fractions of OH as a function of time (left axis) and of absolute differences between the calculations (right axis).

As can be seen in Figures 6.10-6.13, the differences between the calculations are small. For more precise comparison purposes, the absolute differences between the calculations are also given. For each figure, the thin line represents POSM calculations, the thick dots are for standard mechanism calculations and the thin dotted line shows the absolute differences between the two sets of calculations. The differences in temperature between the standard calculations and POSM, shown in Figure 6.10 are too small for it to be possible to distinguish between them. As the difference curve indicates, the differences are well below 0.01% or 0.2 K throughout the calculations. The maximum difference is found at 16 CAD but is so small that it can be neglected.

The pressure curves in Figure 6.11 show exactly the same type of behavior as that for the temperature curves. Just as in Figure 6.10 the differences are very small, less than 0.02 % or 600 N/m<sup>2</sup>, and they also peak at the same time as the temperature curves in Figure 6.10 do. Regarding the mass fractions calculated for the species OH and CH<sub>2</sub>O, Figures 6.12 and 6.13, one can note the same very small differences. It is obvious that the POSM performs almost as well as the standard mechanism. For CO the largest difference occurs at 16 CAD and is less than 1 %.

The largest deviation in the calculations occurs for CH<sub>2</sub>O at 16 CAD and is in the order of 20 % where POSM has the lower value. This deviation can be attributed to the fact that the phase mechanism used by most of the particles during these time-steps is the smallest. Most of the time, the difference is well below 0.1 %. OH which was expected to be difficult to match, in fact

shows close agreement for the calculations. The largest difference, less than 0.1 %, appears at 38 CAD coinciding with the end of the Wiebe-function.

### Reduction in calculation time

Once again POSM show excellent agreement with the standard mechanism, at the same time as it is roughly three times as fast. On a laptop having a 3.2 GHz Pentium processor the calculations using the standard mechanism required 154 s to be completed, while the POSM calculations were completed in 49 s. This translates to a factor of about 3 in terms of computational savings.

### 6.2.5 Analysis of the calculation with POSM

The POSM that was created and used for investigation 2, have six different phase optimized skeletal mechanism in place of the single standard skeletal mechanism. In Figure 6.14 one can see how the different particles are using the different phase mechanism over the calculation time.

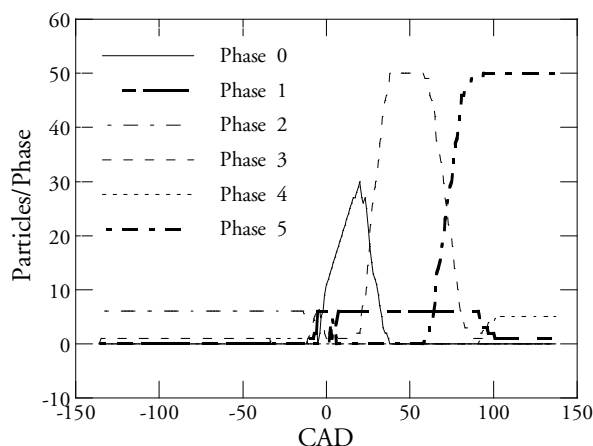


**Figure 6.14** Number of particles using different phases, over the complete calculation.

The calculations start with 5 particles of fuel + air and one particle of EGR, all located in the unburned zone. All the fuel + air particles use phase 2, which is a fairly large phase mechanism (80 species), one used when there are low levels of the *hydroperoxy radical*, *carbon-monoxide* and *iso-octane*. The EGR particle makes use phase 5 since the level of the *hydroperoxy radical* is low, but the levels of *carbon-monoxide* and of *methanol* are relatively high.

From the time of ignition at -11.5 CAD (see Figure 6.15) on through the combustion period of 50 CAD a new particle is created from mass taken from the unburned particles, and is added to

the burned zone at each CAD. The first seven new particles use phase 3, which is employed when intermediate to higher levels of the *hydroperoxy radical* but lower levels of *propene* are present. Phase 3 is also the dominant phase for the burned particles between 25 CAD and 70 CAD, where it is eventually replaced by phase 6 as the concentration of the hydroperoxy radical decreases. During the combustion period from -11.5 CAD until 38.5 CAD, the dominant phase for the burned (new) particles is phase 0 and for the unburned particles, phase 1.

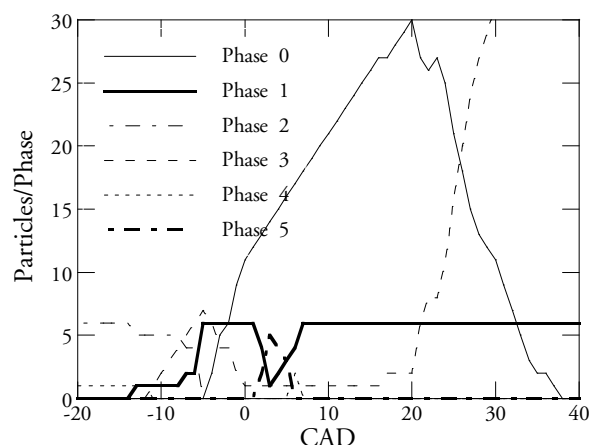


**Figure 6.15** Number of particles using different phases over the actual combustion period (CAD -11.5 – 38.5).

Phase 0 is the smallest mechanism, one employed when there are substantial amounts of the *hydroperoxy radical* and *hydrogen-peroxide*, but low levels of *propene* and of *formyl radical*, which is typical of combustion products at high temperature. Phase 1, which is used by the unburned particles during combustion, is the largest phase mechanism containing all but one species (HCCO), as compared with the standard mechanism. It is no surprise that this phase mechanism is used for the unburned particles, since it contains most of the species and the chemistry there is the most active.

The whole point of using the POSM approach is to gain calculation time by using smaller mechanisms while still maintaining accuracy. Figure 6.16 shows the timing for the phase mechanisms used for the calculations. The time is given in relative CPU time as compared with the mean time for the completion of the calculations for the standard mechanism. The figure is a bit deceptive. It implies that the largest phase mechanism involving 95 species is slower than the standard mechanism involving 96 species, which of course is not the case. Any mechanism is slower or faster depending on how difficult the problem is to solve at any given instant. This means that since during the combustion itself the problem is typically difficult to solve, this is

the point where use of the largest phase mechanism is called for. Use of a smaller mechanism at this point could be slower and less accurate.

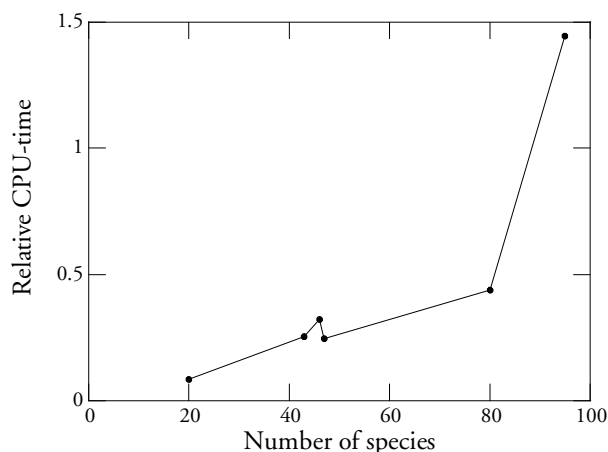


**Figure 6.16** Relative CPU-time for the six different phase-mechanisms employed.

Still, this figure provides some information. The mechanism consisting of 80 species (phase 2) is much faster than that consisting of 95 species (phase 1), and further reductions in size give additional improvements in performance, except for the mechanisms consisting of 43 and 46 species, respectively (phases 5 and 3), as compared with the mechanism consisting of 47 species (phase 6). The latter can be explained by the fact that phase 6 is employed for the most part after the combustion has been completed, when the calculations are “easy” from a numerical point of view. The same explanation can be given for the mechanism consisting of 80 species (phase 2) being very much faster relative to the other mechanisms. Phase 2 is used almost exclusively prior to combustion, when the calculations are also “easy”.



### 6.2.6 Investigation 3

A third investigation was performed to study a less conservative level of reduction, using the POSM approach. Once again, the engine and the calculation parameters were the same as in investigation 1, shown in tables 6.1-6.3. Just as in investigation 2 the fuel employed was a mixture of n-heptane and isooctane.

#### The POSM Created

This investigation uses the same chemical model and base data for the creation of POSM as in investigation 2, but a less conservative level was employed to achieve a further reduction in calculation times. The process of creating POSM that was adopted resulted in six different phases, with one phase optimized skeletal mechanism each (Table 6.5). The phases involved represent a further reduction in size as compared with the standard reduced skeletal mechanism. The created phase decision model created for these mechanisms employs the same massfractions as used in investigations 2.

*Table 6.6 Number of species and reactions for the employed mechanisms.*

Original mechanism	96 species / 647 reactions
Phase 0	17 species / 91 reactions
Phase 1	64 species / 434 reactions
Phase 2	55 species / 257 reactions
Phase 3	24 species / 112 reactions
Phase 4	15 species / 60 reactions
Phase 5	13 species / 34 reactions

#### Results

The aim of this study was to compare the POSM approach with the standard mechanism in terms of computational time and accuracy.

#### Calculation Accuracy

Pressure and temperature profiles as well as mass fractions over time for the species OH and CH<sub>2</sub>O are presented.

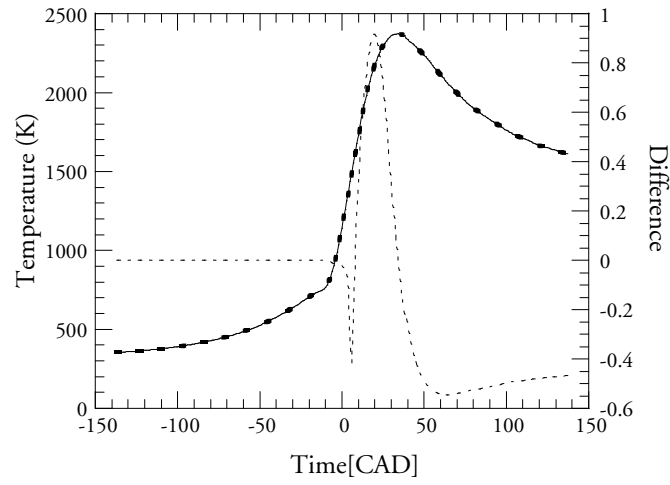


**Figure 6.17** Calculated temperatures as a function of time (left axis) and of absolute differences between the calculations (right axis).

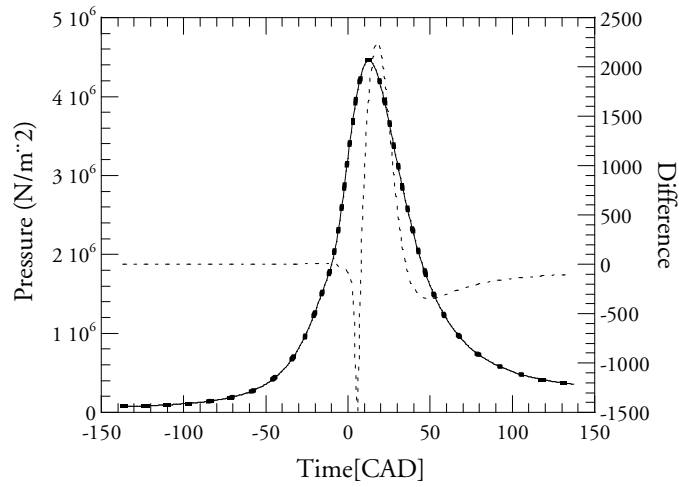


**Figure 6.18** Calculated pressures as a function of time (left axis) and of absolute differences between the calculations (right axis).

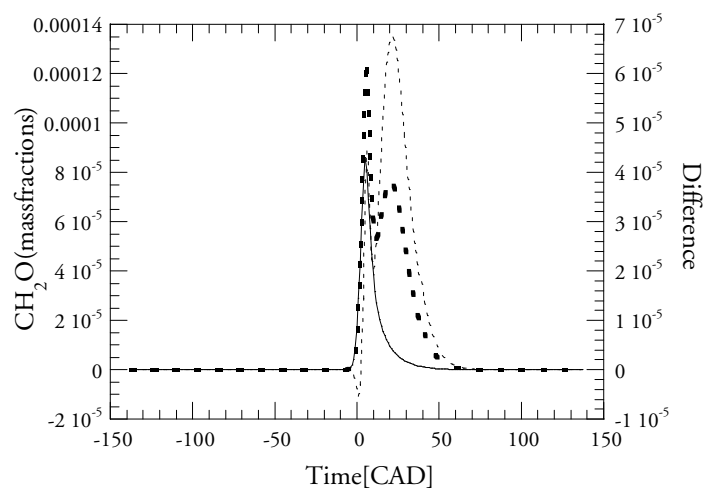


**Figure 6.19** Calculated mass fractions of  $\text{CH}_2\text{O}$  as a function of time (left axis) and of absolute differences between the calculations (right axis).

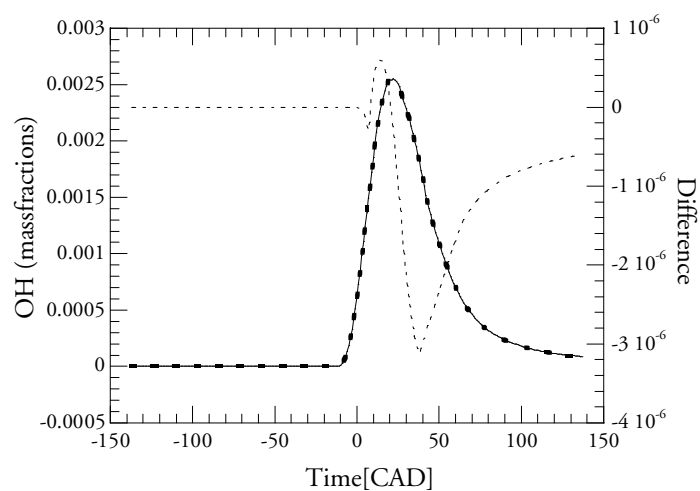


**Figure 6.20** Calculated mass fractions of  $\text{OH}$  as a function of time (left axis) and of absolute differences between the calculations (right axis).

The accuracy achieved is not of the same level as in investigation 2. Formaldehyde, in particular, is not well predicted (Figure 6.19). The second peak has vanished completely and the difference in this region being nearly 90 %, although the difference is fortunately less than 1 % most of the time. OH (Figure 6.20) is still well predicted, however, with a maximum difference being less than 0.2 %, coinciding this time too with the end of the Wiebe-function at 38 CAD.

Although the predictions of individual species are of varying quality, the global conditions are well captured. The pressure curve shows almost exactly the same behavior as before, as can be seen in Figure 6.18. The maximum difference is very small, less than 0.1 % or 2300 N/m<sup>2</sup>, peaking at 16 CAD. The difference in temperatures between the standard calculations and POSM in Figure 6.17 is so small that it is impossible to distinguish them from each other. As the difference curve indicates the difference is well below 0.05% or 1 K throughout the calculations.

Although such ambitious reduction as this could make the model less useful for studies of individual species during the combustion, a study of the model's ability to predict global conditions and emissions at EVO was carried out. Global conditions such as pressure and temperature has already been shown to be predicted sufficiently well. Since the original chemical model did not contain any NO<sub>x</sub> chemistry those emissions could not be studied.

CO was well predicted, the difference at EVO being less than 1%. Hydrocarbons was not well predicted, the difference being a factor of 100 at a mass fractions level of  $1.6 \cdot 10^{-11}$ . The difference was due entirely to the difference for the *formyl radical*. The hydrocarbon level was very low and it is questionable whether the predicted difference would be as great for cases involving higher levels of hydrocarbons.

### Reduction in calculation time

This POSM, in which the reduction is less conservative, agrees less well with the results for the standard mechanism than was the case in the two previous investigations. Nevertheless, the levels of agreement achieved for the global parameters of pressure and temperature, as well as for emissions at EVO, are quite acceptable. On a laptop with a 3.2 GHz Pentium processor, the calculations based on the standard mechanism required 154 s to complete, whereas the POSM calculations were completed in 12.6 s. This translates to a factor of about 12 in terms of computational savings.

### 6.2.7 Conclusions

Although all POSMs in this work were based on already strongly reduced skeletal mechanisms, use of POSM was found, nevertheless, to result in gains in calculation speed with retention of accuracy. The first two investigations showed almost no accuracy to be lost, at the same time as

there was a gain in calculation time by a factor of 3. These two investigations differed not only in the original chemical model that was employed, but also in how the database for Phase creation was calculated. Investigation 1 employed several sets of constant volume calculations, whereas investigation 2 used only a single SRM calculation. It was expected that the SRM calculation would provide a more realistic data set than the constant volume calculations, an expectation that could be neither confirmed nor rejected since the two cases had almost exactly the same accuracy and gain in calculation time. The second case did have a smaller original chemical model, however, which gave less latitude for reduction, so it can well be the case that the SRM calculation did provide a better data set.

Investigation 3 involved a further reduction than carried out in investigation 2. It showed clear losses in accuracy, although the global conditions were well captured and there was a gain in calculation speed by a factor of 12. One should note that the number of species in the phase mechanisms had become so small that it is not at all surprising that higher losses in accuracy appeared.

There is still a lot to be gained by further division into a greater number of phases, rather than simply reducing the number of species in the phases. Especially for phases having only a small reduction in size and possessing a size similar to the original chemical model, further division would be likely to result in substantial gains.

Further, the POSM approach showed excellent robustness as a concept. Even with different base chemistries as in investigation 1 and 2, and also by varying octane rating and mixture strength, accuracy was retained. Several studies to investigate the sensitivity of the numerical and modeling parameters by varying the number of particles, time step size and mixing and heat transfer parameters that were performed, confirmed the robustness of POSM.

### 7 The DI-SRM

Part of the work described in this chapter has been submitted and tentatively accepted for publication at the 2008 SAE International Powertrains, Fuels and Lubricants Congress.

The DI-SRM is an extension of the HCCI-SRM that includes the direct injection modeling. The model is intended to be a computationally efficient one yet able to provide predictive information of engine performance and emissions. The model is suitable for use in simulating diesel engines (CI) and pHCCI. With some extensions it would be useful for DISI (gasoline direct injection) engines as well.

#### 7.1 Introduction

For direct injection engines, such as diesel engines (CI) the combustion process is known to be mainly decided as a function of the mixing processes involved [23,33]. Nevertheless the actual initiation of the combustion during the mixing process is a kinetics decided phenomenon. For this reason a kinetics model could be found valid if the mixing processes can be modeled in an accurate way. Thus far, the SRM has been used little for the investigation of pure diesel engines.

Studies of direct injected HCCI engines using the SRM have appeared in recent years. In terms of implementation these engines have certain similarities with diesel engines but run with early injection that gives partially premixed conditions. [91] has studied the effects of early direct injection on combustion in an HCCI engine while [92] has studied the implementation of a simple spray model and a mixing model in an engine a similar type.

There is a study in [42] reporting calculations using the extreme inhomogeneous conditions found in a pure directinjection diesel engine employing the SRM, in which ignition conditions and soot formation are compared with CFD calculations.

The DI-SRM presented in the this work is based on the HCCI-SRM described in chapter 4, with a fuel injection model employed being one that was developed from the fuel injection model developed originally by [93]. The aim of [93] was to create a model applicable to the investigation of early injection engines, for instance of pHCCI type. Validation was performed in qualitative terms. The model was later developed further and was then applied directly to the modeling of 2-stroke marine diesel engines by [94]. In such implementations, the user of the model has to set the ratio of the number of fuel particles to the total number of particles used. This results in the fuel particles having a weight that differs from that of the other particles. Accordingly, the C/D mixing model had to be modified to deal with particles of differing weight.

During the parametric studies, sensitivity to the fuelparticle ratio was discovered to be an unwanted feature of the model.

The work presented here addresses such issues and also aims at creating a more robust and physically correct model, one that also has the option of coupling with external tools. The main changes in the fuel injection model and additions to it that the author undertook were to make the model fulfill the assumption of equi-weighted particles in the mixing models employed, adapt it to the dynamic time stepping and to integrate a mass fraction burned calculation that are needed for coupling to external tools. The final model developed termed the DI-SRM, was then integrated into the DARS-ESM/ESSA package the author constructed which provides additional functionality, such as coupling to external simulation tools [84,96].

## 7.2 Direct injection model

As compared with the HCCI-SRM model described in chapter 4 and the formal features of the SRM itself, the DI-SRM has additional features, direct injection into the cylinder during the closed cycle being one of these. The operator splitting loop is also expanded to include the direct injection and an additional pressure correction step (Figure 7.1).

### The DI-SRM

The DI-SRM, or direct injection stochastic reactor model, is based on the partially stirred reactor model (PaSPFR) described in chapter 4. It also contains the same PDF based Monte Carlo type simulation assumption, involving use of an MDF and an operator splitting loop. The operator split loop has been extended with one additional step for fuel injection. The DI-SRM model does not include any model for ignition assistance but relies entirely on chemical kinetics.

The fuel injection model employed can model multiple direct injections in which the injection profiles can be of any shape. To simplify implementation, the fuel is assumed to be vaporized instantaneously at the moment of injection, and no vaporization model is employed. There are two implications that follow from this.

1. Rather than a fuel mass injection curve, a vaporized mass injection curve needs to be used as input to the model.
2. The energy needed for vaporization of the injected fuel needs to be taken into account in the model.

During the combustion calculations a control is made at each time step to determine whether there is any fuel to be injected. If such is the case, the vaporized amount to be injected is determined by a linear interpolation of the fuel injection profile provided.

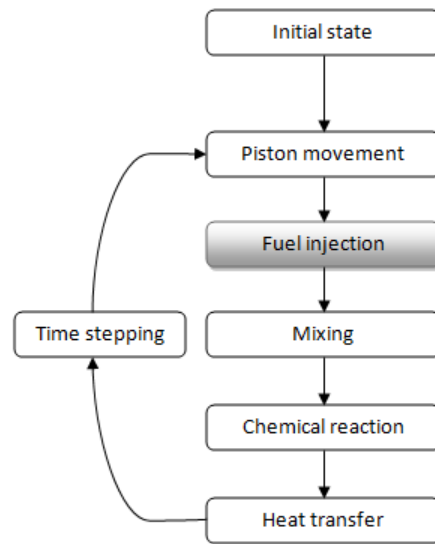


**Figure 7.1** Operator split loop in the DI-SRM involving an added fuel injection step.

The energy needed to vaporize the fuel is determined by lowering the temperature on a sufficiently large mass in the cylinder to the level of the fuel vaporization temperature. This mass, referred to here as the mixing mass, is taken from the already existing particles and is combined with the mass of the injected fuel that forms new particles (Figure 7.2).



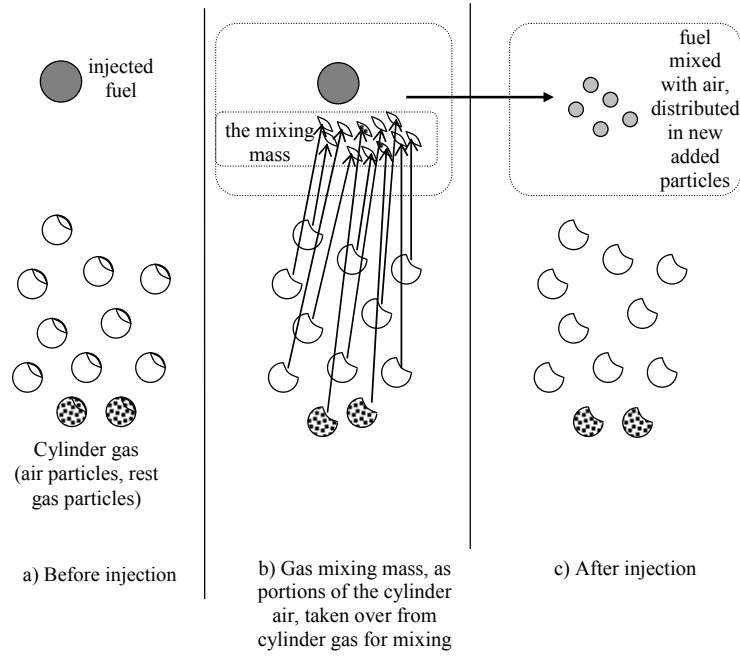


**Figure 7.2** Particle handling during injection.

When fuel  $\dot{m}_f$  is added to the cylinder, the mass fractions and the temperatures of the current set of particles is changed, in line with the composition of the fuel and its liquid injection temperature. Thus, for each particle the source terms need to be supplemented by extra terms that are added (superscript *inj*):

$$G_i^{inj} = \frac{\dot{m}_f}{m} (Y_{i,f} - Y_i), \quad i = 1, \dots, S \quad (7.1)$$

$$G_i^{inj} = \frac{\dot{m}_f}{m} (M_{i,f} - M_i), \quad i = S + 1, \dots, S + n_m - 1 \quad (7.2)$$

$$G_{S+n_m}^{inj} = \frac{1}{\rho c_p} \frac{\dot{m}_f}{V} \sum_{i=1}^S Y_{i,f} (h_{i,f} - h_i) \quad (7.3)$$

where  $S + n_m$  is the index of the temperature, if first  $n_m$  soot moments are included in calculations. The total mass of the cylinder gas  $m$  also changes in accordance with the fuel that is added. The mixing mass is taken from the existing cylinder gas particles. Figure 7.3 presents a sche-

matic for redistribution of the mass and species in a particle after a certain portion of it, represented by a dashed line, is removed and is used for mixing with the fuel.

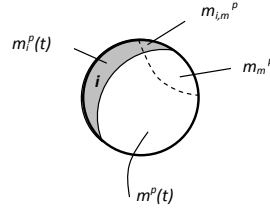


**Figure 7.3** Schematic of an existing particle and of the ratios of masses transferred from it.

A given species  $i$ , represented as gray in the figure, is proportionally distributed between the remaining particles and the mass collected for mixing with the fuel. For each individual particle used in mixing, account is taken of the distribution of the particles species.

If  $m_{i,m}^p$  denotes the mass of species  $i$  taken from particle  $p$  for contributing to the mixing mass, for the old particles the mass fraction of the updated species in particle  $p$  is:

$$Y_i^p(t + \Delta t) = \frac{m_i^p(t) - m_{i,m}^p}{m^p(t) - m_m^p}, \quad p = 1, \dots, N \quad (7.4)$$

whereas the new and added particles all have the same species mass fractions, where  $m_{i,m}$  is the mean mass of species  $i$  for particles present:

$$Y_i^p(t + \Delta t) = \frac{m_{i,f} - m_{i,m}}{m_f - m_m}, \quad p = N + 1, \dots, N' \quad (7.5)$$

The updated temperatures of the old particles and the new and added ones respectively are:

$$T_i^p(t + \Delta t) = T^p(t), \quad p = 1, \dots, N \quad (7.6)$$

$$T_i^p(t + \Delta t) = T_v, \quad p = N + 1, \dots, N' \quad (7.7)$$

## Stochastic Reactor Models for Engine Simulations

The gas mass needed for vaporizing the fuel is calculated, account being taken of the pressure at which the process occurs being constant, and of the final temperature of both the injected fuel and the mixing mass after completion of the process being equal to the vaporization temperature, which corresponds to that specific pressure:

$$m_m = \frac{h_{f,liq}(T_f) - h_{f,gas}(T_v)}{h_m(T_v) - h_m(T_m)} m_f \quad (7.8)$$

where the index  $f$  denotes the injected fuel, and the index  $v$  vaporization.

In the case in which the fuel is a mixture of several different species, each species is dealt with separately in terms of Equation 7.8, since each has a specific vaporization temperature.

The process of fuel injection is considered in itself as being a distinct event in the series of operator splits. The final step in the fuel injection process is the re-initialization of the PDF particles when the new fuel particles are introduced, the masses of all existing particles being adjusted accordingly.

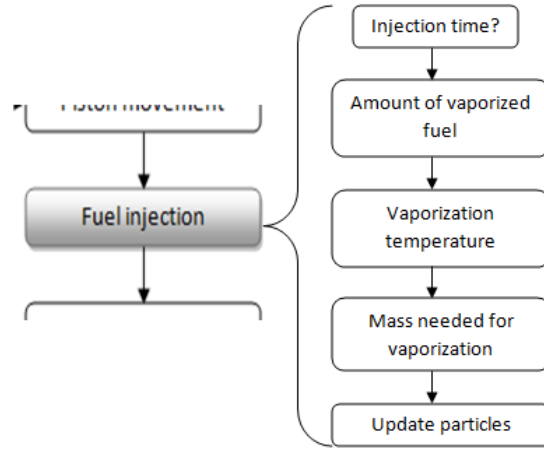


**Figure 7.4** Basic steps in the fuel injection model.

The algorithm for the fuel injection event at each time step in the calculations, shown in Figure 7.4, is as follows:

1. Check if current time is in the range of any of the injection events. If true, follow steps 2...5, otherwise step out.

2. Calculate the amount of vaporized fuel (for each fuel species) from the externally prescribed vaporization rate that corresponds to the time step.
3. Determine the vaporization temperature that corresponds to the current pressure.
4. Calculate the amount of mixing mass that corresponds to the vaporization energy.
5. Reset the particles properties, when new particles are added, in accordance with Equations (7.5) – (7.8).

Figure 7.5 provides a picture of what occurs when one investigates the evolution of the particle masses during a set of calculations. The x-axis is evolution over time (CAD), y-axis is the particle mass and z-axis is the number of particles. Only a small number of particles are represented. At the start, only equal particles are present.

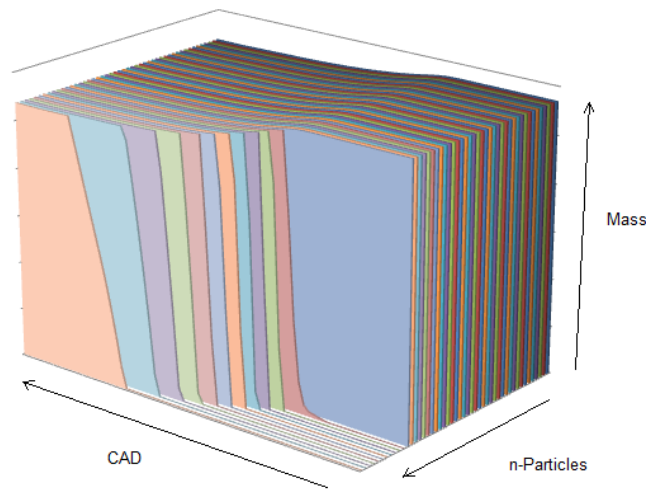


*Figure 7.5 Representation of a selection of the particle masses during fuel injection.*

In the course of time, fuel particles are added consuming mass from all the existing particles, which leads to the mass of the particles decreasing, but since it is assumed that all the particles are of the same weight each fuel particle is only allowed to grow until it reaches the mass of all of the other particles. When this happens, any fuel mass remaining at a given time step leads to the creation of new fuel particles, all of them obeying this condition, except for the single fuel particle created last which at any given time step can have a smaller mass than any of the others. At the next time step, this last particle is filled up, this process being repeated until all the fuel has been injected. Figure 7.5 shows the smooth evolution of the particle masses.

## 7.3 Coupling to Wave

Part of the thesis work was the novel implementation of the DI-SRM (DARS-ESM), to be coupled with the 1-D-EST, Ricardo Wave [95]. Considerable emphasis was placed on making the interfacing of the DARS-ESM suite work both with other 1-D-ESTs as well as with Wave, while using the same DARS-ESM executable. A few tricks had to be employed to be able to send all the data acquired back and forth between the models. Detailed information on how to use DARS-ESM and all its submodels, together with its coupling to Wave, can be found in the DARS-ESM/Wave manual [96].

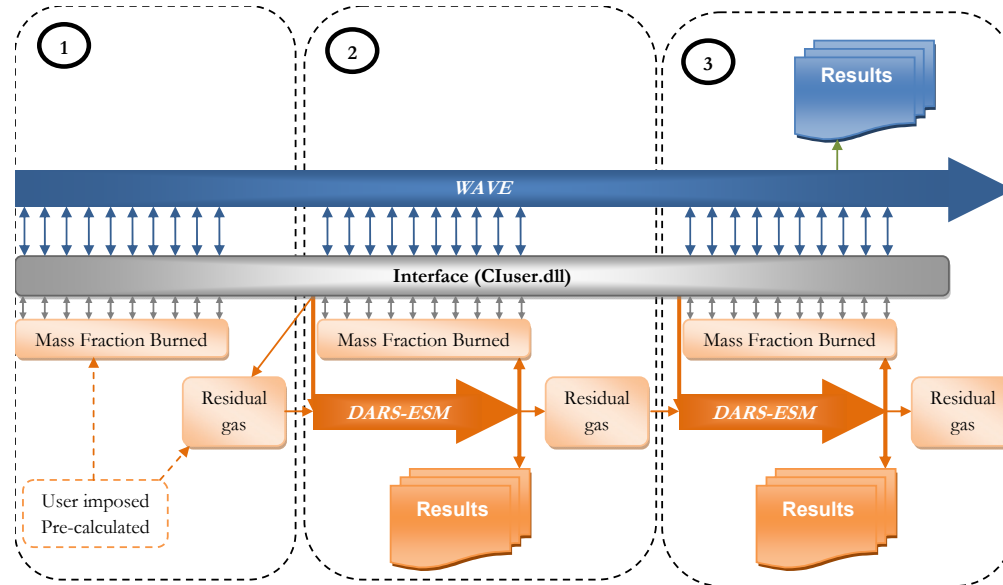


**Figure 7.6** Temporal representation of the Coupling between DI-SRM (DARS-ESM) and Wave.

In section 7.4 all of the calculations, performed by two numerical codes that are coupled with each other, Wave and DARS-ESM, are presented. Wave is a commercial 1-D full engine simulation tool licensed by Ricardo Inc [95]. DARS-ESM is a combustion calculation code that contains the DI-SRM code developed and used in this investigation.

Figure 7.6 indicates the temporal coupling between the 1-D-EST and DARS-ESM. The 1-D-EST, which contains the full engine model (Figure 7.7-7.8), calculates the flow dynamics at each location in the engine, together with all the basic engine parameters and the engine performance, whereas DARS-ESM predicts the in-cylinder combustion.

The coupling is based on the fact that the 1-D-EST provides information regarding the initial conditions at IVC in terms of the cylinder temperature, pressure and amount of residual gases. DARS-ESM provides a cumulative mass fraction burned (MFB) curve that the 1-D-EST uses then to evaluate the cylinder properties during combustion.

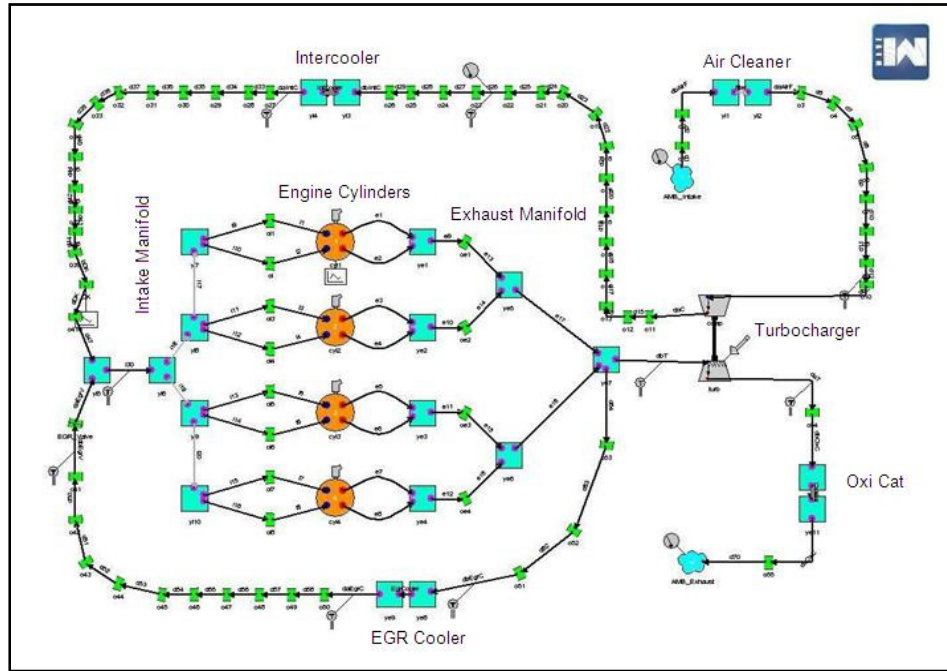


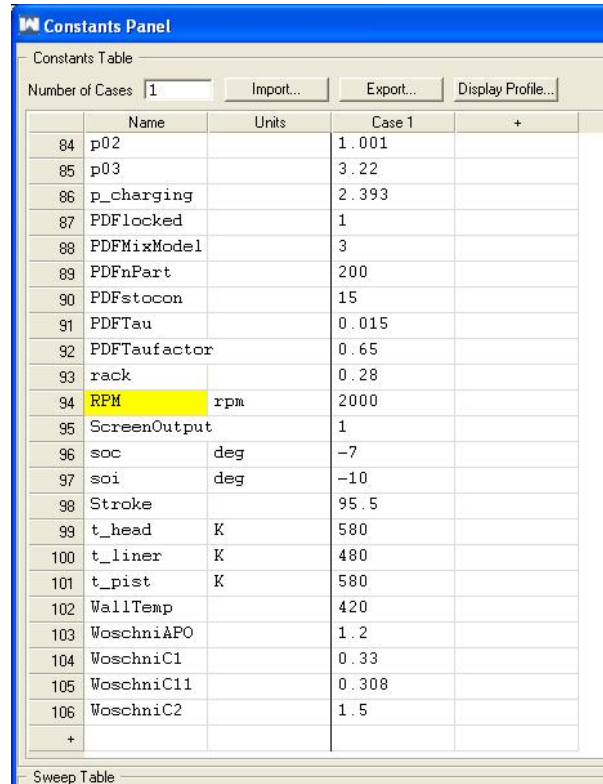
*Figure 7.7 Representation of the TDI engine Wave model.*

If one looks closer at Figure 7.6, the steps of the coupling are:

1. The initial cycles are calculated so as to obtain flow convergence in the 1-D-EST model. For each 1-D-EST time step during the combustion period, the 1-D-EST interrogates DARS-ESM for the cumulative MFB. Since the combustion event has an immediate effect on the flow conditions in the engine, a pre-calculated MFB that is appropriate to the conditions should be employed.
2. The first calculated DARS-ESM cycle takes as its initial conditions the cylinder temperature and pressure and the amount of residual gases from the 1-D-EST. Information concerning the species mass fraction of the residual gases is limited in the 1-D-EST. Although this information

## Stochastic Reactor Models for Engine Simulations

can be utilized, achieving faster convergence for both the flow and the combustion calculations a detailed species mass fraction list for the residual gases may be provided by the user. DARS-ESM performs the complete calculation while the 1-D-EST waits. DARS-ESM updates the MFB and provides the result data for this cycle as outputs. The 1-D-EST continues its calculations then and collects the updated MFB data.



	Name	Units	Case 1	+
84	p02		1.001	
85	p03		3.22	
86	p_charging		2.393	
87	PDFlocked		1	
88	PDFMixModel		3	
89	PDFnPart		200	
90	PDFstocon		15	
91	PDFTau		0.015	
92	PDFTaufactor		0.65	
93	rack		0.28	
94	RPM	rpm	2000	
95	ScreenOutput		1	
96	soc	deg	-7	
97	soi	deg	-10	
98	Stroke		95.5	
99	t_head	K	580	
100	t_liner	K	480	
101	t_pist	K	580	
102	WallTemp		420	
103	WoschniAPO		1.2	
104	WoschniC1		0.33	
105	WoschniC11		0.308	
106	WoschniC2		1.5	
	+			

**Figure 7.8** Part of the Constants Panel in Wave where data needed for the coupling with DARS-ESM can be included.

3. All calculated DARS-ESM cycles thereafter take as their initial conditions the cylinder temperature and pressure and the amount of residual gases from the 1-D-EST, but for all of these cycles DARS-ESM uses the final species mass fractions from the previously calculated DARS-ESM cycle as the residual gas species. As before DARS-ESM will perform the complete calculations while the 1-D-EST waits. For each individual cycle DARS-ESM will update the MFB and output result data. The 1-D-EST continues its calculations then and collects the updated MFB data. When all the cycles are completed the 1-D-EST results data can be accessed.

### Calculation of MFB in DARS-ESM

The main parameter needed for the 1-D-EST to establish the heat release from combustion and thus provide the cylinder pressure and temperature and the species properties, is the mass fraction burned (MFB), which contains the key to this. In DI-SRM the MFB is calculated by use of the change in molar specific enthalpy  $H$  that occurs.

At the start of combustion, calculations are made by the DI-SRM, the enthalpy  $H(t_0)$  for the initial condition of the species, including the fuel to be injected. The adiabatic or burned enthalpy  $H_{ad}(t_0)$  is calculated for the same conditions. The current enthalpy  $H(t)$  is calculated for each time step that follows, account being taken of any fuel that is yet to be injected, which provides an MFB of between 0 to 1 in the range of  $H(t_0)$  to  $H_{ad}(t_0)$ .

The expression for MFB in this model is:

$$MFB = \frac{H(t) - H(t_0)}{H_{ad}(t_0) - H(t_0)} \quad (7.9)$$

$$H(t) = \frac{m_{cyl} Y_{i,cyl} + m_{tbi} Y_{i,tbi}}{m_{cyl} + m_{tbi}}(t) h_i(298.0) \quad (7.10)$$

$$H(t_0) = \frac{m_{cyl} Y_{i,cyl} + m_{tbi} Y_{i,tbi}}{m_{cyl} + m_{tbi}}(t_0) h_i(298.0) \quad (7.11)$$

$$H_{ad}(t_0) = \frac{m_{cyl} Y_{i,cyl,ad} + m_{tbi} Y_{i,tbi,ad}}{m_{cyl} + m_{tbi}}(t_0) h_i(298.0) \quad (7.12)$$

The denotation  $tbi$  stands for “to be injected”.



## 7.4 Validation of DI-SRM coupled to a 1-D-EST

### The Chemical Model

The chemical kinetic mechanism used is an n-heptane mechanism based on a model developed for the NICE project [11]. The complete mechanism is reduced and contains 108 species and 882 reactions.

### Experiment and engine data

The experiments were performed on a VW TDI diesel engine. The engine is a 2.0 liter, 4 valve turbocharged in-line 4 cylinder, normally used as a personal car engine. The most important engine parameters are presented in Table 7.1. Regular diesel was used as fuel in the experiments and no active EGR was employed.

*Table 7.1 Basic engine parameters*

Total displacement [cm <sup>3</sup> ]	1968
Compression ratio	17.5:1
Bore [mm]	81
Stroke [mm]	95.5
IVC [CAD BTDC]	-115
EVO [CAD ATDC]	111

### Results and discussion

To study the performance of the DI-SRM two reference cases were set up and compared with experimental data. Since the actual injection profiles applied to the experiments were not accessible, invented injection profiles had to be constructed, based on the experimental information available, such as the start of injection, injection duration and total injected fuel mass. The DI-SRM does not use, as explained previously, fuel mass injection profiles but fuel vaporization mass profiles. For simplicity, and since the 1-D-EST (Wave) do provide a fuel vaporization model, the 1-D-EST was used to create the fuel vaporization mass profiles based on the provided, constructed fuel mass injection profiles. Further, the experiments were performed with diesel as fuel while the calculations were all performed with n-heptane as fuel. For these reasons the reference cases should be regarded as basic validation cases and as a basis for the parametric studies and demonstration of the fundamental performance of DI-SRM

## Reference case 1

**Table 7.2** Engine operating conditions and model parameters for reference case 1.

Engine speed [rpm]	3250
BMEP [bar]	13.2
Cylinder pressure at IVC [N/m <sup>2</sup> ]	$3.00 \cdot 10^6$
Number of particles	200
Mixing time $\tau$ [s]	0.0001
Stochastic heat transfer constant $Ch$	15
Time step size [CAD]	1.0

Reference case 1 is a medium-to-high speed and medium-to-high load case. The fuel injection mass profile was fed to the 1-D-EST which transferred it to a fuel vaporization mass profile, which could be used by the DI-SRM (Figure 7.9). Please note that the rates are normalized. The vaporization profile is quite much delayed and extends much further than the injection profile and does not show almost any trace of the pilot injection.

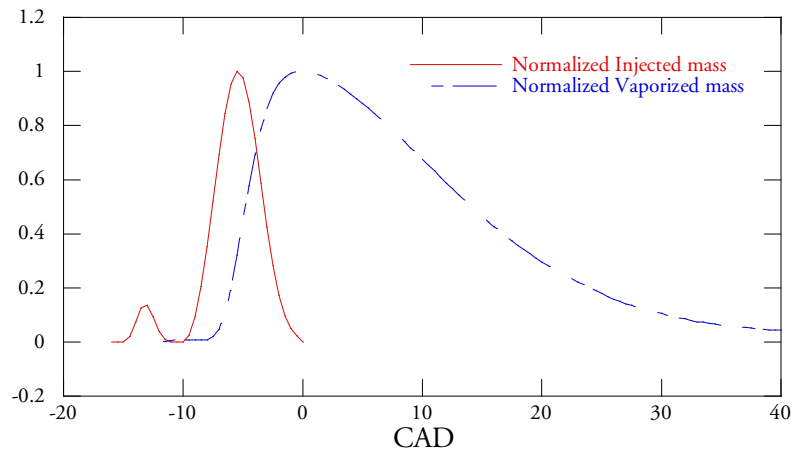


**Figure 7.9** Normalized injection rates for reference case 1.

The calculated pressure has the same maximum pressure as the experimental pressure trace and a reasonable timing. The pressure rate during combustion is clearly overpredicted and the expansion to early for the calculated case (Figure 7.10).

## Stochastic Reactor Models for Engine Simulations

---

The heat release rate is very noisy and fluctuating compared to the experimental heat release and the early part of the experimental heat release, CAD -10 to -5, has not been captured at all (Figure 7.10). The general correlation is fairly good though. The reason for the noisy heat release is mainly the coarse discretization with only 200 particles.

If we study the vaporization profile, the heat release rate and the pressure simultaneously it is clear that the experimental heat release starts before there is any major amount of fuel in the model according to the vaporization rate profile. This leads to the author's belief that the difference in the experimental and calculated pressure is a consequence of a not perfectly described vaporization rate profile.

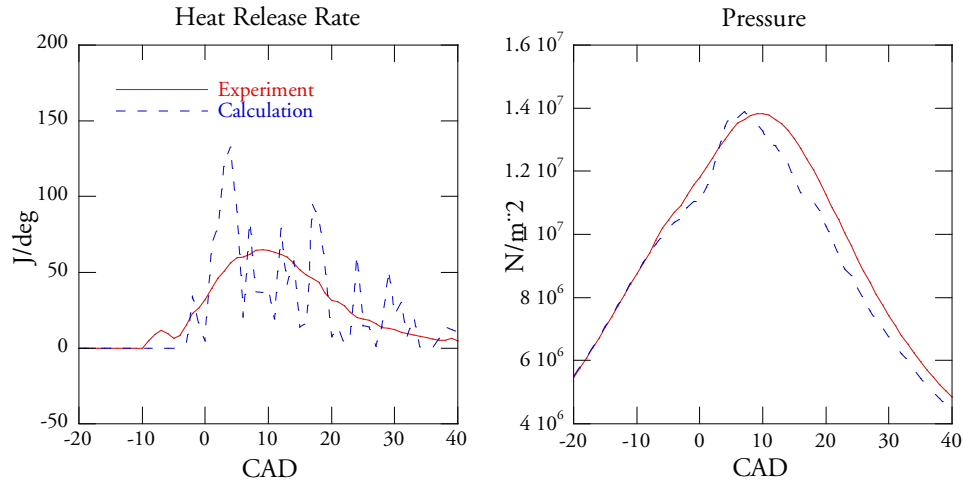


**Figure 7.10** Comparison of experimental and calculated heat release rate (left) and pressure (right) for reference case 1.

## Reference case 2

**Table 7.3** Engine operating conditions and model parameters for reference case 2.

Engine speed [rpm]	1500
BMEP [bar]	14.3
Cylinder pressure at IVC [N/m <sup>2</sup> ]	$2.98 \cdot 10^6$
Number of particles	200
Mixing time $\tau$ [s]	0.0002
Stochastic heat transfer constant Ch	15
Time step size [CAD]	1.0

Reference case 2 is a low speed and high load case. Just as for reference case 1 the fuel injection mass profile was fed to the 1-D-EST which transferred it to a fuel vaporization mass profile that could be used by the DI-SRM (Figure 7.11). Also in this case is the vaporization profile has the same basic profile and does not show any trace of the pilot injection.

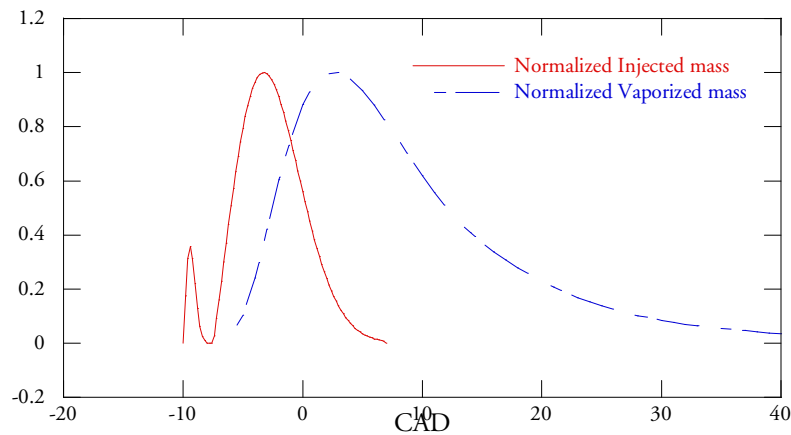


**Figure 7.11** Normalized injection rates for reference case 2.

The calculated pressure show the same maximum pressure as the experimental pressure trace and a good timing and an overall good agreement (Figure 7.12). The heat release rate is also for this case very noisy, for the same reason of coarse discretization, and the early part of the experimental heat release, CAD -8 to -3, has not been captured at all (Figure 7.12). The overall correlation is better than for reference case 1, with more of the heat release centered in time.

Once again it is clear that experimental heat release starts before there is any major amount of fuel in the model according to the vaporization rate profile.

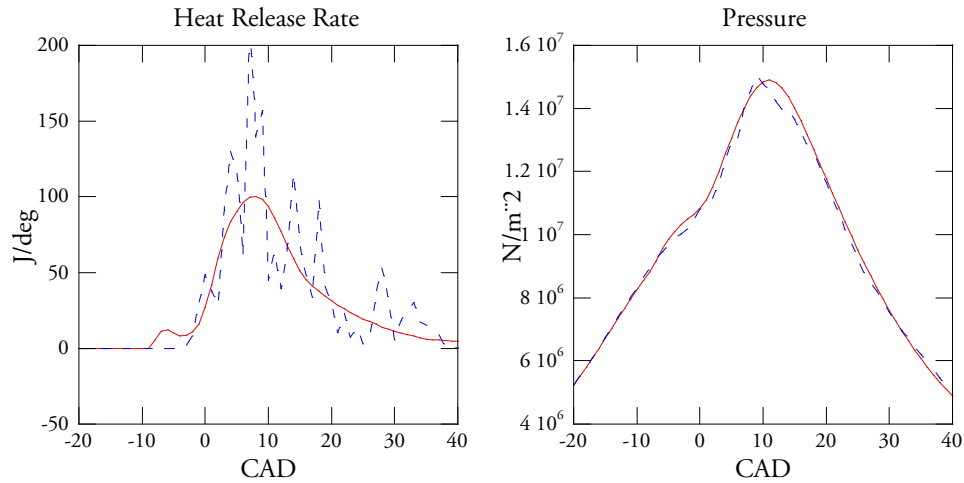


*Figure 7.12 Comparison of experimental and calculated heat release rate (left) and pressure (right) for reference case 2.*

### Parametric studies

All the parametric studies were performed with reference case 2 as the baseline. For clarity all the Figures 7.13-7.18 presents the experimental results as well.

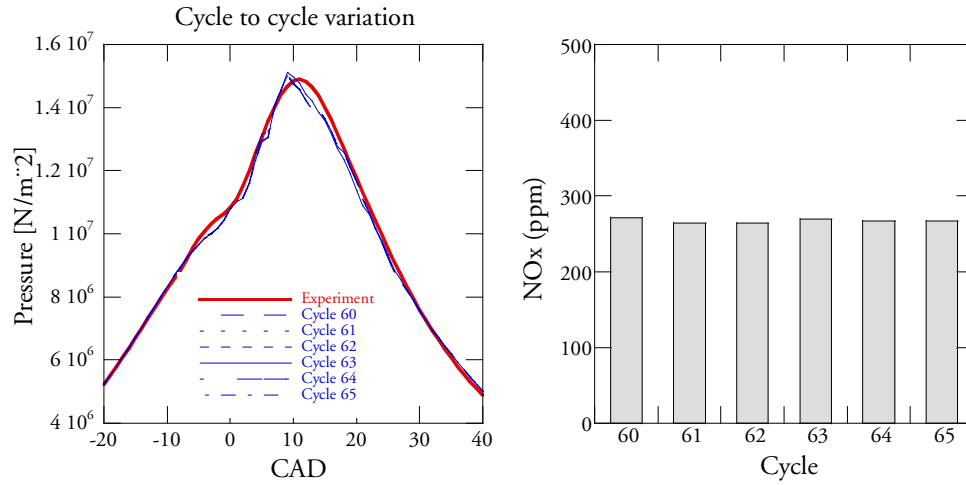
### Cycle-to-cycle Variation

Figure 7.13 demonstrates that the calculated engine conditions were stable from cycle to cycle, meaning that combined flow convergence and combustion convergence were maintained and that steady state operation was reached. Stochastic models themselves inherently show increasing cyclic variations when the discretization is getting coarser, but for the calculations presented in this study that has not been an issue. NO<sub>x</sub> levels are also stable confirming the small cyclic variations.

### Number of particles variation

There is a tradeoff for stochastic models between accuracy and calculation time as a function of the discretization. For the DI-SRM the discretization is a function of the number of particles used to describe the in-cylinder conditions and also a function of the time step length. The assumption of statistical modeling is based on infinite discretization, which in our case would

translate to an infinite number of particles. Now for those of us who do not have infinite time to solve engineering problems the modeling approach is to have a finite number of particles.



**Figure 7.13** Comparison of calculated pressures and NOx levels for cycles 60-65.

With a smaller number of particles the calculation times becomes shorter and one of the important objectives with the DI-SRM is to have a fast and efficient tool. Of course with a smaller number of particles the process gets less precise eventually boarding to a homogenous process which for this investigation would be completely useless.

Figure 7.14 shows the effects on the calculations with different number of particles. Especially obvious is how the heat release rate evolution gets smoother and more realistic with an increasing number of particles. The penalty in calculation time for the increasing number of particles is more or less a linear factor, so that the difference between the 200 particles and 2000 particles is a factor 10. The pressure and other general parameters are still with only 200 particles quite well captured. Investigations with fewer than 100 particles gave very erratic results, which are contributed to the fuel injection process not being modeled reasonable with that small number of particles. The NOx levels are increasing with the number of particles, which cannot be explained by the mean cylinder temperature. Possibly the individual particle temperatures may have a larger spread. Since no experimental value for NOx was given the values with the higher number of particles should be regarded as more correct. The values are typical for this kind of engine.

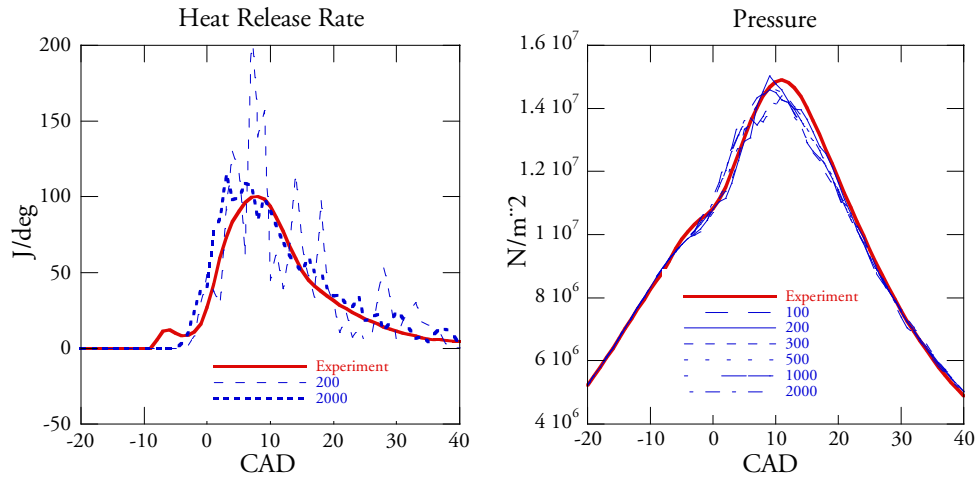


**Figure 7.14** Comparison of calculated heat release rates (left) and pressures (right) for cases with a number of particles ranging from 100 to 2000.

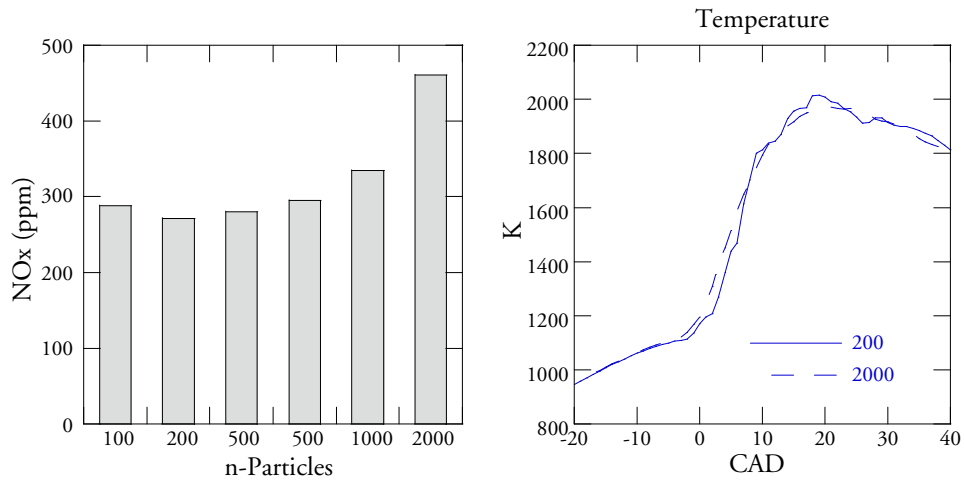


**Figure 7.15** Comparison of calculated NOx levels (left) and temperatures (right) for cases with a number of particles ranging from 100 to 2000.

## Time step size variation

With different time step sizes there were not much difference in the results. Combined with the small amount of particles used, 200, the most noticeable difference is in the peak pressure where

with a time step size of 0.2 CAD the peak pressure has dip. This particular case showed a less good combination of events with fuel injection and the stochastic mixing process. The NO<sub>x</sub> levels move in an opposite direction compared with the number of particles variation.

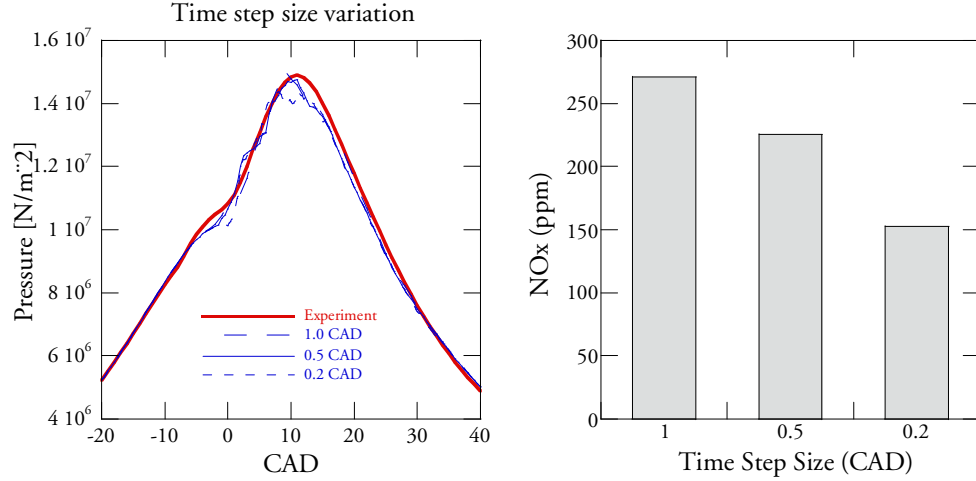


**Figure 7.16** Comparison of calculated pressures for three cases with different time step lengths (left) and for four cases with different mixing times (right).

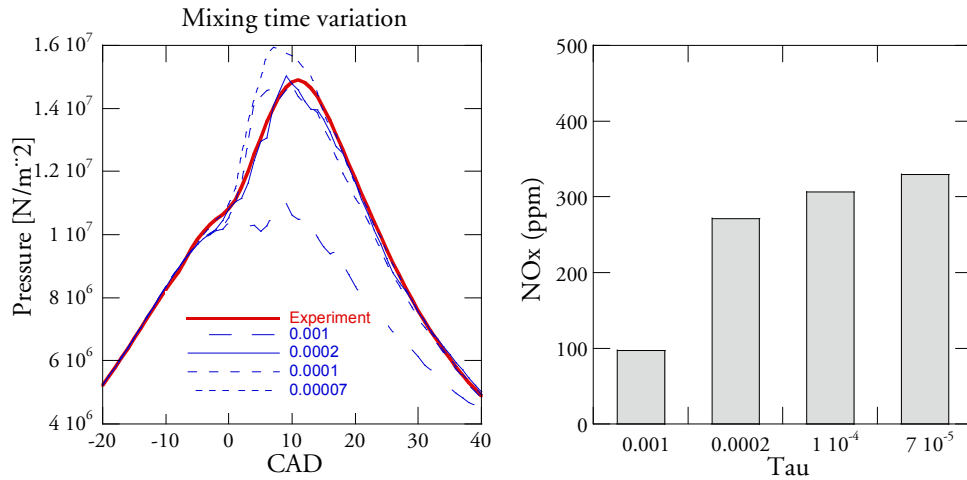


**Figure 7.17** Comparison of calculated pressures for three cases with different time step lengths (left) and for four cases with different mixing times (right).



## Mixing time variation

One of the parameter for the DI-SRM is the mixing time  $\tau$  that either can be given from experiments or CFD calculations. If this is not obtainable  $\tau$  needs to be fitted. The variations of  $\tau$  in Figure 7.17 shows the expected behavior for the heterogeneous conditions of a DI engine, where more intense mixing leads to earlier combustion timing and heat release. With a slow mixing process, 0.001 s, the mixing of fuel and air gets so delayed that favorable conditions for combustion are not reached. The levels of NO<sub>x</sub> have a similar, realistic behavior.

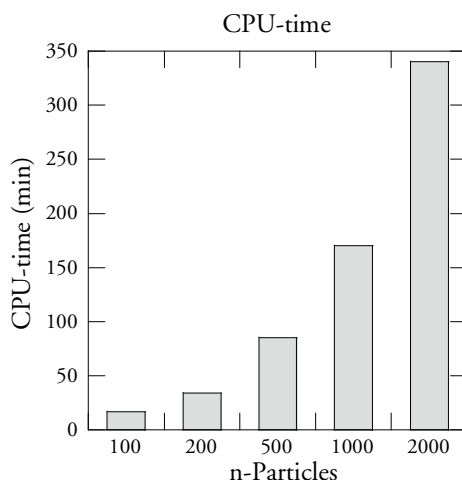


*Figure 7.18 Comparison of calculated pressures for three cases with different time step lengths (left) and for four cases with different mixing times (right).*

## Mixing time variation

The simulations were performed on one of the cores of a 1.8 GHz dual core having 1 GB of RAM. Calculation time for a coupled cycle with a 1-D-EST and the DI-SRM ranges from 17 minutes for 100 particles up to 5 hours and 40 minutes (340 minutes) for 2000 particles (Figure 7.18).

## 7.5 Conclusions

A PDF-based direct injection stochastic reactor model, DI-SRM, was developed. An interface to couple the DI-SRM to the full engine simulation tool was also developed and coupled calculations were performed and compared to experiments to demonstrate the performance of the DI-SRM.

## Chapter 7 The DI-SRM

---

The performed calculation showed reasonable agreement with the experiments. Parametric studies were performed to show the sensitivity from modeling parameters. The DI-SRM is behaving as predicted and even with a coarse discretization the results are comparable to the experiments.

Future work will be focused on making stringent comparisons with new experiments with well verified injection profiles. The models inherent capabilities to predict emissions of HC, NO<sub>x</sub> and soot is also planned to be validated.



### 8 Modeling of HCCI-NVO engines

NVO or Negative Valve Overlap is a strategy that can be used in 4-stroke engines to achieve a second compression and expansion period for every cycle. Possibly combustion may appear during the NVO period but that is most often rather a further oxidation of the residual gases, than a normal combustion.

In a normal 4-stroke engine the expansion stroke is ended with the opening of the exhaust valve(s) for the exhaust stroke that evacuates the exhaust gases from the engine. While the exhaust valve is still open the intake valve (s) opens to start the induction stroke. The period during which both the exhaust and intake valves are open is known as the overlap period. It is since long standard practice to use Variable Valve Timing systems in production engines for regulating the performance of the engine by shifting the valve timings and the overlap period.

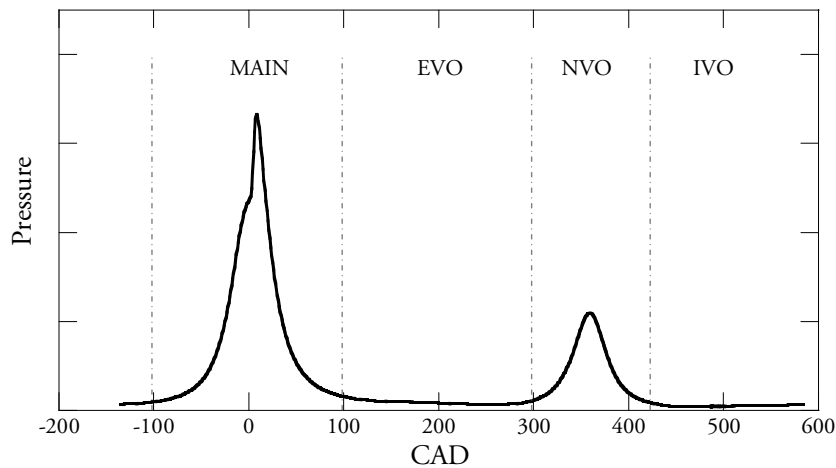


*Figure 8.1 Typical pressure trace for an NVO engine.*

To take this one step further, the valve timings may be set so that the exhaust valve (s) closes before the intake valve (s) opens, thus forming a negative valve overlap period, NVO. What happens is that emptying and filling of the cylinder is decreased and that the amounts of hot residual gases remaining in the cylinder increases. The reason to do this may be several.

- By having a second expansion, more of the energy in the gases may be extracted for work.

- The hot remaining residual gases may be used in the normal combustion period to help the ignition in a HCCI engine.

The concept is interesting but also places particular demand on the modeling due to all possible effects and approaches that are possible with NVO. For instance consideration needs to be taken for that exhaust gases are expelled backwards into the induction system of the engine.

In the present work 3 new reactor models were developed and a substantial number of validations were performed for various clients. Since the models developed are owned by the clients, for reasons of confidentiality not much of details can be presented in this thesis.

## 8.1 Modeling approaches

The studies were done on both port injected and direct injected engine cases with up to 4 injection periods per cycle. The HCCI-SRM code in chapter 5 was modified and two new direct injection models, DI-HRM-SC and DI-SRM-SC, were developed where all three models could be coupled to 1-D-EST or to the in the work carried out here developed Reactor Network Tool.

1-D-EST models were used, coupled to the 3 reactor tools to simulate all the engine performance properties. For parametric studies of the combustion and the emissions, the Reactor Network Tool was used but with starting conditions provided by 1-D-EST calculations.

Throughout the studies n-heptane/isooctane chemical models were used.

The DI-HRM-SC model is based on the HCCI-HRM and is a homogeneous reactor model with direct injection. One of the requests for this model was that it should be as fast as possible to be an efficient tool for parametric studies of the influence of different injection strategies. To further speed up the model, it was implemented with a “cut off” function that could pause the calculation of chemical reactions below temperatures that would be regarded as less important from a chemical point of view. The model utilizes the details of chemical kinetics and fast calculations, but with the limitations of a homogenous reactor model. Heat transfer is modeled with a modified Woschni function.

The DI-SRM-SC model is based on the HCCI-SRM and is a stochastic reactor model with direct injection. The finished model is suitable for use in full cycle simulations of partial HCCI engines (pHCCI) and diesel engines (DICI engines) with or without NVO combustion period. Heat transfer is modeled with a stochastic approach with modified Woschni function. Mixing is performed with the C/D or IEM.

### 8.2 Direct injection model

The direct injection models developed for these studies have little in common with the model presented in chapter 8. Instead of feeding vaporization rates these two models contain a specific vaporization model and the provided injection data should be normal liquid fuel mass rates.

The basic idea is to use an empirical relation of the change of enthalpy due to the evaporation of the fuel during injection, with the knowledge of fuel temperature, heat of vaporization and injected mass during each time step. The cylinder pressure is adjusted due to the increased mass and enthalpy change, continuously. Evolution of the combustion and chemical species (for instance emissions) is solely decided by chemical kinetics. No fundamental limit is set upon number of injection events, which can be spread over the main combustion period or the NVO combustion period or both.

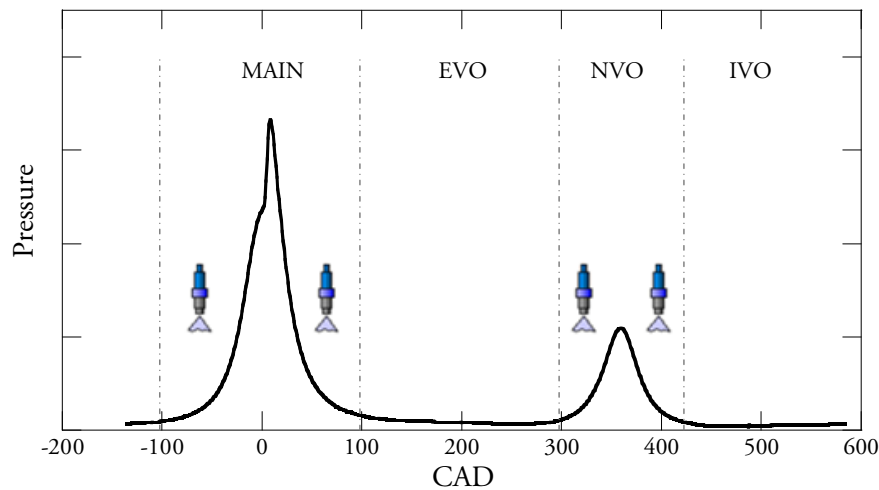


*Figure 8.2 Main and NVO combustion periods with 4 direct injection periods as specified for the DI-HRM-SC and DI-SRM-SC.*

### 8.3 Reactor Network

When the exact composition of EGR and residual gases are unknown, common practice is to run the SRM codes sufficiently many cycles until convergence is obtained. With increasing amounts of EGR and residual gases the combustion itself gets increasingly more sensitive to the composition of those gases. The combustion is always sensitive to initial cylinder pressure, temperature and fuel and oxidizer mass, which are generally given from either experiments or 1-D full engine simulation tools.

If a 1-D full simulation tool is applied to the SRM code, the flow and thus the above mentioned initial conditions are in turn sensitive to the pressure and temperature given from the combustion calculation. To obtain convergence for both the combustion and the residual gases composition but also for the mass flows in the engine at the same time, can be very difficult indeed. However, if the initial conditions at IVC (and EVC for NVO engines) are reasonably well known, either through experiments or through 1-D simulations with deterministic combustion models, it is good practice to run the combustion calculation with the SRM by its own to obtain convergence for the residual gas composition. After such a procedure, combined convergences for the coupled calculations are easier to obtain.

This procedure works fine for standard combustion events in engines, meaning engines that has only single combustion events, since the same modeling settings may be used and the model will simply iterate sufficient many cycles until convergence is reached. For engines with more than one combustion event, like for instance NVO engines, the situation is more complicated. Each of the two combustion events is different. They have different initial conditions and they will produce different composition, temperature and pressure for the residual gases. If the engine has substantial amounts of EGR/residual gases, which is almost always the case for NVO engines, each of the combustion periods are strongly dependent on the other. If it is difficult to reach convergence with a normal combustion period simulation, it is certainly not easier if one needs to consider two different combustion processes alternating each other.

To be able to get simultaneously convergence for both Main and NVO combustion periods, the tool “Reactor Network” was developed. The tool is created in such way that it is a general tool for calculation with up to three different reactors for solving chemical processes that are either separated in time (as for NVO) or separated in space, with either looping or linear dependencies for any number of iterations. Details on the Reactor Network can be found in the manual [97].

For the creation of residual gas composition information for NVO engines the tool is applied in a loop. The Main combustion is simulated and the resulting residual gas composition is fed as input to the next calculated NVO combustion. The resulting residual gas composition from the NVO combustion is in turn fed as input to the next Main combustion. This process is iterated until both the Main and NVO combustion processes has converged. The final residual gas composition is then ready for use in a coupled calculation between the SRM code and a 1-d simulation tool, just one remembers in which order the cycles will be simulated.

The Reactor Network is also a quite efficient tool to use for parametric studies of NVO engines, where initial conditions are known or a 1-d simulation is not desirable.

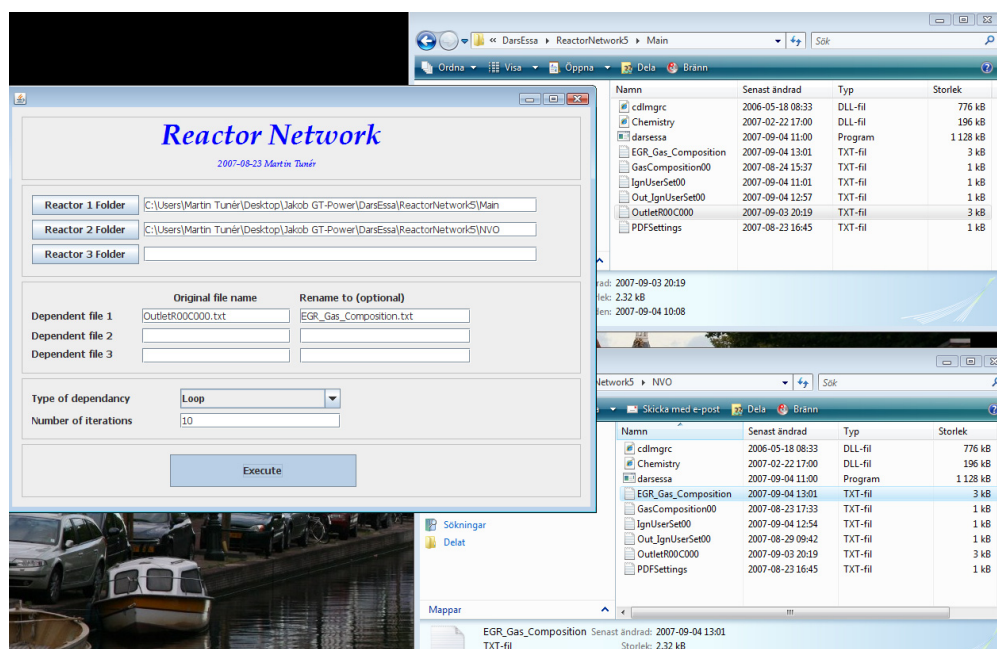
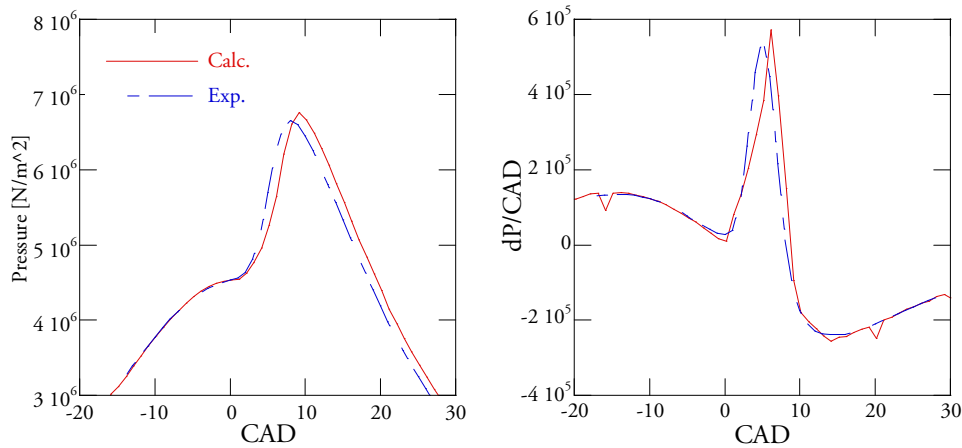


Figure 8.3 The Reactor Network tool.

## 8.4 Validation

The validation of the 3 developed models typically followed the pattern described in the previous Chapter. A 1-D simulation tool and Reactor Runner was used, complementing each other, for fast and efficient parametric variations and simulations until complete convergences were reached. Basically all physical parameters known from experiments could be used without tuning, except compression ratios that were adjusted to fit motored cycles with the heat transfer parameters set for motoring conditions. Parameters that were tuned, involved typically stoicon and tau. For explanation on stoicon and tau see sections 4.4-4.5 and 5.1. Validations were performed against experiments performed by clients, with targets of ignition timing, pressure rates and pressure. Typical results are demonstrated in Figure 8.4.





*Figure 8.4 Typical validation results for NVO engine.*

## 8.5 Peculiarities of NVO engines. Modeling and chemistry issues.

As discussed in section 9.3, from a Chemical Kinetics point of view, validation of NVO engines cannot be divided into separate combustion events since the resulting gas composition (and the remaining chemical energy) has a direct and strong influence on each of the following combustions.

In fact the sensitivity in modeling has nothing to do with sensitivity in the combustion process. The combustion process does not differ to the normal HCCI, pHCCI or DICI combustion process in sensitivity. The sensitivity lies in the models ability to predict the residual gas composition.

In one of the early attempts to model a NVO engine with the SRM coupled to a 1-D code unusual behavior was noted. The case is a quite typical case where the main combustion consists of 41% residual gases and the NVO combustion of 100%. The chemical model used was a PRF chemical model. Note that the gas compositions for the combustion gas (residual gases) from the main and the NVO combustion cycles are quite different.  $C_8H_{18}$ ,  $C_2H_4$ ,  $CO$ ,  $C_6H_{13}$  have differences in the order of up to 10 times.  $C_8H_{18}$ , isooctane, is one of the fuel species and is not completely consumed in the main cycle. The other fuel species,  $C_6H_{17}$ , n-heptane, was completely consumed.

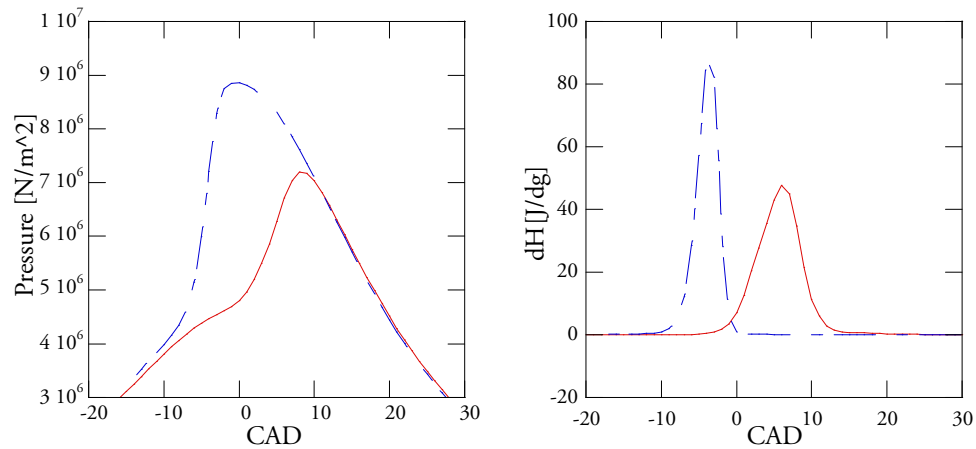


**Figure 8.5** Two calculations with the HCCI-SRM using the same initial conditions except for the residual gas mass fractions. Solid line is when using residual gas species calculated by the previous SRM and defined by the PRF chemical model while the dotted line is for residual gases calculated with the 1-D tool and defined with its chemical model.

While running the calculations coupled with the 1-D code the residual gas species as determined by the 1-D code was used. As most 1-D codes the number of species in the model is limited to less than 17. Even though exactly the same initial conditions, pressure, temperature and fuel, oxidizer and residual gas masses and the same modeling parameters as well as the same chemical model, were used the results were dramatically different (Figure 8.5).

When compared, all species of major amounts, N<sub>2</sub>, O<sub>2</sub>, CO<sub>2</sub>, H<sub>2</sub>O, and fuel remains are similarly predicted by both models. What differs is the amount of the radical OH. Although the mass fraction of OH in the 1-D code is as little as  $2.56 \cdot 10^{-5}$  this is enough to trigger the whole combustion to the massive difference in Figure 8.5. In the SRM code the OH was calculated to  $5.31 \cdot 10^{-11}$ , giving a difference of a factor  $10^6$ .

The reason for the overprediction of OH is most likely not a bug in the 1-D code but probably a consequence of the simplified chemical description used and the way the mass fractions are determined. In the 1-D code the species mass fractions are at each time step during the combustion determined from the mass fraction burned which is calculated and passed from the SRM code. In the case of modeling a NVO engine the mass fraction burned curve is divided into two parts, one for each of the combustion periods (Figure 8.6).

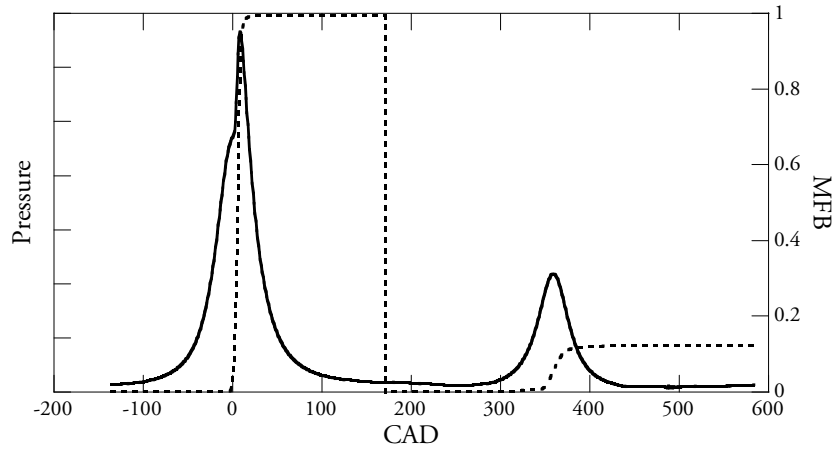


**Figure 8.6** Cylinder pressure and corresponding mass fraction burned for a NVO engine.

The mass fraction burned is normalized where the range is determined by the available chemical energy from the chemical composition of the gases at the beginning of the calculation or through coming fuel injections. In Figure 8.6 the second mass fraction burned curve reaches only 12 %. For this case there is no fuel injected during the EVO period or during the NVO period, so the chemical energy at the start of the NVO combustion is actually very small. In fact only what is left to burn from the main combustion that already reached close to unity in mass fraction burned. The result is that the second mass fraction burned curve is much more sensitive to determine than the one for the main cycle, and can be seen as a normalized MFB that could be placed on top of the first one.

The conclusion one might draw from this, is the importance of having a sufficient kinetic model to be able to model NVO engines at all.

### 9 Conclusions

The thesis work aimed at the further development of practical engine simulation models based on Stochastic Reactor Models, SRMs. Novel and efficient implementations were made of a variety of SRMs adapted to different engine types. The models in question are the HCCI-SRM, the TwoZone SI-SRM and the DI-SRM. The specific models developed were incorporated into two different interfaces: DARS-ESSA, which is a stand-alone tool, and DARS-ESM through which all the models can be operated in a simple and effective manner with use of several commercial 1-d engine simulation tools. The tools and couplings to commercial 1-D codes were successfully developed and employed to simulate such complex combustion processes as of HCCI engines with NVO combustion. It was shown that kinetic models containing detailed chemistry are necessary for modeling such engines, since commercial codes, with the limited chemical models they include, fail to predict the supersensitive residual gases.

SRMs are able to model cyclic variations, but these may be overpredicted if discretization is too coarse. The range of cyclic variations and the dependence of the ability to correctly assess their mean values on the number of cycles simulated were investigated. In most cases, the average values were assessed correctly on the basis of as few as 10 cycles, but assessing the complete range of cyclic variations could require a greater number of cycles. It is obvious that under unstable operating conditions one single calculation may differ from another substantially. A study involving calculation of a single case, if an unfortunate combination of starting conditions and modeling parameters were selected, might yield results that could be easily be misinterpreted. The remedy for such problems is to use sufficiently many particles and to check on a regular basis the cyclic variations from the results obtained. The ability to predict cyclic variations is certainly useful in studying engine operating regimes, but one should bear in mind for the SRM that apparent effect can originate from the incorrect use of discretization, and thus not be a physically correct feature of the engine's functioning. In assessing the range of cyclic variations in pressure, employing the HCCI-SRM, the variation obtained is found to decrease with the number of particles considered, leveling out in the range of 500 to 1000 particles. For determining whether the given results are valid a range of simulations with 400, 600, 800 and 1200 particles could be needed to perform. Judging from the other result parameters it feels safe to say that for this HCCI-SRM configuration a reasonable number should be 500 particles. Regarding the timestep size, the results are less clear. For many of the parameters, notably time of ignition and combustion duration, time step sizes ranging from 0.5 CAD to 0.1 CAD, give slightly differing results. One could nevertheless conclude that a time step size of 0.5 CAD is a reasonable choice in most cases. In studying average values, variations due to coarse discretization when 100 particles and when a time steps of 0.5 CAD are employed are smaller than variations originating

from changes in physical parameters, such as heat transfer and mixing parameters. Thus it feels safe to conclude that, even with such coarse discretization, the findings obtained with use of the HCCI-SRM are basically correct.

For studies of cyclic variations in engines, discretization needs to have a higher level of resolution, 500 particles and 0.5 CAD time steps, to provide trustworthy results. In the case of high levels of turbulence and evenly distributed heat transfer, the in-cylinder conditions become homogeneous more quickly. The results indicate that in HCCI engines inhomogeneities tend to promote earlier ignition and more stable operating conditions as well as lesser cyclic variations. The pressure derivative was shown to generally tend to increase under homogeneous conditions, which could lead to unwanted noise and even to engine damage. According to calculations for HCCI engines, the level of turbulence and the heat transfer distribution had little impact on the duration of combustion or on the amount of HC and NO at EVO, except for HC which rocketed in the odd misfiring cycles.

The calculated concentrations of hydroxyl radicals and formaldehyde were compared with LIF-measurements made in an optically accessed iso-octane / n-heptane fuelled HCCI engine. The profiles of averaged concentrations of  $\text{CH}_2\text{O}$  and OH could be predicted quite well by the SRM, as determined by comparison with averaged LIF-signals of the respective species. A moderate deviation in  $\text{CH}_2\text{O}$  was attributed to the chemical model, which gave too slow a growth of formaldehyde in the low-temperature regime. The minor deviations in the hydroxyl radicals that could be noted were probably due to minor deviations in the physical model, a view that was supported by investigations using different mixing times, that showed the rates of heat release to differ accordingly, a behavior that had a direct impact on the shape of the hydroxyl radical concentration profile. The main heat release could be predicted rather well, whereas low-temperature heat release in the cool flame region could be predicted less accurately. The close agreement between SRM and LIF PDPs clearly proves the validity of the stochastic reactor model. It also shows that well-performed SRM calculations with use of a good detailed kinetic model are a valid method of gaining insight into the ignition characteristics of homogeneous ignition. The method can also be extended to other species that are difficult to measure but still give important information on the combustion and the information sought. The fact that the SRM can be used to extend the concentration range of the species that were investigated, far beyond the LIF detection limit, is also significant. The interrelations of OH and  $\text{CH}_2\text{O}$  during HCCI combustion were investigated. It was found that at the very onset of ignition, during the growth phase of  $\text{CH}_2\text{O}$ , the particles having the highest concentrations of  $\text{CH}_2\text{O}$  also had the highest concentrations of OH. At the peak of low-temperature heat release, particles having relatively high concentrations of OH (for the stage of ignition) become fewer. Just beyond that peak the highest OH levels disappear. During the transition stage from low to high-temperature ignition, all particles seem then to have the same high levels of  $\text{CH}_2\text{O}$ , whereas the OH-concentrations

## Chapter 9 Conclusions

---

are generally low and unevenly distributed. It was observed that during the growth phase of  $\text{CH}_2\text{O}$  there is a temporal OH peak, coinciding with the first heat release peak.

The formation of exothermic centers was modeled with the SRM to investigate their impact on HCCI combustion. By varying the exhaust valve temperature, and thus assigning more realistic wall temperatures, the formation of exothermic centers and the ignition timing was shifted in time. To be able to study the exothermic centers, their formation and their distribution, Scatter plots, standard deviation plots and PDF plots were constructed on the basis of the data the SRM calculations provided. The standard deviation for the particle temperatures was found to be an excellent indicator of the degree of homogeneity within the combustion chamber, and thus of how efficient the combustion process was. It was observed that when the standard deviation of the temperature was higher, the emissions of CO and of hydrocarbons present at the end of the closed cycle were higher. It was thus concluded that the standard deviation of the temperature, provided some indication of such emissions as those of hydrocarbons and CO. Since no  $\text{NO}_x$  model was used for the calculations, no conclusions can be made on the relation of  $\text{NO}_x$  formation and the standard deviation of temperature. The standard deviation does not provide any absolute levels concerning the parameter in question. PDF plots do just this, while at the same time providing a detailed picture of the spread of the parameters being studied. According to the PDF results obtained, higher absolute temperature implies more  $\text{NO}_x$  to be present in the “hot” case. Still, the temperatures were so low that the typically very low levels of  $\text{NO}_x$  in HCCI engines could be expected to be maintained. It was shown that promoting exothermic centers could be one way of counteracting emissions of hydrocarbons and CO which are a problem in HCCI engines.

Implementations of the SRM codes in the present work involved stricter handling of the parameters and combined with the use of a new solver, a reduction of the execution time as well of the memory allocations, were achieved by almost a factor of 10 respectively, compared to similar existing models. Still, part of the work aimed at investigating whether a novel approach developed, involving use of adaptive chemistry, could improve calculation speed still further without much loss in accuracy. Already reduced skeletal mechanisms were divided into sets of sub mechanisms, each representing a phase in the combustion events. These Phase Optimized Skeletal Mechanisms, POSM, as well as establishing the phases in question, were created by an automated tool making use of machine learning, clustering and decision tree algorithms. The phases were established on the basis of constant volume calculations. The POSM model created was incorporated into the two-zone SRM code, comparative calculations being made between the standard mechanisms and the POSM with the aim of determining the accuracy and the calculation speed of this novel technique. Although all of the POSMs considered were based on already

strongly reduced skeletal mechanisms, POSM was found to provide gains in calculation speed while still retaining a high degree of accuracy. The first two investigations showed almost no accuracy to be lost, at the same time as there was a gain in calculation time by a factor of 3. These two investigations differed not only in the original chemical model that was employed, but also in how the database for Phase creation was calculated. Investigation 1 employed several sets of constant volume calculations, whereas investigation 2 used only a single SRM calculation. It was expected that the SRM calculation would provide a more realistic data set than the constant volume calculations, an expectation that could be neither confirmed nor rejected since the two cases had almost exactly the same accuracy and gain in calculation time. The second case did have a smaller original chemical model, however, which gave less latitude for reduction, so it can well be the case that the SRM calculation did provide a better data set. Investigation 3 involved a further reduction than carried out in investigation 2. It showed clear losses in accuracy, although the global conditions were well captured and there was a gain in calculation speed by a factor of 12. One should note that the number of species in the phase mechanisms had become so small that it is not at all surprising that higher losses in accuracy appeared. There is still a lot to be gained by further division into a greater number of phases, rather than simply reducing the number of species in the phases. Especially for phases having only a small reduction in size and possessing a size similar to the original chemical model, further division would be likely to result in substantial gains. Further, the POSM approach showed excellent robustness as a concept. Even with different base chemistries as in investigation 1 and 2, and also by varying octane rating and mixture strength, accuracy was retained. Several studies to investigate the sensitivity of the numerical and modeling parameters by varying the number of particles, time step size and mixing and heat transfer parameters that were performed, confirmed the robustness of POSM.

A direct injection model for the SRM, DI-SRM, allowing multiple and complex injection strategies to be followed was implemented. This model can be used to simulate pHCCI and DICI and with some further development of it DISI as well. Simulations of diesel engine combustion, DICI, using the newly developed model coupled with a 1-D full engine simulation tool were found to agree well with the results of experiments that were conducted. Parametric studies were performed to indicate the sensitivity of the modeling parameters. The DI-SRM behaved as predicted, and even with use of coarse discretization the results were comparable to those of the experiments. Future work will be focused on making stringent comparisons with new experiments with well verified injection profiles. Validation of the models inherent capabilities for predicting emissions of HC, NO<sub>x</sub> and soot is also planned to be validated.

### References

1. National Research Council, <http://www.nap.edu/catalog/11676.html>
2. World Resources Institute, <http://www.wri.org>
3. The Stern Report, [http://www.hm-trea-sury.gov.uk/independent\\_reviews/stern\\_review\\_economics\\_climate\\_change/sternreview\\_index.cfm](http://www.hm-trea-sury.gov.uk/independent_reviews/stern_review_economics_climate_change/sternreview_index.cfm)
4. Kunze, R., "Climate Change and Road Transport Challenges", <http://www.ertrac.org>
5. <http://www.dieselnet.com/standards/eu/ld.php>
6. Tunér, M., "A Java-based Full Engine Simulation Tool", M.Sc. Thesis, Lund University, 2003.
7. [http://en.wikipedia.org/wiki/Oil\\_refinery](http://en.wikipedia.org/wiki/Oil_refinery)
8. Noehre, C., Andersson, M., Hultqvist, A., Johansson, B., "Characterization of Partially Premixed Combustion", SAE 2006-01-3412
9. Persson, H., Remaon, A., Johansson, B., "The Effect of Swirl on Spark-Assisted Compression Ignition (SACI)", SAE 2007-01-1856
10. Arvidsson, A., Løvås, T., Mauss, F., "An Automatic Sparse Matrix Solver for Reduced Reaction Kinetics". 21<sup>st</sup> ICDERS, 2007.
11. Ahmed, S. S., Mauss, F., Moréac, G., Zeuch, T., "A comprehensive and compact n-heptane oxidation model derived using chemical lumping", Phys. Chem. Chem. Phys., 9, 1107–1126, 2007.
12. Pitsch, H., Barths, H., and Peters, N., "Threedimensional modeling of NO<sub>x</sub> and soot formation in DI-Diesel engines using detailed chemistry based on the interactive flamelet approach", SAE 962057.
13. Steiner, R., Bauer, C., Kruger, C., Otto, F., and Maas, U., "3D-simulation of DI-diesel combustion applying a progress variable approach accounting for complex chemistry". SAE 2004-01-0106.



14. Lehtiniemi, H., Mauss, F., Magnusson, I., Balthasar, M., "Modeling Diesel Engine Combustion with Detailed Chemistry Using a Progress Variable Approach", SAE 2005-01-3855.
15. Vermorel, O., Richard, S., Colin, O., Angelberger, C., Benkenida, A., Veynante, D., "Multi-cycle LES simulations of flow and combustion in a PFI SI 4-valve production engine". SAE 2007-01-0151.
16. Lehtiniemi, H., Zhang, Y., Rawat, R., Mauss, F., "Efficient 3-D CFD Combustion Modeling with Transient Flamelet Models". SAE 2008-01-0957.
17. Vibe (Wiebe), I., "Halbempirische Formel für die Verbrennungsgeschwindigkeit, in Kraftstoff-aufbereitung und Verbrennung bei Dieselmotoren", ed G Sitkei, pp 156-159, Springer Verlag, Berlin, 1964.
18. Watson, N., Pilley, A. D. and Marzouk, M., "A Combustion Correlation for Diesel Engine Simulation", SAE 800029.
19. Woschni, G., "A Universally Applicable Equation for the Instantaneous Heat Transfer Coefficient in the Internal Combustion Engine", SAE 670931
20. Amnéus, P., Nilsson, D., Mauss, F., Christensson, M., Johansson, B., "Homogenous Compression Ignition Engine: Experiments and Detailed Kinetic Calculations", Proceedings of the Fourth International Symposium COMODIA 98, Kyoto, Japan, 1998.
21. Erlandsson, O., Einewall, P., Johansson, B., Amnéus, P., Mauss, F., "Simulation of HCCI –addressing compression ratio and turbo charging", SAE 2002-01-2862.
22. Bellanca, R., "*BlueBellMouse; A Tool for Kinetic Development*". Doctoral thesis, Lund University 2004.
23. Heywood, J. B., "Internal Combustion Engine Fundamentals", p 506, McGraw Hill, New York, 1988.
24. Kraft, M., Stochastic Modelling of Turbulent Reacting Flow in Chemical Engineering, 1998, Reihe 6 (391), pp. 1-109 (VDI Verlag, Fortschrittsberichte des VDI).
25. Maigaard, P., Mauss, F. and Kraft, M., 2003, Homogeneous Charge Compression Ignition Engines: A Simulation Study on the Effect of Inhomogeneities, ASME J. Engineering for Gas Turbines and Power, 125, pp. 466-471.
26. Montorsi, L., Mauss, F., Bianchi, G. M., Bhawe, A. and Kraft, M., "Analysis of the HCCI Combustion of a Turbocharged Truck Engine Using a Stochastic Reactor Model", ASME ICE Division, ICES-2003-681.

## References

---

27. Bhave, A., Balthasar, M., Kraft, M., Mauss, F., "Analysis of a natural gas fuelled homogeneous charge compression ignition engine with exhaust gas recirculation using a stochastic reactor model", *Int. J. Engine Res.*, 5(1):93-103, 2004a.
28. Amnéus, P., Tunér, M., Mauss, F., Collin, R., Nygren, J., Richter, M., Aldén, M., Kraft, M., Bhave, A., Hildingsson, L., Johansson, B., "Formaldehyde and Hydroxyl Radicals in an HCCI Engine - Calculations and LIF-Measurements", SAE 2007-01-0049.
29. Warnatz, J., Maas, U. and Dibble, R.W. "Combustion; Physical and Chemical Fundamentals, Modeling and Simulation, Experiments, Pollutant Formation". Springer-Verlag 2001.
30. Hundsdorfer, W. and Verwer, J. "Numerical Solution of Time-Dependent Advection-Diffusion-Reaction Equations". Springer-Verlag 2003.
31. Yang, B., Pope, S. B., "An investigation of the accuracy of manifold methods and splitting schemes in the computational implementation of combustion chemistry", *Combustion and Flame*, 112:16-32, 1998.
32. Gogan, A., Lehtiniemi, H., Sundén, B. and Mauss, F., "Stochastic Model for the Investigation of the Effect of Turbulent Mixing on Engine Knock", SAE 2004-01-2999.
33. Challen, B., Baranescu, R., "Diesel Engine Reference Book", Second edition, SAE International, 1999.
34. Frisch, U., "Turbulence: The Legacy of A. N. Kolmogorov". Cambridge University Press, 1995.
35. Boulanger, J., Liu, F., Neill W. S., Smallwood G. J., "Investigating renewable fuel combustion II: DNS of DME and n-heptane ignition in a turbulent non-homogeneous flow with high dissipation". *International Journal of Environmental Studies*, 64:4, pp 419-432, 2007.
36. Dopazo, C., "Relaxation of initial probability functions in the turbulent convection of scalar fields". *The Physics of Fluids*, 22(1), pp. 20-30, 1979.
37. Dopazo, C., "Recent developments in PDF methods". In P.Libby and F.Williams, Eds., *Turbulent reactive flows*, pp. 375-474. Academic press, London, 1994.
38. Valino, L., Dopazo, C., "A binomial Langevin model for turbulent mixing". *The Physics of Fluids, A*, 3(12), pp. 3034-3037, 1991.
39. Curl, R. L., *Dispersed Phase Mixing: I. Theory and Effects in Simple Reactors*, A.I.Ch.E. Journal, Vol. 9, No. 2, pp. 175-181, 1963.

40. Wouters, H.A., Nooren, P. A., Peeters, T.W.J., Roekaerts, D., "Effects of micro-mixing in gas-phase turbulent jets". 2<sup>nd</sup> Int. Symp. On Turbulence, Heat Transfer and Mass Transfer, pp. 389-398, 1997.
41. Janicka, J., Kolbe, W., Kollmann, W., "Closure of the transport equation for the probability density function of turbulent scalar fields". Journal of Non-Equilibrium Thermodynamics, 4, pp. 47-66, 1979.
42. Samuelsson, K., Gogan, A., Netzell, K., Lehtiniemi, H., Sundén, B., Mauss, F., "Modeling Diesel Engine Combustion and Pollutant Formation Using a Stochastic Reactor Model Approach", Intl. Conf. Clean Diesel Combustion, Lund, 2005
43. Karlsson, M., "The Influence of microscale inhomogeneties on the combustion process in an HCCI engine". B.Sc. Thesis, Lund University, 2007.
44. Withrow, L and Rassweiler, G.M: "Absorption Spectra of Gaseous Charges in a Gasoline Engine", *Industrial and Engineering Chemistry, Vol 25, No 8, pp 923-931*
45. Rassweiler, G.M. and Withrow, L: "Spectrographic Detection of Formaldehyde in an Engine Prior to Knock" *Industrial and Engineering Chemistry, Vol 25, No 12, pp 1359-1366*
46. Withrow, L. and Rassweiler, G.M: "Formaldehyde formation by preflame reactions in an engine" (*Industrial and Engineering Chemistry, Vol 26, No 12 pp1256-1262*).
47. Amnéus, P., PhD Thesis, Lund Institute of Technology, 2002, ISBN 91-628-5508-5
48. Chun, K.M., Heywood, J.B. and Keck, J.C., 22nd Symp. (Int.) on Combustion, pp.1055-1062, The Combustion Institute 1988
49. Cowart, J.S., Keck, C., Heywood, J.B., Westbrook, C.K., Pitz, W.J., 23rd Symp. (Int.) on Combustion, pp.1055-1062, The Combustion Institute 1990
50. Hajireza, S., Mauss, F. and Sundén, B., SAE 971671
51. Hajireza, S., Mauss, F. and Sundén, B., 4th Int Symposium COMODIA 98 pp. 203-209, JSME 1998
52. Hajireza, S., Sundén, B., and Mauss, F., SAE 1999-01-0219
53. Litzingen, T.A., Prog. Energy Combust. Sci. 1990, Vol.16, pp 155-167
54. Schissl, R., Dreizler, A., Maas, U., Grant, A.J. and Ewart, P., SAE 2001-01-1925

## References

---

55. Maly, R.R., 25th Symp. (Int.) on Combustion, pp. 111-124, (1994)
56. Bäuerle, B., Warnatz, J. and Behrendt, F., 26th Symp. (Int.) on Combustion, pp. 2619-2625, (1996)
57. Schissl, R. and Maas, U., Combust. Flame 133 pp. 19-27 (2003)
58. Nygren, J., Hult, J., Richter, M., Aldén, M., Christensen, M., Hultqvist, A. and Johansson, B., 29th Symp. (Int.) on Combustion. Pp 679-685 (2002)
59. Graf, N., Gronki, J., Schulz, C., Baritaud, T., Cherel, J., Duret, P. and Lavy, J., SAE 2001-10-1924
60. Sato, S., Jun, D., Kweon, S., Yamashita, D., Iida, N., SAE 2005-01-0149
61. Konno, M., Chen, Z., SAE 2005-01-0182
62. Becker, H., Arnold, A., Suntz, R., Monkhouse, P., Wolfrum, J., Maly, R. and Pfister, W., Appl. Phys. B 50, pp. 473-478 (1990)
63. Andresen, P., Schlüter, H., Wolff, D., Voges, H., Koch, A., Henstschel W., Oppermann, W. And Rithe, E., Applied Optics, Vol. 31 no. 36, pp.7684-7689, (1992)
64. Tamura, M., Sakurai, T. and Tai, H. Opt. Soc. Am
65. Pixner, P., Schiessl, R., Dreizler, A. and Maas, U., Combust. Sci. and Tech., Vol. 158, pp. 485-509
66. Dec, J.E. and Coy, E.B., SAE 960831
67. R. Collin, J. Nygren, M. Richter, and M. Aldén; L. Hildingsson, and B. Johansson (2003). *Simultaneous OH- and formaldehyde-LIF measurements in an HCCI engine*. SAE 2003-01-3218
68. Ahmed, S., Zeuch, T., Amneus, P., Blurock, E., Soyhan, H. and Mauss, F: "Validation of the iso-octane/n-heptane mechanism PL 2.0 in HCCI and shock tube calculations", Planet D4 report. The European Community
69. Ahmed, S., Blurock, E., and Mauss, F: Detailed mechanism for n-Heptane and iso-Octane relevant for HCCI engine calculations. Joint meeting of Scandinavian-Nordic and Italian Sections of the Combustion Institute. 2003, session 3.3.

70. Klaus, Ph., PhD Thesis, Interdisziplinäres Zentrum für Wissenschaftliches Rechnen, Ruprecht-Karls-Universität Heidelberg (1997)
71. Mauss, F., Blurock, E. and Amneus, P: "Complex chemical scheme for HCCI auto-ignition relevant for engine conditions", Planet D4 report Work Package MD, The European Community.
72. Hoyernann, K, Mauss, F. and Zeuch, T., Phys. Chem. Chem. Phys. 6 (2004) 3824-3835.
73. Chevalier, C., Dissertation, Institut für Technische Verbrennung, Ruprecht-Karls-Universität Heidelberg (1993)
74. Curran, H., Gaffuri, P., Pitz, W. and Westbrook, C., Combust. & Flame 129:253-280 (2002)
75. Ahmed, Syed Sayeed, Licentiate thesis, Lund Institute of Technology, 2004
76. Metz, T., Bai, X., Ossler, F. and Aldén, M., Spectrochim. Acta A 60:821-828, 2004.
77. König, G., Bradley, D., Lau, A., Sheppard, W., Maly, R., "Role of Exothermic Centers on Knock Initiation and Knock Damage", SAE 902136.
78. Ethyl Corporation: "Engine Combustion Noises", Ethyl technical note PCDTN-MS 117768.
79. Vressner, A., Lundin, A., Christensson, M., Tunestål, P., Johansson, B., "Pressure Oscillations During Rapid Hcci Combustion". SAE 2003-01-3217
80. Ahmed, S. S., Moréac, G., Zeuch, T. and Mauss, F., "Reduced Mechanism for the Oxidation of the Mixtures of n-Heptane and iso-Octane", Proceeding of the European Combustion Meeting "ECM 2005", Louvain-La-Neuve, Belgium, April 3-6, Paper No. 40, 2005.
81. Gamma Technologies Inc., GT-Power User's Manuals 5.2-6.2, [www.gtisoft.com](http://www.gtisoft.com)
82. Montorsi, L., Cantore, G., Amnéus, P., Mauss, Erlandsson, O., Johansson, B., Morel, T., "Analysis of a 6 Cylinder Turbocharged HCCI Engine using a Detailed Kinetic Mechanism", ASME ICE Division, 2002-ICE-457.
83. Gogan, A., Sundén, B., Montorsi, L., Ahmed, S., Mauss, F., "Knock Modeling: an Integrated Tool for Detailed Chemistry and Engine Cycle Simulations", SAE 2003-01-3122.
84. Tunér, M., "Manual for DARS-ESM/GT-Power", Version 2007-10-04, LOGE AB.

## References

---

85. Tunér, M., Blurock, E. S., Mauss, F., “Phase Optimized Skeleton Mechanisms for Stochastic Reactor Models for Engine Simulation”, SAE 2005-01-3813.
86. Soyan, H, Mauss, F., and Sorousbay, C., “Chemical Kinetic Modelling of Combustion in Internal Combustion Engines using Reduced Chemistry”, Combust. Sci. Technol., 2002, 174, 73-91.
87. Blurock, E. S., “Automatic Characterization of Ignition Processes with Machine Learning Clustering Techniques”, accepted for publication International Journal of Chemical Kinetics.
88. Blurock, E. S., “Characterizing Complex Reaction Mechanisms using Machine Learning Clustering Techniques”, International Journal of Chemical Kinetics, 2004, 36, pp.107-118.
89. J.J. Emdee, K. Brezinsky, I. Glassman, J. Phys. Chem 96 (1992) 2151-2161.
90. Turns, S., “An Introduction to Combustion”, McGraw-Hill, 1993.
91. Su, H., Vikhansky, A., Mosbach, S., Kraft, M., Bhave, A., Kim, K., Kobayashi, T., Mauss, F., “A computational study of an HCCI engine with direct injection during gas exchange”, Combustion and Flame, 147, 118-132, (2006).
92. Mosbach, S., Su, H., Kraft, M., Bhave, A., Wang, Z., Wang, J., Mauss, F., “Dual Injection HCCI Engine Simulation using a Stochastic Reactor Model.”, The International Journal of Engine Research, 8 (1), 41-50, (2007).
93. Samuelsson, K., “Development and Validation of a Fuel Injection Model for the SRM Code”, MSc. Thesis, Lund University, 2004.
94. Gogan, A., “Full Cycle Engine Simulations with Detailed Chemistry”, PhD. Thesis, Lund University, 2006.
95. Ricardo Inc., Wave 7.0-7.1 User’s Manuals, [www.ricardo.com](http://www.ricardo.com)
96. Tunér, M., “Manual for DARS-ESM/Ricardo Wave”, Version 2007-05-15, LOGE AB.
97. Tunér, M., “Reactor Runner user Manual”, Version 2006-04-26, LOGE AB.